EXPLORING THE IMPACT OF HEMODYNAMIC AND HEMORHEOLOGY IN THE DESIGN OF CARRIER FOR VASCULAR-TARGETED DRUG DELIVERY IN ATHEROSCLEROSIS

by

Katawut Namdee

A dissertation submitted in partial fulfillment
of the requirements for the degree of
Doctor of Philosophy
(Biomedical Engineering)
in the University of Michigan
2015

Doctoral Committee:

Associate Professor Omolola Eniola-Adefeso, Chair
Professor David J Pinsky
Professor Takayama Shuichi
Assistant Professor Greg Thurber

To Dad and Mom

For your love, support and encouragement

ACKNOWLEDGMENTS

This thesis, “Exploring the Impact of Hemodynamic and Hemorheology in the Design of Carrier for Vascular-Targeted Drug Delivery in Atherosclerosis”, studies the efficacy of drug carriers in animal models and microvascular systems with the purpose of understanding co-relation and differences from humans. Research such as this requires financial support, availability of animal subjects, and technical and intellectual support. I wish to acknowledge with grateful thanks the enormous support to those who have made this thesis possible. I sincerely appreciate all the assistance and suggestions from all directions.

My advisor, Professor Omolola Eniola-Adefeso (Associate Prof. at Chemical Engineering), gave me an opportunity to work in the Drug delivery and Cell adhesion Lab for the past five years. I am deeply indebted to her support, suggesting on my research directions, her editorial comments on all my manuscripts and presentations and was patience with my limited knowledge in engineering. Her energy and enthusiasm has inspired me to continue working in this field.

Dr. David J. Pinsky, Director and Science Lead of Cardiovascular Medicine at the University of Michigan, provided me the chance to collaborate with his lab and treated me like one of his lab members for five years. The animal studies were conducted in his lab

with huge supports from his lab members; Dr. Diane Bouis, Dr. Anuli Anyanwu, Dr. Natasha Dolgacheva and Dr. Yogendra Kanthi. I honestly appreciate all the assistance.

Professor Shuichi Takayama, Department of Biomedical Engineering, allowed me to share facilities in his Micro/Nano/Molecular Biotechnology Lab. I am very grateful to Dr. Chuan-Hsien Kuo who trained me in microfluidic channel fabrication. I also would like to thank to Professor Takayama for serving on my committees and for his thoughtful suggestions.

I would like to thank Professor Greg Thurber, Department of Chemical Engineering, for serving on my thesis committee. He is an expert in animal models and cancer therapeutics. He provided me valuable discussions, time and attention on my studies.

Co-workers also provided greatly valued aid and assistance. I am deeply grateful to Dr. Phapanin Charoenphol, Dr. Alex J Thompson, Peter Onyskiw, Dr. Ryan Huang, Daniel Sobczynski, Margaret Fish and Mariana Carrasco-Teja. I specially thank all the diligent undergrad students who worked with me including Alexander Golinski, Lois Garba, Christopher McMullen, Erica Jane Tiedeman, Kayla Curtis and Jessica Zilberberg. I really enjoyed doing research and sharing their opinions and discussion with you all.

I express special gratitude to ULAM Managed Breeding Colony for supplying and donating thousands of mice over the last four years, which enabled me to conduct these experiments. I especially thank, Kelli Rule, Andrew Cave and Sara Grove whose kindness collecting and transferring mice every week for experimental work was much appreciated.

Human blood for this study was usually obtained freshly from donors on experiment days. I would like to thank all of my blood donors for their time over the years of my research. I appreciate every drop of their blood.

I am also especially grateful for acknowledgement to the Royal Thai Government scholarship, which has provided me long term financial support over ten years from high school until now. Without the support of this scholar, I would not have had the great opportunities I have had in my life.

I would like to thank the Thai Student Association at University of Michigan and Thai friends for their precious friendships and support. It would be a long paragraph for me to thank all of them, but I would like to extend thanks in particular to Nattaporn Dhitirojana, Kochapun Dhitirojana, Rattima Sirihorachai, Thitaphat Ngernsutivorakul, Varinee Srimahachota, Nakorn Thurajane, Pattanapon Hangboonsukkul, Wirithphol Ek-Ularnpun, Pornchai Leelasinjaroen, Kamin Manatpon, Art Verapal, Chanisa Niljinda and Watchsun Sookhawatako. They always stood by my side and cheered me on through good and bad times.

Finally, I would like to thank my family, Narongsak Namdee (Dad), Wanna Namdee (Mom), Bancha Namdee (Tuu-elder brother), Nattapon Namdee (Nat Auon-younger brother) and my grandmom (Tee Jaiboon) for always supporting and encouraging me with their best wishes.

TABLE OF CONTENTS

LIST OF FIGURES

LIST OF TABLES

LIST OF ABBREVIATIONS

CAD	Coronary artery disease
ApoE	Apolipoprotein E
VTC	Vascular targeting carrier
VCAM-1	Vascular cell adhesion molecule 1
ICAM-1	Intercellular Adhesion Molecule 1
PSGL-1	P-selectin Glycoprotein Ligand 1
RBC	Red blood cell
WBC	White blood cell
PPFC	Parallel plate flow chamber
EC	Endothelial cell
ESD	Equivalent spherical diameter
sLe^A	sialyl Lewis A
PBS	Phosphate buffered saline
PFA	Paraformaldehyde
SEM	Scanning electron microscopy
ID/g	Injected dose/gram organ
RCC	Right common carotid
RS	Right subclavian
LCC	Left common carotid
LS	Left subclavian
H&E	Hematoxylin and Eosin
AR	Aspect ratio
CFL	Cell free layer

RES	Reticuloendothelial system
EPR	Enhanced permeability and retention
PDMS	Polydimethylsiloxane
HUVEC	Human umbilical vein endothelial cell
IL-1β	Interleukin-1 beta
WSR	Wall shear rate
Q	Volumetric flow rate
h	Channel height
w	Channel width
TLR	Transport-limited adhesion regime
RLR	Reaction-limited regime
Hct	Hematocrit
PS	Polystyrene
PLGA	Poly(lactic-co-glycolic acid)
DCM	Dichloromethane
PVA	Polyvinyl alcohol
PEMA	Poly(ethylene-alt-maleic anhydride)
EDAC	1-Ethyl-3-(3-Dimethylaminopropyl)carbodiimide
MES	2-(N-morpholino)ethanesulfonic acid
HEPES	4-(2-hydroxyethyl)-1-piperazineethanesulfonic acid
ACD	Acetate-citrate-dextrose
WB	Whole blood
BSA	Bovine serum albumin
VB	Viscous buffer
P	1 hr plasma opsonized
VSFC	Vertical-step gasket flow chamber
VDR	Volume to diameter ratio

ABSTRACT

Exploring the Impact of Hemodynamic and Hemorheology in the Design of Carrier for Vascular-Targeted Drug Delivery in Atherosclerosis

by

Katawut Namdee

Chair: Omolola Eniola-Adefeso

Recently, targeting drug carriers (VTCs) have become one of the most distinguished aspects in the field of pharmaceutical engineering. In order to sustain the ability of localized drug release over time, a carrier must survive through the circulatory system, travel to and be retained at a specific site. Therefore, a multitude of strategies have to be considered and implemented to achieve an optimal performing VTC design. Herein, the presented studies aim to elucidate the coupled effect of VTC physical and material properties and the characteristics in prescribing the efficiency of VTCs to localize and bind

to the vascular wall in atherosclerosis via in vitro flow assays and a mouse model atherosclerosis.

In the first study, we explore the impact of VTC shapes on their functionality in targeting atherosclerosis and found that targeted microrods were more effective at adhering to mouse aortas than micro and nanospheres, while nanorodsparticles displayed the same minimal adhesion levels as nanospheres due to poor localization to the vessel wall. We also found that targeted microparticles were retained at high levels in the lungs, likely due to molecular interaction with the pulmonary endothelium.

In the second study, we explore how particle size, along with hemodynamics (blood shear rate and vessel size) and hemorheology (blood hematocrit) affect the adhesion of VTCs in a microfluidic assays. Microspheres also were found to exhibit disproportionately higher vascular wall adhesion than nanospheres in all hemodynamic conditions, due to the higher ability to localize to the wall.

Moreover, we also investigate the role of hemorheology (RBC's dimension) on dictating the binding efficiency of spherical VTCs. Our results suggest that the ratio of RBCs size to the carrier size dictate the particle binding.

Finally, we study the potential role of plasma proteins and material types which affect the adhesion efficiency of VTCs under the blood flow assays. The results show that the plasma proteins in different species have different effects on particle binding, especially porcine, which show strong negative effect on particle adhesion. This study offers the first evaluation of plasma proteins in different animal species to determine how they affect VTCs.

In conclusion, we address the crucial factors of hemodynamics, hemorheology and plasma protein to VTC design. This important for many research fields, particularly for the design of drug delivery and diagnostics in cardiovascular diseases as these parameters can be used to improve carrier performance.

CHAPTER 1

INTRODUCTION

1.1 Background and significance

In recent decades, drug delivery systems have become one of the most distinguished aspects of the field of biomedical and pharmaceutical engineering, especially the targeting of carriers for delivery of therapeutics in human diseases via the vascular system. Drug delivery systems enhance drug effectiveness at the targeted sites with the ability to sustain drug release over time, which increases patients' compliance. In addition, targeted drug carriers also minimize the harmful side effects generally caused by systemic administration of highly potent drugs. Regarding both conceptual and practical benefits, many variants of vascular targeting carriers have been investigated for therapeutics in cancer as well as in pulmonary and cardiovascular diseases [1-4]. One major role that the vascular wall and its endothelial lining play in human physiology is the regulation of inflammation response. The regulated expression of leukocyte adhesion molecules during inflammation and their specificity provides a way for targeting therapeutics to the vascular wall in human cardiovascular diseases. Moreover, in order to sustain the ability of drug release over time, a carrier must survive through the circulation system and travel to a specific site without being filtered by reticuloendothelial system (RES) or coalesce in the vessel network.

Carriers such as polymer particles, liposome, dendrimers, polymersomes and microbubble have been explored for diagnostic and therapeutic approaches [1, 4]. Conjugated antibody and other targeting moieties provide specific targeting to molecules expressed on the surface of the cell to enhance a drug therapeutic effect. In addition, biological parameters including hemodynamics such as shear stress and flow pattern also impact the ability of targeted carriers to reach a specific tissue [5]. However, little attention has been given to understanding the fluid mechanic forces akin to blood flow dynamics (hemodynamics) that would provide a concrete ground of understanding such processes and connections in the pathogenesis of diseases. Therefore, carrier design features, not only their chemistry, avidity, carrier concentration, targeting molecule, but also hemodynamic properties (rheology, shear rate and flow patterns) and physical properties (size and shape) should be considered as key to the design of a delivery system with optimal targeting properties.

1.1.1 Vascular-Targeted Drug Carrier Design

There are several criteria that need to be considered in order to design an effective vascular-targeted drug carrier including targeting property, hemodynamics and physical property.

1.1.2 Targeting Property (targeting molecule on drug carrier)

Endothelial cells represent a significant target for therapeutic invention in numerous acute and chronic diseases; thus, the optimization of targeted delivery of therapeutics to vascular wall represents an important medical goal [1, 3, 4]. However, most of pharmaceutics lack intrinsic affinity to target cells, and exhibit rapid clearance from the blood. These limitations can be surmounted by coupling drug carriers to targeting vectors,

such as antibody or protein, where they will recognize an expressed molecule on the cell surface at the sites of disease.

In cardiovascular disease, leukocytes, triggered by inflammatory signals, accumulate at the lesion site.[6]. During this process, leukocytes, mainly monocytes and neutrophils, roll and adhere on the vascular wall via surface expressed ligands, e.g. P-selectin Glycoprotein Ligand 1 (PSGL-1), which interact with endothelial-expressed selectins for initial capture and rolling action and Intercellular Adhesion Molecules (ICAM), which leads to firm adhesion on the endothelium wall. According to their specific and regulated expression, the selectin and other endothelial-expressed leukocyte adhesion molecules are suitable for targeted delivery of therapeutics to the vascular wall. Drug carriers can be designed to mimic leukocyte adhesion by conjugating neutrophil adhesion ligands or antibodies binding to endothelial expressed molecules to the surface of drug-loaded carriers [7-9].

According to previous studies, the multiple-receptor targeting, both selectin and ICAM, has higher efficiency than the single targeting receptor alone. This confirmed the similarity in adhesion cascade of polymeric particle and leukocyte to endothelial cell [8, 9]. One appropriate set of ligands for conjugation on polymeric particles interacting with the multiple-receptor on endothelial cell are Sialyl-Lewis$^{A \text{ or } X}$ ($sLe^{A/X}$) and anti-ICAM-1 [10, 11]. $sLe^{A/X}$, a sialylated fucosylated carbohydrate naturally found on PSGL-1, is selected due to its fast on-rate and off-rate characteristic, whereas anti-ICAM-1, which has a low on-rate and off-rate, can bind to ICAM-1 with strong binding and cause firm adhesion.

1.1.3 Hemodynamics Property

Blood flow dynamics

In order to enhance the efficiency of the drug carrier to the targeted site, carriers must be able to survive in blood circulation and migrate through the blood cell core layer to the vascular wall. Hemodynamics, the movement of blood cells in the circulatory system, is enforced by flow dynamics that can be changed by the characteristic of blood vessel [12-14]. Physiological blood flow in most vessels has an unsteady flow pattern depending on the size and location of the vessel. The cyclic heart pump also creates a pulsatile condition in most arteries[15]. At the curve and bifurcation vessel, the secondary flows can be generated in recirculating flow or vortex pattern which might enhance local shear stress to the luminal endothelial cell and induce adhesion of active platelets and WBCs causing thrombosis and atherosclerotic plaques, respectively[15-17]. Much research show that flow pattern and flow velocity play an importance role in the initiation and enhancement of the adhesion of platelets to the vascular wall [18, 19]. They found that the platelet adhesion is larger in steady flow than in pulsatile flow, and high share stress also can increase platelet adhesion[18]. Therefore, this behavior could be manipulated to optimize the binding efficiency of a drug carrier in blood flow as well, particularly, at the atherosclerotic plaque area.

Notably, to date, only few investigators have explored this relationship between blood flow dynamics and the adhesion of a vascular-targeted drug carrier that could provide a useful application in imaging or therapeutics of cardiovascular disease.

Cell-free layer in blood vessels

The cell free layer near the vascular wall occurs due to the tendency of RBC aggregation to migrate away from the vessel wall by cell-cell interaction, deformability and asymmetric shapes of RBC [20]. The formation of RBC core layer in a flow stream is influenced by several factors: extrinsic factors, including component of suspending media (e.g. plasma, buffer), hydrodynamic forces and dimension of flow system; intrinsic factors, including component of cell types (RBC, WBC and platelet), size and shape of RBC (species or age); and hematocrit [21]. Recently, the formation of the cell-free layer in the microcirculation has gained interest due to it contributions to the rheological properties of blood in arterioles and venules [22] and distribution of red blood cells in the capillary network [23].

The width of the cell free layer is mainly dependent on the vessel diameter. According to Kim and colleagues [24], it was found that the cell-free layer in rat arterioles increased slightly in the vessel range of 10-20 μm. diameter, but gradually decreased as the diameter increased in the 20-50 μm range. While Yamaguchi et al. [25] found that the cell-free layer formation in cat brain microvessels (arterioles and venules) doesn't depend on vessel diameter in the range of 30-86 μm diameter. Other factors that need to be considered are the relationship between mean flow velocity and RBC aggregation. Without the RBC aggregation condition, the width of the cell-free layer increase with flow rate due to enhanced axial migration of RBC high shear rate. However, RBC aggregation is the main factor that impacts the layer formation at low shear rate [24].

Hematocrit, one of the most important rheological factors that influence flow resistance in microcirculation, also majorly effects the formation of the cell-free layer due

to the volume fraction occupied by the RBC core layer in the vessel. The RBC core layer width is inversely related to the cell-free layer. In addition, the interactive force between RBC will be altered with increased hematocrit counteracting axial migration of RBC, which decreases the cell free layer width and its variation [26].

Although the formation of this layer in vitro and in vivo has been of interest for many years, little information on the cell-free layer in terms of carrier delivery and cell adhesion in the microcirculation has been available due to the limitation of measurement techniques and the complexity of mimicking physiological microcirculation conditions.

Red blood cell size

Beside hematocrit, one of the main factors enhancing platelet adhesion to the vessel wall is the RBCs size [27, 28]. Due to the potential role of RBCs size in enhancing platelet adhesion, the slightly different animal species with various size of RBCs in various animal species [29] may have an impact on the adhesion of a vascular-targeted drug carrier as well. Nowadays, only few studies have investigated the differences between animal and human blood rheology that could affect on the margination of blood cells and also a vascular targeted carrier. Grabowki *et al.* claimed that the significant differences in platelet adhesion were observed in several mammalian species which could be due to the variation in size of RBC in these different species [28]. This could be explained by the presence of a "skimming layer" or "cell free layer". In blood flow, the RBCs mainly occupy in the center of the flow, which results in the cell free layer of platelet rich plasma at the vessel wall. If the RBCs are large, platelets simply migrate into the cell free layer region by RBCs-platelets interaction resulting in an increase in platelet concentration and an increase in platelet adhesion as well. On the other hand, the small RBCs are expected to be more

equally mixed with the platelets and no RBCs induced platelet transport mechanism occurs, which cannot increase platelet adhesion.

Existing studies in the literature focus only on RBC size with platelet adhesion. However, it is still not clear how different RBC size along with other blood cell components can affect to the binding efficacy of a vascular-targeted drug carrier in different size and material types.

1.1.4 Physical Property

Geometrics of Drug Carrier

For the general vascular targeting system in atherosclerosis, the carriers are transported by blood flow and interact by specifically binding (ligand-receptor) and non-specifically binding (electrostatic and steric interactions) to the vessel walls, seeking the diseased lesion [5] as the final objective. The intravascular delivery of a carrier can be divided into three steps: margination, adhesion and cell internalization [30]. The role of the physical properties of particle (size and shape) is important in each of these steps.

In general, leukocyte and platelet margination (localization and adhesion) to the vascular wall require interaction with red blood cells in blood flow. Thus, a high marginating drug carrier is one designed to move preferentially in close proximity to the blood vessel walls by process of escaping the red cell core and efficient lateral drifting of the particle to the wall once in the cell-free layer [31]. Whereas red blood cells have the opposite behavior to margination by accumulating preferentially within the core of the vessel, staying larger in macro-circulation, which is described as *plasma skimming effect* and the formation of a *cell free layer* [32]. Therefore, in order to be efficient drug carriers,

they would break through the RBCs core layer to accumulate in the cell free layer where an almost laminar flow is observed [33]. According to Goldmann *et al.,* the motion of spherical particles in linear laminar flow does not show lateral drift unless applying an external force, such as gravitational or magnetic [34], while non-spherical particles show more complex motion with tumbling and rolling which can be broken to control their margination without any lateral external forces. The longitudinal, lateral forces and torque by blood flow depend on the size, shape, orientation of the particle to the stream direction and changes over time during transportation [35, 36]. Based on the previous study, it has been shown that the lateral drifting velocity is related to the carrier's aspect ratio; the rod particle can be rotated and translated downstream drifting laterally from one side to the other side of the capillary, which tends to marginate more than spherical particles [35].

Adhesion to the vascular walls is dependent upon the balance of ligand-receptor interaction, which is the density of ligand molecule over the particle surface; and receptor molecules expressed at the cell membrane; and detaching forces such the shear stress at the blood vessel walls. Moreover, size and shape also have an influence on carrier adhesion: for submicron particles, the hydrodynamic force is small but the area of interaction at the particle/cell interface is smaller, leading to small number of ligand-receptor bonds available for capture that can withstand detachment forces. For the large particles, the number of ligand-receptor bonds that can be formed grows but hydrodynamic force also grows even more [37]. Chareonphol *et al.* [38] elucidated the potential role of hemodynamics and size in prescribing the binding efficiency of vascular-targeted spherical carriers in flow via parallel plate flow assays. Specifically, spherical particles with diameters ranging from 200 nm up to 5 μm conjugated with sialyl Lewis (sLe^A) were

evaluated for their ability to effectively bind activated endothelial cells (aECs) from blood flow. It was found that spherical particles with 2-5 μm range display significantly better margination to the wall at intermediate high shear rate and channel height than the sub-micron sized sphere.

However, the most recent studies about the margination and adhesion of carrier have been observed with assays in the absence of blood cells particularly RBC and WBC. Likewise very few studies have been observed in animal model and micro-vascular systems.

Plasma protein corona

For administered drug delivery system, prolonging blood circulation time with low blood clearance rate is advantageous. However, it is known that biomaterial properties effect their protein corona formation, which is recognized by macrophages and rapidly clearance in the reticuloendothelial system (RES). In biological fluids (plasma or otherwise), a range of protein can associate with vascular drug carriers, which forms a "protein corona" around the particle that defines the biological character of the particle. The protein corona formation depends on the physicochemical properties of a targeted drug carrier and biomaterial such as size, charge, material type, curvature and targeting moieties on their surfaces [39-41].

Some studies have found that for copolymer, gold, or other metal nanoparticles with various diameters, the amount of absorbed protein on surface varied with size and surface curvature, and the qualitative changes of protein also depend on the size of the particles in the obtained corona protein[39, 42, 43]. The potential explanation is a larger ratio of surface to volume which allows more protein to bind to smaller particles than to particles of larger sizes, and total surface area differences [39, 42]. Moreover, some investigators also pointed

out that nanoparticles with different material and different sizes are associated with different corona proteins [44].

A few studies have shown that corona protein interferes with the ligand-receptor interaction on particles [45-47]. Sobcyznski *et al.* [42] show that the negative plasma protein effect on adhesion of PLGA particle is dependent on targeting ligand density along with specific blood donors under physiological blood flow. Additionally, some studies also claim that PEGylation of nanoparticle reduce the plasma protein corona allowing the particles to avoid clearance in the RES and prolong circulation time [48, 49].

We have not yet explored how the plasma protein in different animal species affects protein corona formation on various material surfaces and also affects on VTCs adhesion under blood flow condition.

1.2 Organization of the dissertation

This dissertation thesis consists of 6 chapters.

Chapter 1 introduces background and significance, literature review and the scope of my experiment works.

Chapter 2 evaluates the role of size and shape in the capacity for a vascular-targeted carrier system to bind inflamed endothelial cells over plaque using ApoE -/- mice with developed atherosclerosis. Specifically, we investigated the adhesion levels along mouse aortas of ellipsoidal and spherical polystyrene particles targeted to the inflammatory molecules E-selectin and VCAM-1. Additionally, we also studied the biodistribution of targeted and untargeted particles in various range of size and shape, particularly, in major organs. For all studies, particles were injected via tail-vein and a 30-min circulation time.

Chapter 3 investigates the role of particle size, along with hemodynamics (blood shear rate and vessel size) and hemorheology (blood hematocrit) on the capacity of spheres particle to marginate to inflamed endothelium in a microfluidic model of human microvessels. In more detail, we use microfluidic chambers that comprise of flow channels with dimensions on the order of human arteriole and venule diameters with an endothelial wall to evaluate the margination of spherical model VTCs from blood flow in the human microcirculation. Specially, 200 nm, 500 nm, 2 μm and 5 μm polystyrene spheres with their surfaces conjugated with sialyl lewis A (sLe^A), a ligand specific to E-selectin expressed by inflamed endothelial cells (ECs). The efficiencies of particles were evaluated for their ability to localize and bind to activated ECs from human blood flow in microfluidic channels of 28 and 43 μm heights, allowing us to understand the behavior of particle under micro-circulation.

Chapter 4 investigates the role of hemorheology (RBC dimension) of various animal models and human on dictating the binding efficiency of spherical VTCs at the wall in physiological blood flows. Specifically, the adhesion of sLe^A-coated particles, 0.2, 0.5, 2 and 5 μm, to inflamed endothelial cells monolayers were conducted via a parallel plate flow chamber assay (PPFC). Particle binding was observed in RBCs-in-buffer (washed RBCs suspended in saline at 40%Hct) and whole blood from different animals species and human: rabbit, pig and mouse. The flow assays were studied under simple laminar and disturbed blood flow (i.e. pulsatile and recirculating flow).

Chapter 5 investigates the potential role of different animal plasma proteins and material types in dictating the adhesion efficiency of both micro and nano sphere to the vascular wall model from blood flow via in vitro assays. Specifically, PS, PLGA, silica and titanium particles were used as vascular-targeted carriers (VTCs) model in this study. We characterize the adhesion of sLe^A conjugated particles to inflamed endothelial cells in laminar blood flow via a parallel plate chamber (PPFC) from different animal species (mouse, rabbit, porcine and human). The experiments were conduct in various blood suspensions (saline buffer, viscous buffer, plasma) compared to whole blood. The result from this chapter would raise awareness of the possible difference in result from animal to represent human.

Chapter 6 draws the conclusion and summary the important result from this dissertation to the field of study, and also proposes the new topics for future research.

References

1. Bendas, G., et al., Selectins as new targets for immunoliposome-mediated drug delivery:: A potential way of anti-inflammatory therapy. Pharmaceutica Acta Helvetiae, 1998. 73(1): p. 19-26.

2. Muro, S., et al., Endothelial targeting of high-affinity multivalent polymer nanocarriers directed to intercellular adhesion molecule 1. Journal of Pharmacology and Experimental Therapeutics, 2006. 317(3): p. 1161.

3. Sakhalkar, H.S., et al., Leukocyte-inspired biodegradable particles that selectively and avidly adhere to inflamed endothelium in vitro and in vivo. Proceedings of the National Academy of Sciences, 2003. 100(26): p. 15895.

4. Schnitzer, J.E., Vascular targeting as a strategy for cancer therapy. New England Journal of Medicine, 1998. 339(7): p. 472-474.

5. Decuzzi, P., et al., A theoretical model for the margination of particles within blood vessels. Annals of biomedical engineering, 2005. 33(2): p. 179-190.

6. Kaneider, N.C., A.J. Leger, and A. Kuliopulos, Therapeutic targeting of molecules involved in leukocyte–endothelial cell interactions. FEBS Journal, 2006. 273(19): p. 4416-4424.

7. Eniola, A.O., S.D. Rodgers, and D.A. Hammer, Characterization of biodegradable drug delivery vehicles with the adhesive properties of leukocytes. Biomaterials, 2002. 23(10): p. 2167-2177.

8. Eniola, A.O., P.J. Willcox, and D.A. Hammer, Interplay between rolling and firm adhesion elucidated with a cell-free system engineered with two distinct receptor-ligand pairs. Biophysical journal, 2003. 85(4): p. 2720-2731.

9. Omolola Eniola, A. and D.A. Hammer, In vitro characterization of leukocyte mimetic for targeting therapeutics to the endothelium using two receptors. Biomaterials, 2005. 26(34): p. 7136-7144.

10. Handa, K., et al., Selectin GMP-140 (CD62; PADGEM) binds to sialosyl-Lea and sialosyl-Lex, and sulfated glycans modulate this binding. Biochemical and biophysical research communications, 1991. 181(3): p. 1223-1230.

11. Rodgers, S.D., R.T. Camphausen, and D.A. Hammer, Sialyl LewisX-Mediated, PSGL-1-Independent RollingAdhesion on P-selectin. Biophysical journal, 2000. 79(2): p. 694-706.

12. Pries, A.R., et al., Blood flow in microvascular networks. Experiments and simulation. Circulation research, 1990. 67(4): p. 826-834.

13. Munn, L.L., R.J. Melder, and R.K. Jain, Role of erythrocytes in leukocyte-endothelial interactions: mathematical model and experimental validation. Biophysical journal, 1996. 71(1): p. 466-478.

14. Turitto, V.T. and H.R. Baumgartner, Platelet interaction with subendothelium in a perfusion system: physical role of red blood cells. Microvascular research, 1975. 9(3): p. 335-344.

15. Ku, D.N., Blood flow in arteries. Annual Review of Fluid Mechanics, 1997. 29(1): p. 399-434.

16. Baumgartner, H.R., The role of blood flow in platelet adhesion, fibrin deposition, and formation of mural thrombi. Microvascular research, 1973. 5(2): p. 167-179.

17. Tricot, O., et al., Relation between endothelial cell apoptosis and blood flow direction in human atherosclerotic plaques. Circulation, 2000. 101(21): p. 2450-2453.

18. Sakariassen, K., P. Bolhuis, and J. Sixma, Platelet adherence to subendothelium of human arteries in pulsatile and steady flow. Thrombosis research, 1980. 19(4): p. 547-559.

19. Lowe, G.D., Virchow's triad revisited: abnormal flow. Pathophysiology of haemostasis and thrombosis, 2005. 33(5-6): p. 455-457.

20. Bishop, J.J., et al., Erythrocyte margination and sedimentation in skeletal muscle venules. American Journal of Physiology-Heart and Circulatory Physiology, 2001. 281(2): p. H951.

21. Kim, S., et al., The cell-free layer in microvascular blood flow. Biorheology, 2009. 46(3): p. 181-189.

22. Bishop, J.J., et al., Effects of erythrocyte aggregation and venous network geometry on red blood cell axial migration. American Journal of Physiology-Heart and Circulatory Physiology, 2001. 281(2): p. H939.

23. Barber, J.O., et al., Simulated two-dimensional red blood cell motion, deformation, and partitioning in microvessel bifurcations. Annals of biomedical engineering, 2008. 36(10): p. 1690-1698.

24. Kim, S., et al., Temporal and spatial variations of cell-free layer width in arterioles. American Journal of Physiology-Heart and Circulatory Physiology, 2007. 293(3): p. H1526.

25. Yamaguchi, S., T. Yamakawa, and H. Niimi, Cell-free plasma layer in cerebral microvessels. Biorheology, 1992. 29(2-3): p. 251.

26. Pries, A., et al., Resistance to blood flow in microvessels in vivo. Circulation research, 1994. 75(5): p. 904-915.

27. Aarts, P., et al., Red blood cell size is important for adherence of blood platelets to artery subendothelium. Blood, 1983. 62(1): p. 214-217.

28. Grabowski, E., et al., Platelet adhesion to foreign surfaces under controlled conditions of whole blood flow: human vs rabbit, dog, calf, sheep, pig, macaque, and baboon. ASAIO Journal, 1977. 23(1): p. 141-149.

29. Gregory, T.R., Animal genome size database, 2001, TR Gregory.

30. Decuzzi, P., et al., Intravascular delivery of particulate systems: does geometry really matter? Pharmaceutical research, 2009. 26(1): p. 235-243.

31. Goldsmith, H.L. and S. Spain, Margination of leukocytes in blood flow through small tubes. Microvascular research, 1984. 27(2): p. 204-222.

32. Fåhræus, R. and T. Lindqvist, The viscosity of the blood in narrow capillary tubes. American Journal of Physiology--Legacy Content, 1931. 96(3): p. 562.

33. Sharan, M. and A.S. Popel, A two-phase model for flow of blood in narrow tubes with increased effective viscosity near the wall. Biorheology, 2001. 38(6): p. 415-428.

34. Goldman, A., R. Cox, and H. Brenner, Slow viscous motion of a sphere parallel to a plane wall--II Couette flow. Chemical Engineering Science, 1967. 22(4): p. 653-660.

35. Gavze, E. and M. Shapiro, Motion of inertial spheroidal particles in a shear flow near a solid wall with special application to aerosol transport in microgravity. Journal of Fluid Mechanics, 1998. 371(1): p. 59-79.

36. Gentile, F., et al., The effect of shape on the margination dynamics of non-neutrally buoyant particles in two-dimensional shear flows. Journal of biomechanics, 2008. 41(10): p. 2312-2318.

37. Decuzzi, P. and M. Ferrari, The adhesive strength of non-spherical particles mediated by specific interactions. Biomaterials, 2006. 27(30): p. 5307-5314.

38. Charoenphol, P., R.B. Huang, and O. Eniola-Adefeso, Potential role of size and hemodynamics in the efficacy of vascular-targeted spherical drug carriers. Biomaterials, 2010. 31(6): p. 1392-1402.

39. Lundqvist, M., et al., Nanoparticle size and surface properties determine the protein corona with possible implications for biological impacts. Proceedings of the National Academy of Sciences, 2008. 105(38): p. 14265-14270.

40. Tenzer, S., et al., Nanoparticle size is a critical physicochemical determinant of the human blood plasma corona: a comprehensive quantitative proteomic analysis. ACS nano, 2011. 5(9): p. 7155-7167.

41. Nel, A.E., et al., Understanding biophysicochemical interactions at the nano–bio interface. Nature materials, 2009. 8(7): p. 543-557.

42. Sobczynski, D.J., et al., Plasma Protein Corona Modulates the Vascular Wall Interaction of Drug Carriers in a Material and Donor Specific Manner. PloS one, 2014. 9(9): p. e107408.

43. Deng, Z.J., et al., Differential plasma protein binding to metal oxide nanoparticles. Nanotechnology, 2009. 20(45): p. 455101.

44. Cedervall, T., et al., Understanding the nanoparticle–protein corona using methods to quantify exchange rates and affinities of proteins for nanoparticles. Proceedings of the National Academy of Sciences, 2007. 104(7): p. 2050.

45. Mirshafiee, V., et al., Protein corona significantly reduces active targeting yield. Chemical Communications, 2013. 49(25): p. 2557-2559.

46. Salvati, A., et al., Transferrin-functionalized nanoparticles lose their targeting capabilities when a biomolecule corona adsorbs on the surface. Nature nanotechnology, 2013. 8(2): p. 137-143.

47. Fleischer, C.C., U. Kumar, and C.K. Payne, Cellular binding of anionic nanoparticles is inhibited by serum proteins independent of nanoparticle composition. Biomaterials science, 2013. 1(9): p. 975-982.

48. Alexis, F., et al., Factors affecting the clearance and biodistribution of polymeric nanoparticles. Molecular pharmaceutics, 2008. 5(4): p. 505-515.

49. Lim, J., et al., The role of the size and number of polyethylene glycol chains in the biodistribution and tumor localization of triazine dendrimers. Molecular pharmaceutics, 2008. 5(4): p. 540-547.

CHAPTER 2

IN VIVO EVALUATION OF VASCULAR-TARGETED MICROPARTICLE DRUG CARRIER IN ATHEROSCLEROSIS

Abstract

Vascular-targeting remains a promising strategy for improving the diagnosis and treatment of coronary artery disease (CAD) by providing localized delivery of imaging and therapeutic agents to atherosclerotic lesions. In this work we evaluate how size and shape affects the capacity for a vascular-targeted carrier system to bind inflamed endothelial cells over plaque using ApoE -/- mice with developed atherosclerosis. We investigated the adhesion levels along mouse aortas of ellipsoidal and spherical particles targeted to the inflammatory molecules E-selectin and VCAM-1, as well as the biodistribution of targeted and untargeted particles in major organs following injection via tail-vein and a 30-min circulation time. We found that targeted ellipsoidal microparticles adhered to mouse aortas at higher levels than microspheres of similar volume, particularly at segments that contained atherosclerotic plaques. Moreover, both ellipsoidal and spherical nanoparticles displayed the same minimal adhesion levels compared to both types of microparticles evaluated, likely due to poor localization of nanoparticles to the vessel wall in blood flow. We found that microparticles targeted to plaque-associated inflammation were retained at higher levels in the lungs than untargeted particles, largely due to molecular interaction

with the pulmonary endothelium. The level of the mechanical entrapment of ellipsoidal microparticles in the lungs was also not significantly different from that of microspheres of the same volume despite a ~3-fold higher major axis length for the ellipsoids. Therefore, particle shape and size should be considered in the design of carrier systems to target atherosclerosis, as these parameters can be tuned to improve carrier performance.

---

*Content of this have been published as Namdee K, Thompson AJ, Golinski A, Mocherla S, Bouis D and Eniola-Adefeso O. *In vivo* evaluation of vascular-targeted spheroidal microparticles for imaging and drug delivery application in atherosclerosis. Atherosclerosis. 2014; 237(1): 279-286.
* This work is collaborated with Dr. Alex J Thompson as equal contribution.

2.1 Introduction

Vascular targeting remains a promising avenue for localized delivery of imaging and/or therapeutic agents to the diseased vasculature in coronary artery disease (CAD), the consistent leading cause of mortality in the western world [1, 2]. Vascular-targeted carriers (VTCs) are of particular interest for the treatment of CAD because specific vascular wall endothelial cell receptors associated with acute and chronic inflammation (selectin, ICAM-1, VCAM-1) play a major role in the pathology of this disease. Naturally, these receptors then also provide a convenient and accessible platform for vascular targeting. Current vascular-targeting strategies in CAD typically involve coating injectable carriers with targeting moieties, e.g. antibodies or peptides, for specific interaction with the relevant endothelial expressed receptors, providing these carriers the ability to navigate the vasculature, adhere, and persist locally in the diseased tissue [3]. Overall, the ability to provide highly localized delivery to atherosclerotic pre-lesions or fully formed plaques in CAD can offer new therapeutic avenues for early diagnosis and treatment of this disease [4].

Many variants of VTCs have been investigated for use as a diagnostic or therapeutic, such as polymer particles, liposomes, dendrimers, and polymersomes; which are typically spherical with nanoscale diameters [5]. However, particle shape and size have recently been presented as tunable parameters for enhancing the vascular wall interaction of VTCs at a targeted site in the presence of blood flow [6-8]. Specifically, numerous mathematical and some simple flow experimental models show that ellipsoidal particles can display greater deposition/adhesion compared to spherical particles of the same volume

[9-12]. Our recent *in vitro* study also shows that under physiological levels of shear, prolate ellipsoidal (rod-like) particles targeted to inflammation display higher levels of adhesion compared to spheres in the presence of human red blood cells (RBCs) in parallel plate flow chamber (PPFC) assays, provided that the equivalent spherical diameter of the rods is ≥ 1 μm [13]. To our knowledge, no *in vivo* study has been performed to compare adhesion of spherical and ellipsoidal polymer VTCs within the context of targeting atherosclerotic plaques in CAD. The areas of the vasculature vulnerable to atherosclerosis tend to be large vessels (on the order of centimeters), which make the successful localization of VTCs to the vascular wall increasingly important in determining their overall performance. Further, these atheroprone areas tend to exhibit pulsatile and disturbed blood flow profiles which are very different in terms of hemodynamics compared to the microvasculature, where much of the previous vascular targeting research has been focused [14]. In this study, we evaluate the role that the size and shape of particles has on their capacity to effectively reach and bind to inflamed aorta using a mouse model of atherosclerosis. Specifically, we investigated the adhesion levels of dual, E-selectin and VCAM-1,-targeted prolate ellipsoidal and spherical particles along sections of the aorta from the aortic root to the iliac branches, and the effect of the targeting ligands on the biodistribution of spherical and ellipsoidal particles in major organs. E-selectin and VCAM-1 are proteins known to be overexpressed by endothelium in atherosclerosis [15-17]. A dual targeting of both E-selectin and VCAM-1 is employed based on previous publications that suggest *in vivo* selectivity to ECs over plaque in ApoE-/- mice is greatest when both VCAM-1 and selectin were targeted.[18, 19] We found that targeted rod-shaped microparticles adhered to mouse aortae at overall higher levels than spherical microparticles, particularly at segments of the

aorta that contained developed or developing plaques. There was no difference in the adhesion of rod-shaped and spherical nanoparticles, which was minimal compared to the adhesion of microparticles.

2.2 Methods

2.2.1 Preparation of vascular-targeted particles

Fluoresbrite® YG carboxylate polystyrene spheres were purchased from Polysciences, Inc (Warrington, PA). Prolate ellipsoidal (rod-shaped) particles were prepared using a previously described polymer film stretching method [13]. Spheres and rods with the same equivalent spherical diameter (ESD), and thus volume, were used in this study (500 nm or 2 μm ESD). Unless otherwise stated, 2 μm ESD rods have aspect ratio (AR) = 4 and 500 nm ESD rods have AR = 6. The dimensions of the particles used to test the effect of AR on particle adhesion are shown in Supplemental Table 1. Rods and spheres were conjugated with Neutravidin® Biotin-Binding Protein (Thermo Scientific), which is used a platform to conjugate biotinylated targeting ligands as previously described [3]. In this study, a multiple ligand system was used to target vascular inflammation. The two targeting ligands used were biotinylated sialyl Lewis A (sLe^A) for binding to E-selectin and biotinylated rat anti-mouse CD106 (aVCAM-1) for binding to VCAM-1. On the day of injection, VTCs were coated with a combination of sialyl Lewis a (Glycotech; Gaithersburg, MD) and aVCAM-1 (BD Pharmingen). Unless otherwise stated, VTCs were saturated at a ratio of 30% sLe^A and 70% aVCAM-1, as this ratio was previously determined to be advantageous for adhesion to inflammation [20]. Particles used in the

untargeted control study were prepared in the same way, except their surfaces remained carboxylated.

2.2.2 Murine model and *in vivo* assay

The procedures of animal experiment were approved by Unit for Laboratory Animal Medicine, The University of Michigan. Twenty-five homozygous ApoE-/- mice and twenty-five wild type at 8-10 weeks old were purchased from Jackson Laboratories (Bar Harbor, ME). Mice were fed a normal diet for 20 weeks. Mice with an average weight of 28 grams were randomly assigned into five groups of five animals, and VTCs were injected via tail vein at a dosage of 20 x 10^6 particles in 200 µl of in phosphate buffered saline (PBS) /mouse. 30 min after injection, mice were anaesthetized with 100 µl of a mixture of 35% ketamine and 5% xylazine in PBS. Additional anesthesia was administered as necessary. Blood was drawn via cardiac puncture from the left ventricle using heparin-coated syringe. Following blood draws, the right atrium was nicked and the vasculature was perfused with ice-cold PBS by injection into the puncture site at the apex of the left ventricle. The lung, liver, spleen, and kidney were harvested and snap-frozen in liquid nitrogen. Consequently, the heart and aorta were perfused again with ice-cold 4% paraformaldehyde (PFA) in PBS at pH 7.5. Whole mice were preserved in 4% PFA until aorta isolation. The aorta were excised from the aortic arch to the iliac branches, including the renal branches and celiac branch, and kept in 4% PFA in PBS. For each heart, the apex was removed in order to increase the penetration of solution into tissue, and placed in ice-cold 4% PFA in PBS for 3 hours. The heart was washed 3 times for 15 minutes with PBS before being soaked overnight with 30% sucrose. The heart was embedded in O.C.T. embedding medium and snap-frozen before cross-sections of the aortic root were collected.

2.2.3 Quantification of particle adhesion *in vivo*

After the fixation process, the aorta was cleaned of fascia and fat deposits adjacent to the vessel before it was excised into segments along the full length including aortic arches, abdominal branches and iliac branches (1000 μm -1500 μm in length/segment). Each segment was tracked by number and position. Aortic segments were bisected and mounted open *en face* on glass slides by 4% PFA, and coverslips were sealed using nail polish agent. The aorta slides were imaged using a Nikon TE 2000-S Inverted Microscope and an attached Photometric CoolSNAP EZ digital camera with a Sony CCD sensor. The *en face* images were quantified using Metamorph® software by counting number of adherent particles on both endothelial area and plaque area. The microparticles were quantified using a 20 X objective while the nanoparticles were quantified with a 40 or 60 X objective. For each group of mice, we averaged the number of adherent particles along the entire aorta. Standard error bars are plotted and statistical significance in the data was determined by one-way ANOVA with Tukey post-test (a value of $p < 0.05$ was considered statistically significant). To account for variation in plaque density and inflammation levels across different mice, particle adhesion was normalized to the adhesion of 500 nm diameter spherical particles. Particle adhesion in the aortic root was imaged by removal of the apex of the heart and sectioning into approximately 130 cross-sections of 6 μm each prepared from the base of the aortic root to the ends of the aortic valve leaflets using cryostat at −20°C. The sectioned tissues were mounted on gelatin-coated microscope slides. The slides were allowed to dry at room temperature for 30 min. Images were then captured by fluorescence microscopy to qualify particles adhesion on aortic root.

Subsequently, the slides were stained with hematoxylin and eosin, and mounted with permount. Mounted tissues were then reimaged by light microscopy.

2.2.4 Scanning electron microscopy (SEM)

Aortic root samples were also prepared by a freeze dry process for SEM imaging. The samples were immersed in liquid nitrogen and placed in a vacuumed desiccator for 2 hr. Then, the samples were sputter coated with gold and imaged using a Philips XL30FEG SEM (EMAL, University of Michigan) at 4000x and 8000x magnification.

2.2.5 Quantification of biodistribution in organs

Harvested and snap-frozen organs (lung, liver, spleen and kidney) were stored at -80C° until ready to analyze for particle accumulation. Organs were thawed and multiple samples from each organ were weighed and homogenized in 1 ml of PBS+/+. The concentration of particles in each homogenized solution was quantified using a hemocytometer under a fluorescence microscope. For the lungs and liver, only a part of the organ was harvested and analyzed for particle accumulation. The same area of these organs was used in all animals. For the lungs, a portion of left lobe with an average sample weight 37 ± 3.5 (S.E.) or 163 ± 6.7 mg was used for assays with ApoE-/- or wild type mice, respectively. For the liver, a portion of the left lobe weighing 110 ± 3.9 (S.E.) or 320 ± 7.5 mg was used. The whole organs were used for analysis of particle accumulation in the spleen and kidney. Particle accumulation was calculated as % injected dose/gram organ (% ID/g), and each data point represented an average of at least 5 samples. Standard error bars are plotted and statistical significance in the data was determined by one-way ANOVA with Tukey post-test (a value of $p < 0.05$ was considered statistically significant).

2.3 Results

2.3.1 Binding efficiency along the aorta

Adhesion of spherical and prolate ellipsoidal (rod-shaped) vascular-targeted particles (VTPs) was quantified along the aortic tree of ApoE -/- mice following intravenous injection via the tail vein and a 30-minute subsequent circulation time. Particles had equivalent spherical diameters (ESD) of either 500 nm or 2 μm with aspect ratios of either 1 (spheres), 6 (500 nm rods) or 4 (2 μm rods). Figure 1 shows representative fluorescent and H&E images of sections of the aortic root for mice injected with dual-targeted spheres and rods with either 2 μm or 500 nm ESD. As shown in these images, VTPs are successfully bound to the aorta after a tail-vein injection. Figure 2-2A shows the average cumulative particle adhesion along the entire length of the aortic tree normalized to the adhesion of 500 nm spheres, from the ascending aorta to the iliac branching points. Particles with 2 μm ESD displayed significantly higher adhesion densities, at least 4 fold, compared to particles with 500 nm ESD. When adhesion data is normalized to the particle volume (relevant for drug loading), the cumulative volume delivered by adherent microparticles is ~500-1500 fold higher than the volume of adherent nanoparticles depending on particle shape (Supplemental Figure 2-1). Sample images of fluorescent microparticles bound to the aorta are shown in Supplemental Figure 2-2. Nanorods displayed no increased adhesion compared to their equivalent 500 nm diameter spheres. Control experiments with targeted 2 μm spheres injected into wild type mice or 2 μm IgG-coated particles (spheres or aspect ratio 4 rods) injected into ApoE-/- mice show minimal accumulation in the aorta (Figure 2-2B), suggesting that the high adhesion of targeted

microparticles observed in the aorta in ApoE-/- mice are due to the expression of the targeted inflammatory molecules by the endothelium.

It is established that atheroprone areas of the aorta are typically near vessel bifurcations or curvature, whereas the blood flow profiles along straight sections of the aorta tend to be atheroprotective. Therefore, we also quantified the adhesion density of targeted particles along different sections of the aorta from the ascending aorta to the iliac branches. At each section investigated, the adhesion density of 2 μm ESD rods was greater than or equal to the adhesion of equivalent spheres (Figure 2-2C). Interestingly, the adhesion density of targeted microrods relative to microspheres and nanoparticles was greatest around the combined area of the brachiocephalic, right common carotid (RCC), and right subclavian (RS) branching points nearby the aortic arch, followed by the thoracic aorta and to a smaller extent the descending aorta. Visual inspection revealed developing/developed plaques near many of the branched and curved regions of the vasculature (Supplemental Figure 2-3). Qualitatively, adhesion of targeted particles was higher on or near these regions of plaque formation. As shown in Figure 2-3, a representative Hoecsht (nucleus) and wheat germ agglutinin (plasma membrane) staining of a segment of the aorta with visible plaque, more microparticles were bound around the periphery of the developing plaque than on the top. Overall, adhesion was minimal for nanoparticles throughout the aorta compared to microparticles, even in areas where very high levels of inflammation are expected.

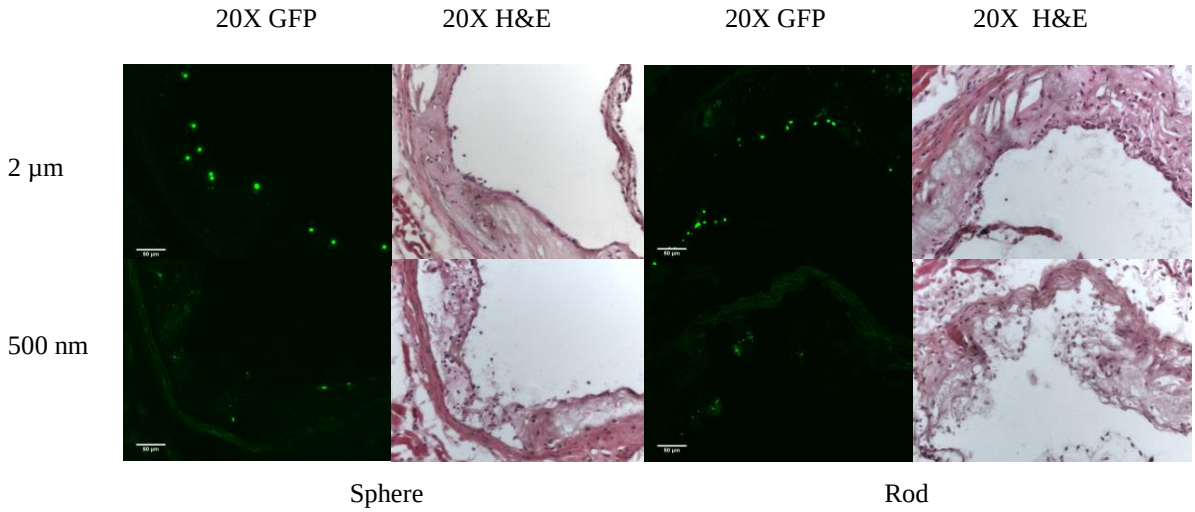

Figure 2-1 Fluorescent and H&E stain images of aortic roots adhesion of micro/nanoparticles of different size/shape on atherosclerotic plaque at 20X magnification.

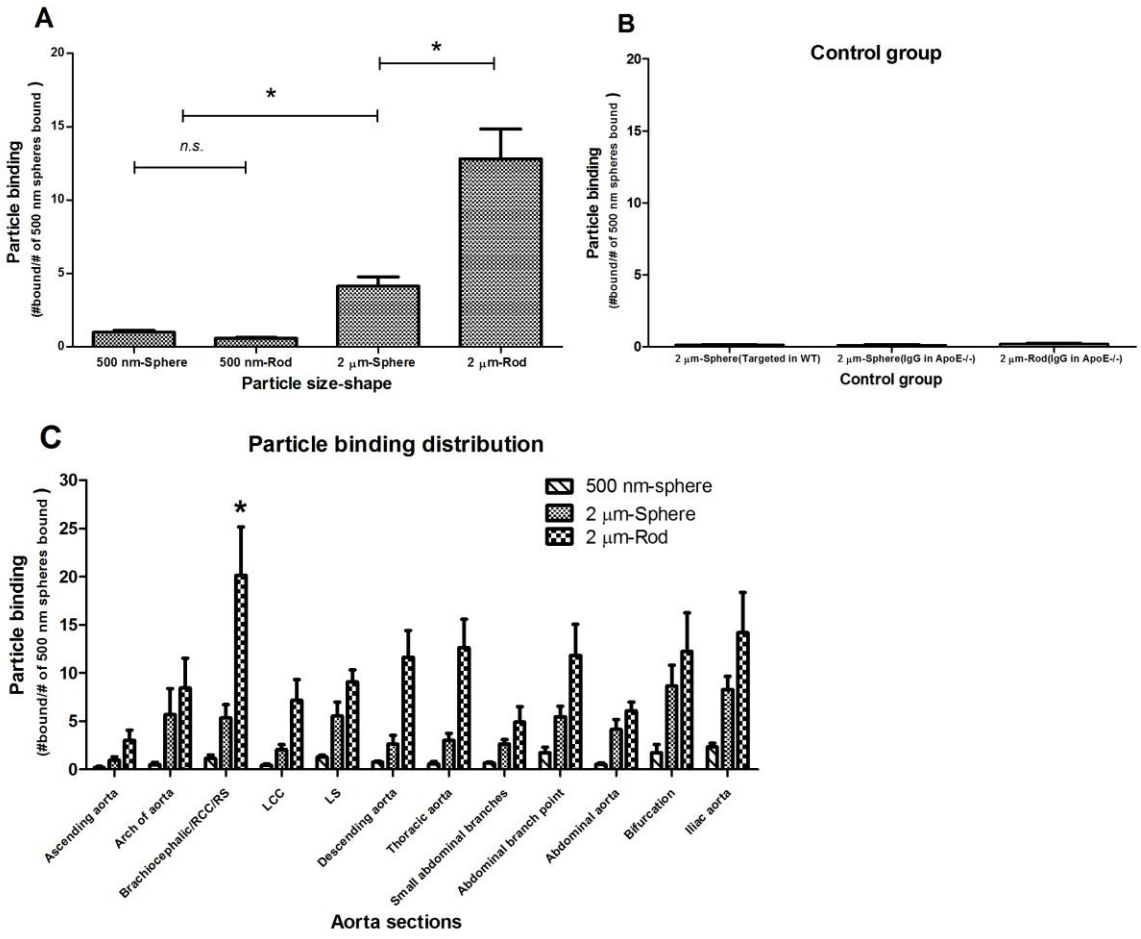

Figure 2-2 (A) Ratio of the adhesion of sLe^a and anti-VCAM coated particles on ApoE $^{-/-}$ mouse aortae following 30 min circulation via tail vein injection. Adhesion data shown is normalized to the adhesion of 500 nm diameter spheres. AR = 6 and 4 for rods with ESD of 500 nm and 2 μm, respectively (* = $p < 0.05$ with respect to 2 μm microspheres and *n.s.*= not significant via one-way ANOVA. $n \geq 5$). (B) Ratio of the adhesion of sLe^A and anti-VCAM targeted 2 μm spheres in wild type mouse aortae or of IgG-coated 2 μm spheres and rods (AR4) in ApoE −/− mouse aortae following 30 min circulation via tail vein injection (C) Ratio of particle binding (normalized to the average number of 500 nm ESD spheres bound per segment) of sLe^A and anti-VCAM coated particles to the endothelium in 12 segments along mouse aorta. (* = $p < 0.05$ with respect to 2 μm microspheres. $n \geq 4$).

2.3.2 Effect of aspect ratio (AR) on particle adhesion

In order to determine the effect that aspect ratio has on targeting ability, targeted rods of three different ARs (2, 4, 9) with 2 μm ESD as well as 500 nm and 2 μm spheres were prepared. Figure 2-4 shows the SEM images of the 2 μm ESD rods and their equivalent spheres. Particles were injected into ApoE-/- mice via tail-vein and the total adhesion along the aortae was quantified for each particle shape as before. The adhesion of the AR4 rods was the highest (~3 times higher) relative to their equivalent microspheres as shown in Figure 2-5. Adhesion of AR2 rods was roughly the same as 2 μm spheres, likely because of the relatively small difference in shape and surface area between these two shapes. Adhesion of AR9 rods was statistically the same as the 2 μm spheres and lower than that of AR4 rods despite having a higher contact surface area, likely due to entrapment in the capillaries as AR9 rods have a major axis length of roughly 9 μm.

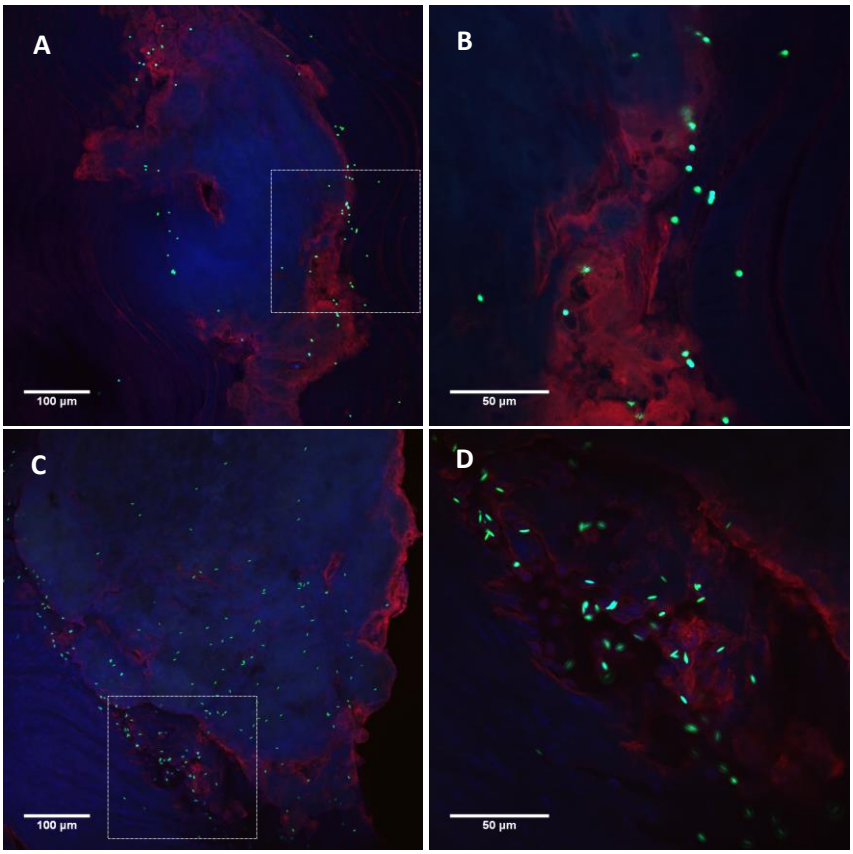

Figure 2-3 Representative images of aortic arch segments (with atherosclerotic plaque present) with adhesion of 2 µm ESD sphere (A and B) and 2 µm ESD rod (C and D) at 20X and 60X magnification, respectively, qualitatively showing the increased adhesion of rods particularly near the periphery of plaques (**Blue** = nucleus stained by Hoechst, **Red** = plasma membrane stained by Alexa Fluor conjugate of wheat germ agglutinin and **Green** = fluorescent particle).

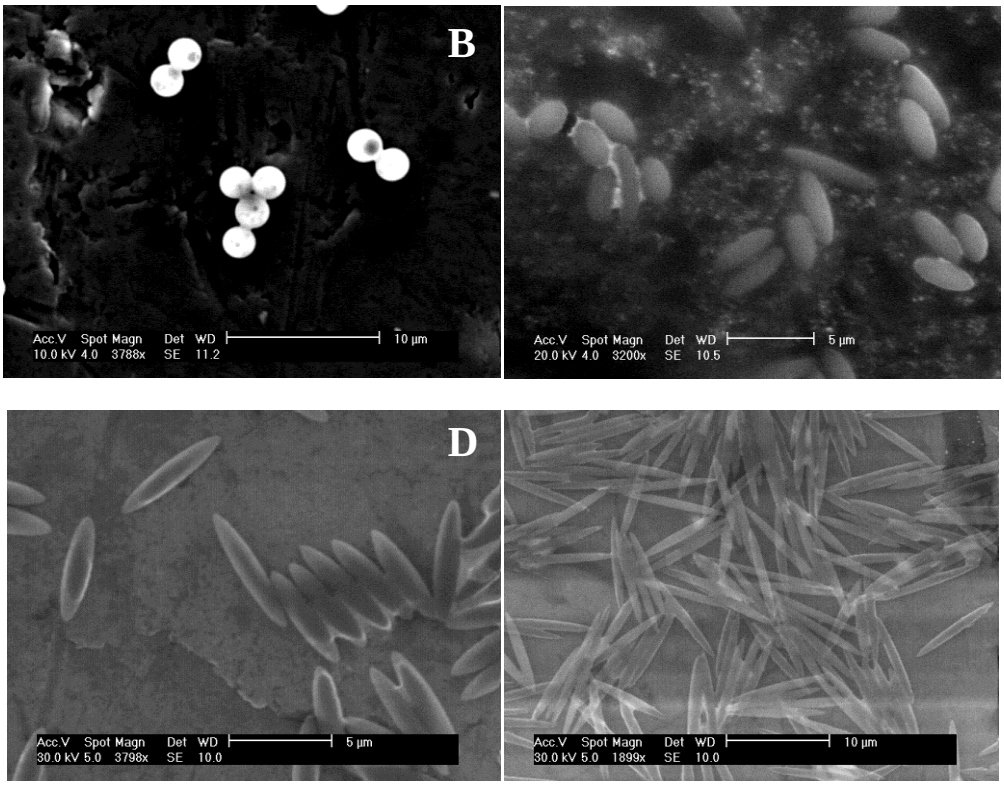

Figure 2-4 SEM image of 2 µm ESD polystyrene (A) spheres, (B) AR-2 rods, (C) AR-4 rods, and (D) AR-9 rods used to test the effect of aspect ratio on particle adhesion on ApoE -/- mouse aorta after 30 min circulation via tail vein injection.

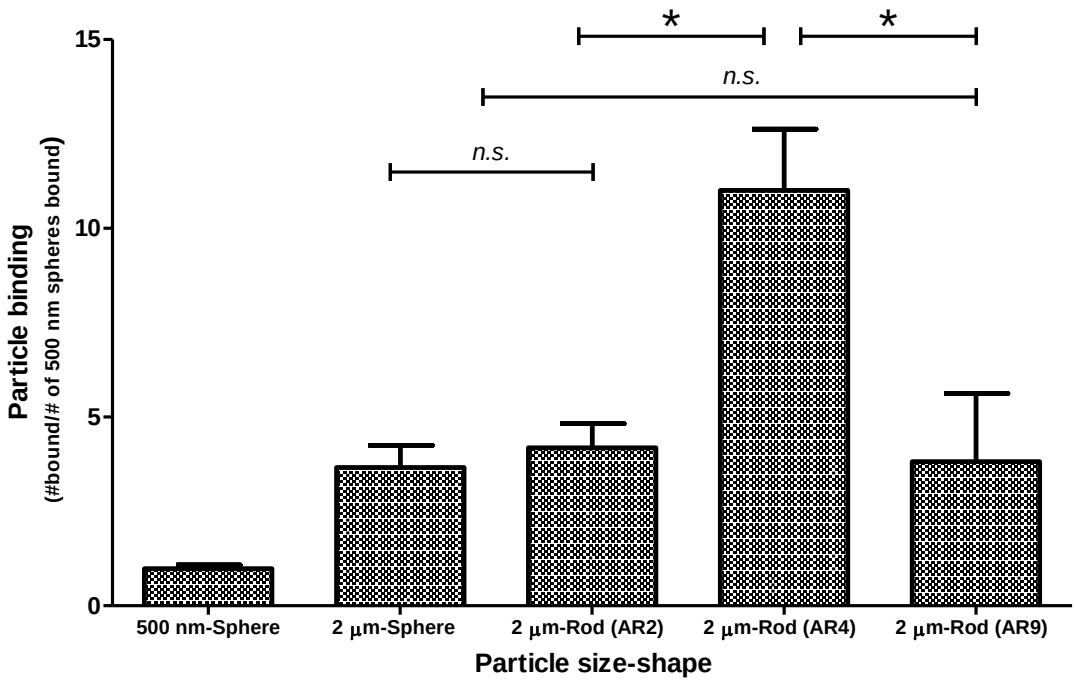

Figure 2-5 Ratio of the binding (normalized to 500 nm ESD sphere) of sLe^A and anti-VCAM coated particles of various AR on ApoE -/- mouse aortae after 30 min circulation via tail-vein injection. (* = $p < 0.05$ and *n.s.*= not significant via one-way ANOVA. $n \geq 3$).

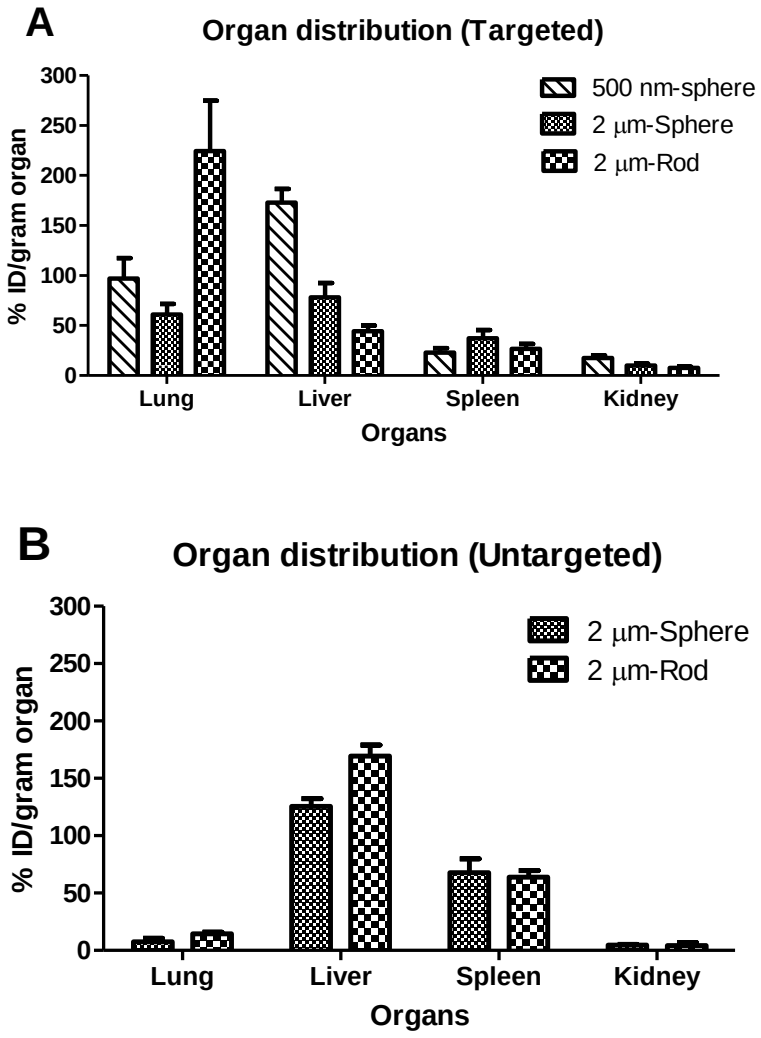

Figure 2-6 (A) Biodistribution of sLe^A and anti-VCAM coated spheres (500 nm or 2 μm diameter) and rods (2 μm ESD, AR4) in ApoE -/- mice following 30 min circulation via tail-vein injection. n≥5 (B) Biodistribution of untargeted spheres (2 μm diameter) and rods (2 μm ESD, AR4) in wild type mice following 30 minute circulation via tail-vein injection. (* = $p < 0.05$ relative to 2 μm spheres and # = $p < 0.05$ relative to the 500 nm spheres via one-way ANOVA. $n \geq 4$).

2.3.3 Particle accumulation in different organs

Major organs were harvested from animals injected with targeted particles to quantify the biodistribution of the microrods with the top performing aspect ratio, AR4, relative to its equivalent sphere and nanospheres. Figure 2-6A shows the accumulation of targeted particles in the lung, liver, spleen, and kidney. Blood collected following a 30-minute circulation time contained negligible amounts of particles (data not shown). Targeted AR4 microrods were retained at a higher level in the lungs than 2 μm or 500 nm diameter spheres. These same rods were retained at either equal or significantly lower levels than micro/nanospheres in the other organs, potentially because their higher level of first-pass lung accumulation and adhesion to the aorta reduces the amount available to accumulate elsewhere. The 500 nm spheres accumulated at higher levels in the liver than the larger microparticles, and there was no appreciable difference in the splenic accumulation of micro and nanoparticles. Retention of particles in the kidneys was low, as particles larger than about 50 – 100 nm are not expected to be removed from blood via glomerular filtration. The higher accumulation of targeted rods in the lungs may be due to physical entrapment of rods (major axis = 5.6 μm) in the small capillaries of the lungs or due to the surface targeting ligands allowing molecular interaction to increase adhesion of particles to lung endothelium. To investigate this further, uncoated rods and spheres were injected into wild type mice via tail-vein and allowed to circulate for 30 minutes before the mice were sacrificed and organs harvested. As shown in Figure 2-6B, retention of untargeted microspheres and the AR4 microrods in the lungs was about 87% and 93% lower, respectively, than targeted particles of the same size and shape. Meanwhile, retention of untargeted microspheres and microrods was about 60% and 280% higher in

the liver, and about 81% and 140% higher in the spleen, respectively, than the equivalent targeted particle. When each dataset presented in Figure 2-6 is normalized to the density of each particle type accumulating in the lungs, the targeted microspheres were found to accumulate in similar amounts in the lung, liver and spleen while targeted microrods accumulated primarily in the lungs (Supplemental Figure 2-4). However, untargeted microspheres and microrods both displayed the majority of accumulation in the liver and spleen.

2.4 Discussion

Physical property of particle, such as particle shape and size, is known to be an important parameter that can be tuned to affect the circulation time, biodistribution, adhesion, internalization, and intracellular trafficking of vascular-targeted drug carriers [21-31]. This study shows that the size and shape of vascular-targeted carriers plays a role in prescribing their adhesion to atherosclerotic area and accumulation in major organs in mouse model. In order for particles to successfully adhere to inflamed endothelium, they must be able to effectively marginate to the vessel wall as well, which is comparable to how circulating WBCs and platelets are able to localize to inflamed endothelium even in large diameter vessels. Previous works have revealed that particle size plays a crucial role in the ability or inability of a particle to preferentially marginate in the presence of human blood components (RBC, plasma) using *in vitro* blood flow assays [3, 8, 13, 20, 32, 33]. Generally, particles that have diameters less than about 2 μm do not segregate through RBC core to the cell-free layer, and then slightly adhere to ECs at the vessel wall, in blood flow as efficiently as particles with diameters ≥2 μm [3, 10, 30, 32]. Instead, the study suggests that these submicron to nanoscale particles mostly remain in the core of flow,

enclosed by RBCs [8]. According to the results, we found that the adhesion of targeted nanospheres and nanorods of 500 nm ESD are significantly lower along the mouse aorta compared to microparticles. In addition, the increased adhesion of microrods to the mouse aorta (roughly 4 fold) compared to equivalent microspheres is similar to our previous study of particle localization in human blood *in vitro* assays which microrods (≥1 μm ESD) were found to adhere at higher levels than equivalent spheres [13]. This increased adhesion for microrods *in vivo* over their equivalent spheres is likely due to more favorable adhesive characteristics rather than improved localization to the wall, including a higher contact surface area and a streamlined shape to reduce drag force in the presence of blood flow induced shear, since no improvement was found in the localization of rod-shaped particles to the RBC-free plasma layer (CFL) in human blood flow in PPFC assays compared to their equivalent spheres [13]. The deficiency of adhesion of nanorods compared to nanospheres is likely due to the incapability of nanoparticles to preferentially segregate to the CFL, which is unrelated to their shape and the impact of higher contact surface area. Whereas particles on the nanometer scale may provide advantages in long circulation time and transmigration across the endothelium, the drawback of nanoparticles to preferentially adhere to the endothelium in the aorta could potentially limit their efficacy as a vascular-targeted carriers in medium/large blood vessels.

"Atheroprone" are specific areas of the arterial tree predisposed to atherosclerotic lesion formation. These atheroprone areas including the aortic root, the curvature along the aortic arch, and major branching points along the arterial tree; usually are exposed to disturbed blood flow, characterized by high pulsatile flow but low net shear [14, 34]. The results shows significantly increased adhesion of microrods compared to spheres in many

atheroprone areas, particularly nearby major branching points in the aorta and curvature along the aortic arch. Particle adhesion at atheroprone was found more binding at the periphery of the plaque, which agrees with previously reported findings for the adhesion of VCAM-1 targeted polymeric particles [35]. This formation is very likely related to the expression patterns of the target molecules, particularly VCAM-1, which have been shown to persist on ECs nearby plaques more so than directly on top of plaques within ApoE -/- mice [15].

According to previous research, particle shape and size associated with presence of targeting ligands can affect biodistribution in mice, [21, 28, 31, 35, 36], and then in this study we would like to include the biodistribution profile altered based on these parameters. As the result, we find accumulation of particles in the lung and liver, with accumulation to a lesser extent in the spleen and kidneys. We find significantly more targeted 2 μm ESD rods in the lungs compared to equivalent spheres, which could be a function of either (1) mechanical entrapment due to the longer axis length of the rod or (2) enhanced molecular interactions of the targeting ligands on rods with pulmonary endothelium. Research has correlated accelerated pulmonary endothelial inflammation with the presence of systemic atherosclerosis[37], so some level of accumulation based on molecular interaction with targeting ligands could be occurring. Certainly, the significantly lower accumulation of untargeted microparticles in the lung suggests that a significant portion of the lung accumulation is due to molecular interaction of the targeting molecule with the pulmonary endothelium and would be exaggerated for the microrods versus spheres due to their larger surface area for contact. Interestingly, the mechanical entrapment of the AR4 microrods (i.e., non-targeted particles) in our study is not significantly different from that of spheres

despite having quite different major axis lengths (see Figure 2-6), which would suggest that the rods preferentially enter the capillaries in an orientation that line their major axis in the direction of flow.

Finally, the overall biodistribution profile of microparticles shows preferential accumulation in the liver and spleen when the targeting ligands are removed from microparticles. This is probable due to the lower first-pass retention of untargeted particles in the lung (immediately following tail vein injection) and more untargeted particles available in circulation for hepatic/splenic clearance compared to their targeted counterparts. The overall observation of particle distribution in this work is agree with a previous study by Muro et al., which reported the accumulation of anti-ICAM targeted polystyrene disks in the lungs and liver of C57Bl/6 mice [21]. This study found that targeted micro-disks accumulated at high levels in the lungs and relatively low levels in the liver, and that retention of nontargeted (IgG coated) particles was diminished in the lungs, with a corresponding increase in liver accumulation [21]. The liver accumulation of microparticles in this study (%ID/g) is slightly higher than in other published reports, which may be due to differences in quantification techniques and also heterogeneity in the liver. In this study, the left lobe of the liver from each animal was harvested after the animal is sacrificed and the circulatory system perfused with buffer and fixing agent. It is possible that more particles were deposited in the left lobe than in the rest of the liver. It has been shown that "portal streamlining" can result in incomplete blood mixing causing variation in blood delivered to liver lobes and hence disproportionate deposition of particles between the two lobes [38]. Also, blood from the spleen or stomach tends toward the left side of the liver.[38] Furthermore, others have published *in vivo* studies with

fluorescent images that seem to suggest heterogeneous particle deposition in the liver as well [39, 40].

In conclusion, the study reveals that ellipsoidal microparticles of an intermediate aspect ratio (AR4) with volume equivalent to 2 μm diameter spheres are higher efficient than microspheres with equal volume and nanoparticles at the aorta of atherosclerotic mice, particularly in atheroprone areas. In addition, the untargeted microrods show a similar level of minimal mechanical entrapment in the lung capillaries compared to their spherical counterparts. Thus, the ellipsoidal geometry with the appropriate aspect ratio may be an advantageous shape for designing drug carriers for targeting the aorta, in order to enhance efficiency of therapeutics or diagnostics intravenously in atherosclerosis. However, targeted microrods, more than microspheres and nanoparticles, are retained in the lungs at higher levels compared to their untargeted counterparts, likely due to molecular interaction with inflammatory molecules in the pulmonary vasculature of atherosclerotic mice. Overall, this work reveals that particle shape, particle size, and targeting moiety all play a role in dictating the adhesion and biodistribution profile in a mouse model of atherosclerosis, therefore all of these parameters should be considered when designing carrier systems to target this disease.

2.5 Supplemental Data

Supplemental Table 2-1. Dimensions of particles used to test the effect of AR on particle adhesion (Figure 2-5)

Particle Shape	ESD (μm)	Aspect Ratio	Major Axis (μm)	Minor Axis (μm)
Sphere	**2.07**	1.00	2.07	2.07
AR-2		2.25	3.55	1.58
AR-4		4.46	5.61	1.26
AR-9		9.45	9.25	0.98

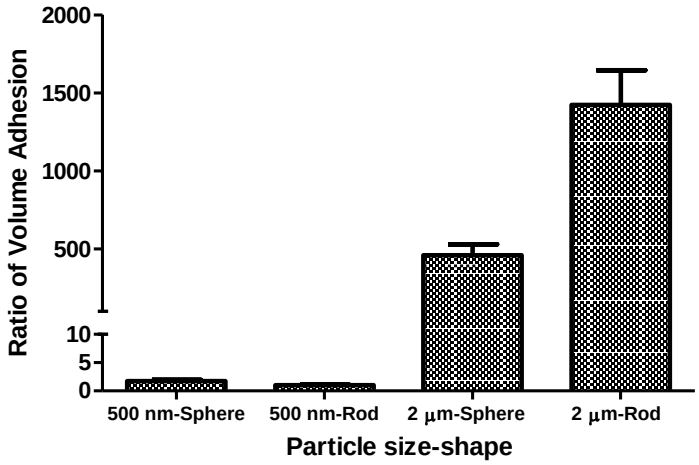

Supplemental Figure 2-1. Ratio of volume binding (normalized to 500 nm ESD rod) of sLe^A and anti-VCAM-coated particle binding on ApoE -/- mouse aorta after 30 min circulation via tail vein injection. $n \geq 5$

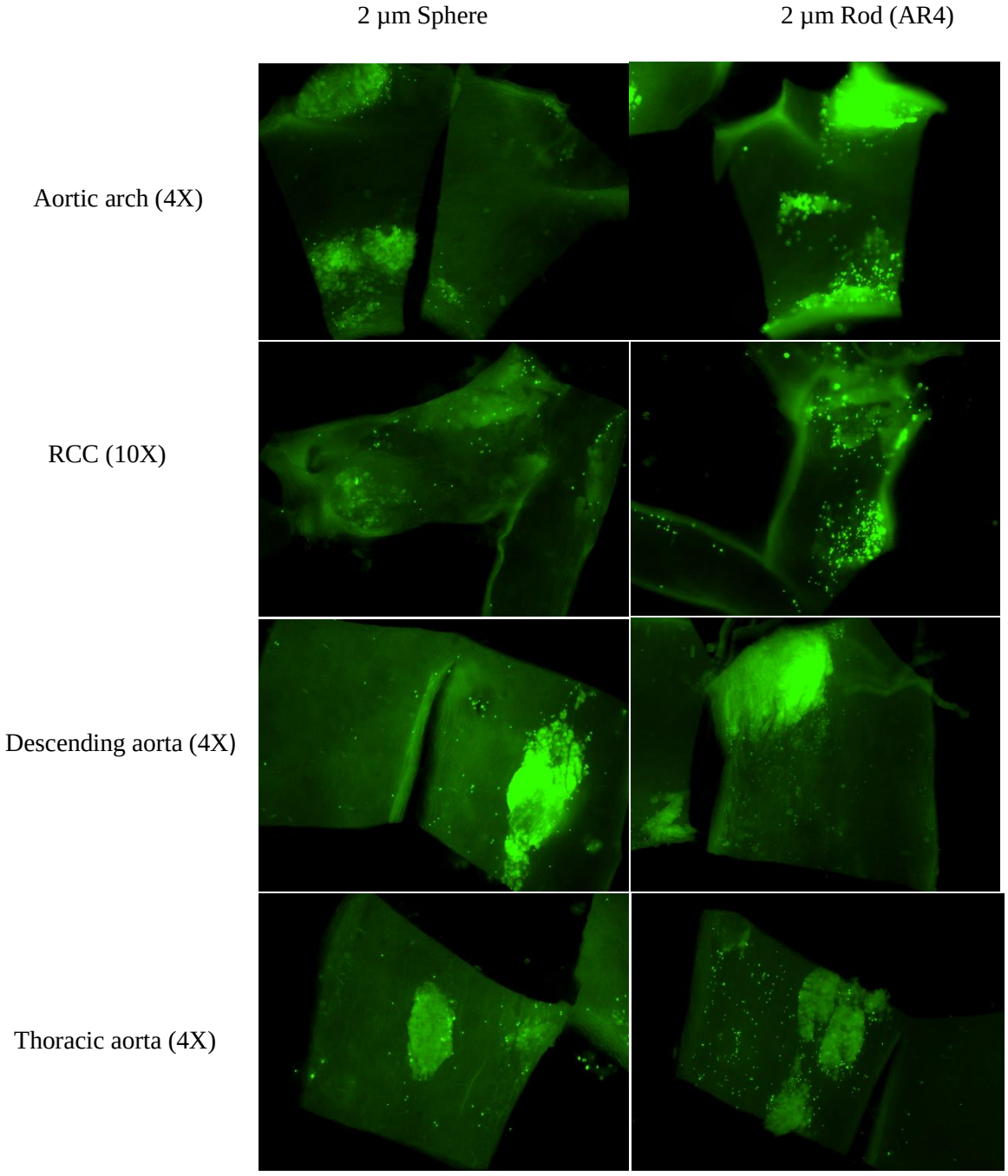

Supplemental Figure 2-2. Fluorescent images of sLe^A and anti-VCAM-coated 2 µm sphere and rod (AR4) particles adhering on ApoE $^{-/-}$ mouse aortas after 30 min circulation via tail vein injection. Five sections of the aorta are shown: aortic arch, RCC, descending aorta and thoracic aorta.

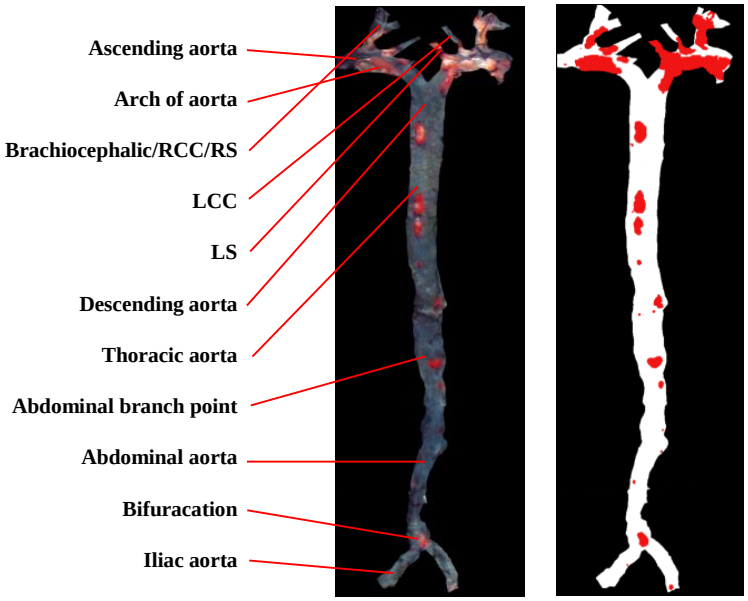

Supplemental Figure 2-3. Anatomical images of *en face* mouse aorta with atherosclerotic plaque area (red) stained with O-red oil, presenting developing plaques near the branched/curved regions of aorta.

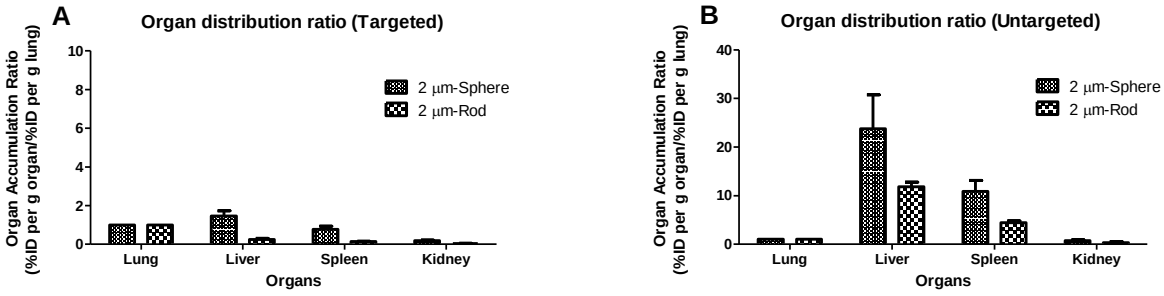

Supplemental Figure 2-4. Ratio of the accumulation density in major organs (%ID/g organ) to the accumulation density in the lungs (%ID/g lungs) for (A) targeted and (B) untargeted 2 μm spheres and rods (2 μm ESD, AR4) in mice following 30 minute circulation via tail-vein injection. $n \geq 4$

References

1. Psarros, C., R. Lee, M. Margaritis, and C. Antoniades, Nanomedicine for the prevention, treatment and imaging of atherosclerosis. Nanomedicine, 2012. 8 Suppl 1: p. S59-68.

2. Hajitou, A., R. Pasqualini, and W. Arap, Vascular targeting: recent advances and therapeutic perspectives. Trends Cardiovasc Med, 2006. 16(3): p. 80-8.

3. Charoenphol, P., R.B. Huang, and O. Eniola-Adefeso, Potential role of size and hemodynamics in the efficacy of vascular-targeted spherical drug carriers. Biomaterials, 2010. 31(6): p. 1392-402.

4. Lobatto, M.E., V. Fuster, Z.A. Fayad, and W.J. Mulder, Perspectives and opportunities for nanomedicine in the management of atherosclerosis. Nat Rev Drug Discov, 2011. 10(11): p. 835-52.

5. Huang, R.B., S. Mocherla, M.J. Heslinga, P. Charoenphol, and O. Eniola-Adefeso, Dynamic and cellular interactions of nanoparticles in vascular-targeted drug delivery. Mol Membr Biol, 2010. 27(7): p. 312-27.

6. Decuzzi, P., R. Pasqualini, W. Arap, and M. Ferrari, Intravascular delivery of particulate systems: does geometry really matter? Pharm Res, 2009. 26(1): p. 235-43.

7. Charoenphol, P., P.J. Onyskiw, M. Carrasco-Teja, and O. Eniola-Adefeso, Particle-cell dynamics in human blood flow: implications for vascular-targeted drug delivery. J Biomech, 2012. 45(16): p. 2822-8.

8. Namdee, K., A.J. Thompson, P. Charoenphol, and O. Eniola-Adefeso, Margination propensity of vascular-targeted spheres from blood flow in a microfluidic model of human microvessels. Langmuir, 2013. 29(8): p. 2530-5.

9. Doshi, N., B. Prabhakarpandian, A. Rea-Ramsey, K. Pant, S. Sundaram, and S. Mitragotri, Flow and adhesion of drug carriers in blood vessels depend on their shape: a study using model synthetic microvascular networks. J Control Release, 2010. 146(2): p. 196-200.

10. Decuzzi, P. and M. Ferrari, The adhesive strength of non-spherical particles mediated by specific interactions. Biomaterials, 2006. 27(30): p. 5307-14.

11. Gavze, E. and M. Shapiro, Motion of inertial spheroidal particles in a shear flow near a solid wall with special application to aerosol transport in microgravity. Journal of Fluid Mechanics, 1998. 371: p. 59-79.

12. Lee, S.Y., M. Ferrari, and P. Decuzzi, Shaping nano-/micro-particles for enhanced vascular interaction in laminar flows. Nanotechnology, 2009. 20(49): p. 495101.

13. Thompson, A.J., E.M. Mastria, and O. Eniola-Adefeso, The margination propensity of ellipsoidal micro/nanoparticles to the endothelium in human blood flow. Biomaterials, 2013. 34(23): p. 5863-71.

14. Ku, D.N., D.P. Giddens, C.K. Zarins, and S. Glagov, Pulsatile flow and atherosclerosis in the human carotid bifurcation. Positive correlation between plaque location and low oscillating shear stress. Arteriosclerosis, 1985. 5(3): p. 293-302.

15. Iiyama, K., L. Hajra, M. Iiyama, H. Li, M. DiChiara, B.D. Medoff, and M.I. Cybulsky, Patterns of vascular cell adhesion molecule-1 and intercellular adhesion molecule-1 expression in rabbit and mouse atherosclerotic lesions and at sites predisposed to lesion formation. Circ Res, 1999. 85(2): p. 199-207.

16. Davies, M.J., J.L. Gordon, A.J. Gearing, R. Pigott, N. Woolf, D. Katz, and A. Kyriakopoulos, The expression of the adhesion molecules ICAM-1, VCAM-1, PECAM, and E-selectin in human atherosclerosis. J Pathol, 1993. 171(3): p. 223-9.

17. Galkina, E. and K. Ley, Vascular adhesion molecules in atherosclerosis. Arterioscler Thromb Vasc Biol, 2007. 27(11): p. 2292-301.

18. Ferrante, E.A., J.E. Pickard, J. Rychak, A. Klibanov, and K. Ley, Dual targeting improves microbubble contrast agent adhesion to VCAM-1 and P-selectin under flow. J Control Release, 2009. 140(2): p. 100-7.

19. McAteer, M.A., J.E. Schneider, Z.A. Ali, N. Warrick, C.A. Bursill, C. von zur Muhlen, D.R. Greaves, S. Neubauer, K.M. Channon, and R.P. Choudhury, Magnetic resonance imaging of endothelial adhesion molecules in mouse atherosclerosis using dual-targeted microparticles of iron oxide. Arterioscler Thromb Vasc Biol, 2008. 28(1): p. 77-83.

20. Charoenphol, P., S. Mocherla, D. Bouis, K. Namdee, D.J. Pinsky, and O. Eniola-Adefeso, Targeting therapeutics to the vascular wall in atherosclerosis--carrier size matters. Atherosclerosis, 2011. 217(2): p. 364-70.

21. Muro, S., C. Garnacho, J.A. Champion, J. Leferovich, C. Gajewski, E.H. Schuchman, S. Mitragotri, and V.R. Muzykantov, Control of endothelial targeting and intracellular delivery of therapeutic enzymes by modulating the size and shape of ICAM-1-targeted carriers. Mol Ther, 2008. 16(8): p. 1450-8.

22. Geng, Y., P. Dalhaimer, S. Cai, R. Tsai, M. Tewari, T. Minko, and D.E. Discher, Shape effects of filaments versus spherical particles in flow and drug delivery. Nat Nanotechnol, 2007. 2(4): p. 249-55.

23. Christian, D.A., S. Cai, O.B. Garbuzenko, T. Harada, A.L. Zajac, T. Minko, and D.E. Discher, Flexible filaments for in vivo imaging and delivery: persistent circulation of filomicelles opens the dosage window for sustained tumor shrinkage. Mol Pharm, 2009. 6(5): p. 1343-52.

24. Champion, J.A. and S. Mitragotri, Shape induced inhibition of phagocytosis of polymer particles. Pharm Res, 2009. 26(1): p. 244-9.

25. Champion, J.A., A. Walker, and S. Mitragotri, Role of particle size in phagocytosis of polymeric microspheres. Pharm Res, 2008. 25(8): p. 1815-21.

26. Gratton, S.E., P.A. Ropp, P.D. Pohlhaus, J.C. Luft, V.J. Madden, M.E. Napier, and J.M. DeSimone, The effect of particle design on cellular internalization pathways. Proc Natl Acad Sci U S A, 2008. 105(33): p. 11613-8.

27. Agarwal, R., V. Singh, P. Jurney, L. Shi, S.V. Sreenivasan, and K. Roy, Mammalian cells preferentially internalize hydrogel nanodiscs over nanorods and

use shape-specific uptake mechanisms. Proc Natl Acad Sci U S A, 2013. 110(43): p. 17247-52.

28. Decuzzi, P., B. Godin, T. Tanaka, S.Y. Lee, C. Chiappini, X. Liu, and M. Ferrari, Size and shape effects in the biodistribution of intravascularly injected particles. J Control Release, 2010. 141(3): p. 320-7.

29. Huang, X., L. Li, T. Liu, N. Hao, H. Liu, D. Chen, and F. Tang, The shape effect of mesoporous silica nanoparticles on biodistribution, clearance, and biocompatibility in vivo. ACS Nano, 2011. 5(7): p. 5390-9.

30. Devarajan, P.V., A.B. Jindal, R.R. Patil, F. Mulla, R.V. Gaikwad, and A. Samad, Particle shape: a new design parameter for passive targeting in splenotropic drug delivery. J Pharm Sci, 2010. 99(6): p. 2576-81.

31. Kolhar, P., A.C. Anselmo, V. Gupta, K. Pant, B. Prabhakarpandian, E. Ruoslahti, and S. Mitragotri, Using shape effects to target antibody-coated nanoparticles to lung and brain endothelium. Proc Natl Acad Sci U S A, 2013. 110(26): p. 10753-8.

32. Eckstein, E.C., A.W. Tilles, and F.J. Millero, 3rd, Conditions for the occurrence of large near-wall excesses of small particles during blood flow. Microvasc Res, 1988. 36(1): p. 31-9.

33. Tilles, A.W. and E.C. Eckstein, The near-wall excess of platelet-sized particles in blood flow: its dependence on hematocrit and wall shear rate. Microvasc Res, 1987. 33(2): p. 211-23.

34. Nakashima, Y., A.S. Plump, E.W. Raines, J.L. Breslow, and R. Ross, ApoE-deficient mice develop lesions of all phases of atherosclerosis throughout the arterial tree. Arterioscler Thromb, 1994. 14(1): p. 133-40.

35. Deosarkar, S.P., R. Malgor, J. Fu, L.D. Kohn, J. Hanes, and D.J. Goetz, Polymeric particles conjugated with a ligand to VCAM-1 exhibit selective, avid, and focal adhesion to sites of atherosclerosis. Biotechnol Bioeng, 2008. 101(2): p. 400-7.

36. Gratton, S.E., P.D. Pohlhaus, J. Lee, J. Guo, M.J. Cho, and J.M. Desimone, Nanofabricated particles for engineered drug therapies: a preliminary biodistribution study of PRINT nanoparticles. J Control Release, 2007. 121(1-2): p. 10-8.

37. Moore, G.W., R.R. Smith, and G.M. Hutchins, Pulmonary artery atherosclerosis: correlation with systemic atherosclerosis and hypertensive pulmonary vascular disease. Arch Pathol Lab Med, 1982. 106(8): p. 378-80.

38. Malarkey, D.E., K. Johnson, L. Ryan, G. Boorman, and R.R. Maronpot, New insights into functional aspects of liver morphology. Toxicol Pathol, 2005. 33(1): p. 27-34.

39. Ballou, B., B.C. Lagerholm, L.A. Ernst, M.P. Bruchez, and A.S. Waggoner, Noninvasive imaging of quantum dots in mice. Bioconjug Chem, 2004. 15(1): p. 79-86.

40. Michalet, X., F.F. Pinaud, L.A. Bentolila, J.M. Tsay, S. Doose, J.J. Li, G. Sundaresan, A.M. Wu, S.S. Gambhir, and S. Weiss, Quantum dots for live cells, in vivo imaging, and diagnostics. Science, 2005. 307(5709): p. 538-44.

CHAPTER 3

MARGINATION PROPENSITY OF VASCULAR-TARGETED SPHERES IN A MODEL OF HUMAN MICROVESSELS

Abstract

Many variants of vascular-targeted carriers (VTCs) have been investigated for therapeutic intervention in several human diseases. However, in order to optimize the functionality of VTC *in vivo*, carriers' physical properties, such as size and shape, are important considerations for a design that evades the reticuloendothelial system (RES) and successfully interacts with the targeted vessel wall. Nonetheless, little evidence has been presented on the role of size in VTC's interactions with the vascular wall, particularly in the microcirculation. Thus, in this work, we explore how particle size, along with hemodynamics (blood shear rate and vessel size) and hemorheology (blood hematocrit) affect the capacity for spheres to marginate to inflamed endothelium in a microfluidic model of human microvessels. Microspheres, particularly the 2 μm spheres, were found to show disproportionately higher margination than nanospheres in all hemodynamic conditions evaluated due to the poor ability of the latter to localize to the wall region from midstream. This work represents the first evidence that nanospheres may not exhibit "near wall excess" in microvessels, e.g. arterioles and venules, and therefore may not be suitable

for imaging and drug delivery applications in cancer and other diseases affecting microvessels.

* Content of this have been published as Namdee K, Thompson AJ, Charoenphol P and Eniola-Adefeso O. Margination propensity of vascular-targeted spheres from blood flow in a microfluidic model of human microvessels. Langmuir. 2013, 29(8): 2530-2535.

3.1 Introduction

Vascular-targeted drug delivery offers the advantage of low drug side effects and the ability to sustain drug release over an extended period, both of which would lead to an increase in patient compliance. Many variants of vascular-targeted carriers (VTCs) have been investigated for therapeutic intervention in several human diseases where a unique or an overexpression of specific biomolecules by the endothelium of the vascular wall can be identified, including in cancer and coronary artery disease [1-4]. However, in order to achieve optimum targeting, VTCs must first successfully travel from midstream of blood flow to the red blood cell (RBC)-free plasma layer adjacent to the vessel wall. Therefore, the physical properties of VTCs (e.g. size and shape) that facilitate optimal margination (localization and adhesion) to the vascular wall are necessary considerations in their design.

To this end, a few works in the literature have evaluated the role of carrier size in the binding efficiency of VTCs to the vascular wall from blood flow. In one study, Decuzzi and co-workers used a theoretical model to show that spherical drug carriers with diameters in the range of 100 nm would have the same short margination time to the vascular wall as 2 μm spheres [5]. However, we recently reported that 2-5 μm diameter spheres display significantly better margination to the wall from bulk human blood flow than nanospheres in channels on the order of medium to large blood vessels [6-8]. Nanospheres were found to exhibit minimal margination in bulk blood flow due to their significant entrapment within the red blood cell (RBC) core that forms when blood flows in blood vessels or confined channels *in vitro* [8]. It remains unclear, though, whether the reported trends for medium and large channels would prevail in the microcirculation that comprises arterioles, venules, and capillaries [9].

Microvessels are critical for the transfer of nutrients and leukocyte diapedesis (extravasation) into tissue spaces. However, these vessels are also known to be involved in the pathology of many human diseases, the most notable of which is cancer. Thus, targeted disruption of the tumor vasculature and/or localization of nanoparticles into tumor tissue, via the enhanced permeability and retention (EPR) effect in tumor capillaries, are often proposed as a strategy for cancer treatment. Though both of these targeting strategies typically focus on the capillaries, the majority of blood vessels in a tumor microvascular network have diameter greater than 20 μm (i.e. the feeding arterioles and post-capillary venules)[10], and are therefore likely to exhibit bulk blood flow. In this work, we use microfluidic chambers that comprise of flow channels with dimensions on the order of human arteriole and venule diameters (~ 20 - 100 μm) and an endothelial wall to evaluate the margination of spherical model VTCs from blood flow in the human microcirculation. Specially, 200 nm, 500 nm, 2 μm and 5 μm polystyrene spheres with their surfaces conjugated with sialyl lewis^{A} (sLe^{A}), a ligand specific to E-selectin expressed by inflamed endothelial cells (ECs), were evaluated for their ability to localize and bind to activated ECs from human blood flow in microfluidic channels of 28 and 43 μm height.

3.2 Method

3.2.1 Microchannel fabrication

Microfluidic chambers (Figure 3-1A) were designed using AutoCAD software. A chamber template was fabricated on silicon wafers using a soft lithography technique [11]. This template was then silanized with tridecafluoro-(1,1,2,2-tetrahydrooctyl)-1-trichlorosilane (United Chemical Technologies, Bristol, PA) for 1 hr at room temperature in a desiccator to prevent polydimethylsiloxane (PDMS) from adhering to the template. PDMS was poured into the mold and cured at 60°C overnight. The solidified PDMS layer was removed from the template. The chamber was exposed to plasma oxygen for 15 min to render its surface hydrophilic. The chamber length was set at 10 mm including the 2 mm diameter reservoirs on both ends. Two 1.5 mm pin holds were punched through on both ends in the reservoir areas to allow access into the channel. A vacuum network was applied around the chamber to allow the sealing of a glass coverslip with a monolayer of endothelial cells.

3.2.2 Preparation of vascular-targeted particles

Carboxylate-modified polystyrene spheres of 0.20, 0.51, 2.07, and 5.72 μm in size (Bangs Laboratories Inc., Fishers, IN) were covalently coupled with NeutrAvidin protein (Pierce Biotech Inc., Rockford, IL) via carbodiimide (EDAC) chemistry as previously described [12]. Avidin-coated spheres were conjugated with biotinylated multivalent sialyl Lewis A (sLe^A; GlycoTech, Gaithersburg, MD) in 50 mM PBS with 1% BSA and resuspended in blood at a fixed concentration, 5 times 10^5 particles/mL, as previously described. A fixed targeting ligand surface density was achieved for all spheres by varying

ligand concentration in the conjugation solution for each particle size. Sphere surface ligand densities were quantified via BD FACsCalibur. A site density of approximate 1000 sites/μm^2 were used for *in vitro* experiments with sLe^A [13].

3.2.3 Preparation of endothelial cell (EC) monolayer

Human umbilical vein endothelial cells (HUVECs) were harvested and cultured as described in [6]. HUVECs) harvested from fresh umbilical cords obtained from Mott Children's Hospital (Ann Arbor, MI) were pooled and cultured in tissue culture flasks pretreated with gelatin (0.2% w/v). Human umbilical cords were obtained from the U of M hospital under a Medical School Internal Review Board (IRB-MED) approved human tissue transfer protocol (HUM00026898). This protocol is exempt from informed consent per federal exemption category #4 of the 45 CFR 46.101. (b). For flow experiments, HUVECs were subcultured onto 30 mm glass cover slips pretreated with 1% w/v gelatin cross-linked with 0.5% glutaraldehyde [14]. The HUVECs were cultured at 37°C in a humidified 5% CO_2 incubator. Confluent HUVEC monolayers were activated with IL-1β (1 ng/ml) for 4 h prior to use in flow assays. E-selectin expression on HUVEC was confirmed by immunofluorescence staining [15].

3.2.4 Preparation of human blood

Venous blood was collected from adult donors into a citrate-containing syringe. Blood samples were collected according to protocols approved by the University of Michigan Internal Review Board and in line with the standards set by the Helsinki Declaration [16]. Red blood cells were sedimented from whole blood using a 6% dextran solution. Cell-free plasma (devoid of leukocytes and platelets) was obtained by

centrifugation of the leukocyte-platelet rich plasma layer at 500×g for 10 min and was kept at 37°C until used. Unless otherwise stated, reconstituted blood, i.e. isolated RBCs resuspended in cell-free plasma, at 30% hematocrit (% Hct) was used in flow assays.

3.2.5 Experimental setup

A monolayer of activated HUVECs was vacuum-sealed to the microfluidic chamber such that the HUVEC monolayer formed the bottom plate of the rectangular flow channel. sLe^A-coated spheres of a given size suspended in reconstituted blood at 5 time 10^5 particles/ml, unless otherwise stated, were introduced into the flow channel from an inlet reservoir via a syringe pump. Adhesion assays were observed on an inverted microscope (Nikon TE 2000-S) fitted with a digital camera (Photometrics CoolSNAP EZ with a Sony CCD sensor). To account for any potential variation in fluxes along the chamber length as well as entrance effects, data was collected at a constant position midway from the entrance and exit of the chamber for all experiments.

The wall shear rate (γ_w; WSR) in the system was calculated from the adjustment of volumetric flow rate (Q) according to

$$\gamma_w(s^{-1}) = \frac{6Q}{wh^2} \quad (1)$$

where h is the channel height (28 μm or 43 μm) and w is the channel width (1000 μm). Adhesion assays were conducted with laminar flow through the channel at WSRs of 100 s^{-1}, 200 s^{-1} and 500 s^{-1}, which are within the range of values reported for human microvessels *in vivo* [17-19]. Data is recorded as the number of particles that adhere to endothelial cells (ECs) after 5 min of flow divided by the area of view (0.152 mm^2).

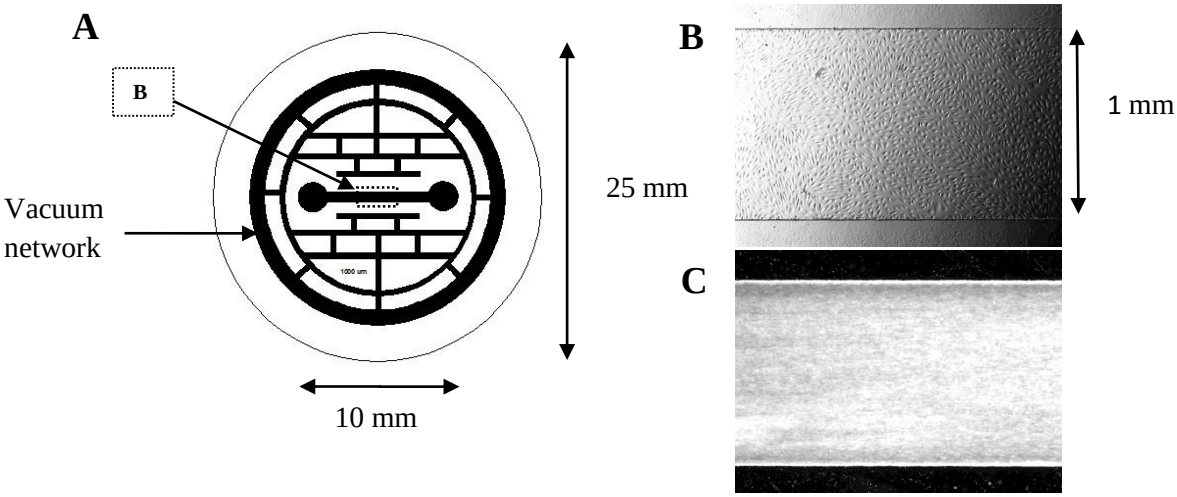

Figure 3-1 Microchannel system. A) Top view of the microfluidic chamber showing the surrounding vacuum network system. Phase images of the microchannel (B) before and (C) during laminar blood flow. Human endothelial cell monolayer is visible in (B).

Standard error bars are plotted and significances in data analyzed by one-way ANOVA with Tukey post-test (a value of $p < 0.05$ was considered statistically significant).

3.2.6 Confocal imaging of particle localization to the chamber wall

A Leica Inverted SP5X Confocal Microscope (MIL, University of Michigan) was used to visualize the distribution of 0.5 and 2 μm spheres to the wall in reconstituted human blood flow at 30% Hct in a parallel plate flow chamber (PPFC) setup. Specifically, particle localization to a focal plane just above that of a resting 2 μm diameter sphere at the bottom of the PPFC was evaluated. Varied concentrations of particles, relative to a 1X concentration of 5 time 10^5 particles/ml, were mixed in blood, and then the mixture was induced into the flow chamber at a WSR of 200 s^{-1}. The images of the focal plane were taken, and the fluorescence intensity for each image was calculated using Leica Microsystems LAS AF Lite Imaging Software. Fluorescence intensity was analyzed comparing to 1X concentration for each flow condition.

3.3 Result and Discussion

3.3.1 Effect of shear rate and channel height on binding dynamics of spheres in microchannels

Vascular-targeted spheres with diameters ranging from 0.2 to 5 μm were allowed to interact with activated HUVEC monolayers in microfluidic channels from laminar reconstituted human blood flow at a fixed hematocrit (Hct) of 30%. As shown in Figure 3-2, particle adhesion densities significantly increased with increasing spherical diameters from 0.5 to 2 μm for all laminar WSRs evaluated in the 43 and 28 μm height channels. The

adhesion densities of 0.2 and 0.5 μm spheres were not significantly different at all WSRs tested in both channels ($p > 0.05$; one-way ANOVA). The 5 μm spheres displayed either statistically the same or significantly lower adhesion density than the 2 μm spheres for all experimental conditions at 30% Hct in both channels with the exception of adhesion in the 28 μm channel at 100 s^{-1}. In general, microspheres were found to be more efficient at binding from blood flow than the nanospheres evaluated, when fed at the same fixed concentration, likely because the latter exhibited minimal localization to the wall. It is well documented that in blood flow, RBCs congregate in the mid-line of flow leaving a RBC-free layer (RBC-FL) near the vessel wall. Leukocytes, platelets and VTCs must localize to this RBC-FL in order to interact with the vessel wall. Several publications have reported that microspheres tend to disproportionately concentrate in the RBC-FL relative to midstream during blood flow in medium to large channels while spheres smaller than 1 μm do not exhibit such "near-wall excess" [6, 20]. Instead, a majority of the submicron to nanospheres in blood flow is retained within the RBC core, filling the void space between RBCs. The result presented in Figure 2 is the first report that nanospheres do not exhibit near-wall excess, or high margination, in human blood in channels on the order of human microvessels. A similar observation was previously reported by King et al. for the trajectory of fluorescent 500 nm particles in small venules of mouse cremaster tissue where it was shown that a high concentration of nanoparticles exist in the centerline of observed vessels while only a few nanospheres were found near the wall [21].

To better understand particle adhesion trends in the context of adhesion kinetics, particle adhesion densities were normalized to the total number of spheres that perfused

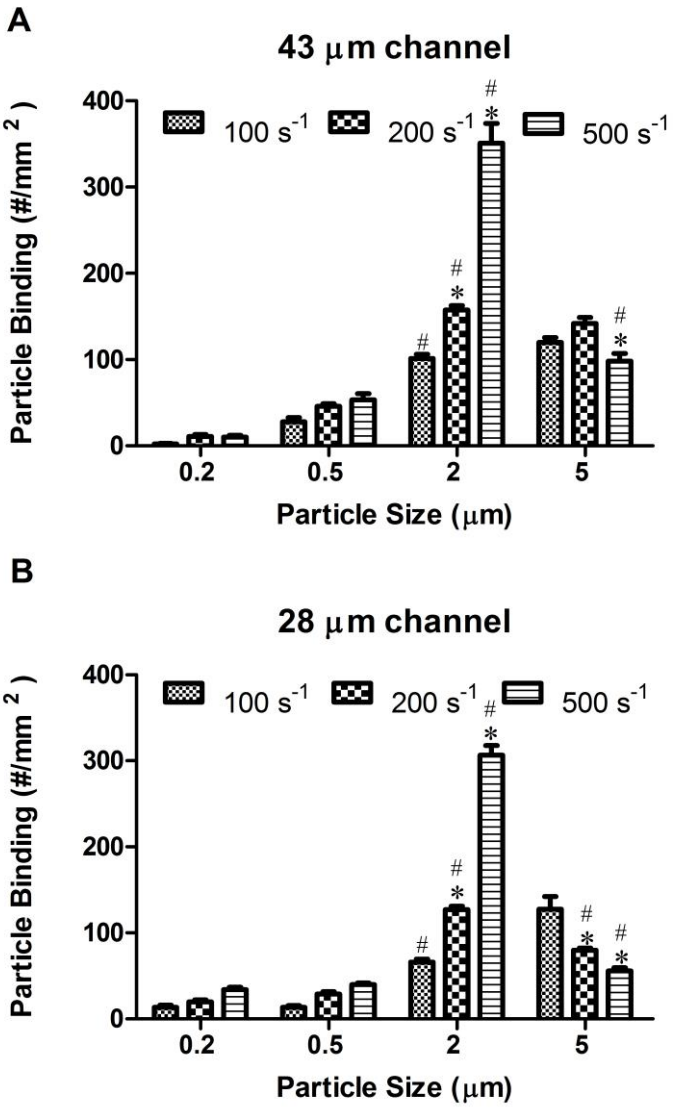

Figure 3-2 Adhesion densities of sLe^A-spheres to EC monolayer from laminar blood flow as a function of wall shear rate (WSR) in the (A) 43 μm and (B) 28 μm height channels. Reconstituted blood at 30% Hct is used. * = $p < 0.05$ compare to binding at the immediate lower WSR and # = $p < 0.05$ compare to binding for the immediate smaller size at the same WSR via one-way ANOVA. $n \geq 3$.

over the EC monolayer at 100 s^{-1} in the 28 μm channel via multiplying adhesion densities for all other conditions by the factor difference between the volumetric flow rates at these conditions and that of flow at 100 s^{-1} in the 28 μm channel. As shown in Figure 3-3, the normalized adhesion densities (i.e. adhesion efficiency) of nanospheres did not significantly change with increases in WSRs from 100 to 500 s^{-1} in both microchannels. For 2 μm spheres, the adhesion efficiency slightly decreased with the WSR increasing from 100 to 200 s^{-1} in the 43 μm channel, but the adhesion efficiency for these spheres did not change with all increases in WSRs in the 28 μm channel. For 5 μm spheres, the adhesion efficiency significantly decreased for all WSR increases in both channels. Overall, the minimal decrease to no change in the adhesion efficiency of nanospheres and 2 μm spheres with WSR increases indicate that these spheres exist in a transport-limited adhesion regime (TLR) at the fixed sLe^A density evaluated [6,22]. In this regime, particle adhesion density increases with increase in WSRs due to the increase in the number of particles, i.e. higher transport of particle, passing over the monolayer at higher WSRs for a fixed experimental time. Conversely, 5 μm spheres exist in a reaction-limited regime (RLR), in which a high slip velocity exhibit by these spheres and higher disruptive force acting on them inhibit their adhesion at high WSRs; hence the decrease in adhesion density observed for the 5 μm spheres as the channel WSR increases. This existence of the 5 μm spheres in the RLR, i.e. poor adhesion kinetics, also explains their significantly lower adhesion relative to 2 μm spheres rather than their poor localization to the wall from RBC core. We have previously shown that sufficiently increasing the ligand site density on particles in the RLR enhances their adhesion kinetics and thus transition their adhesion into the TLR [6].

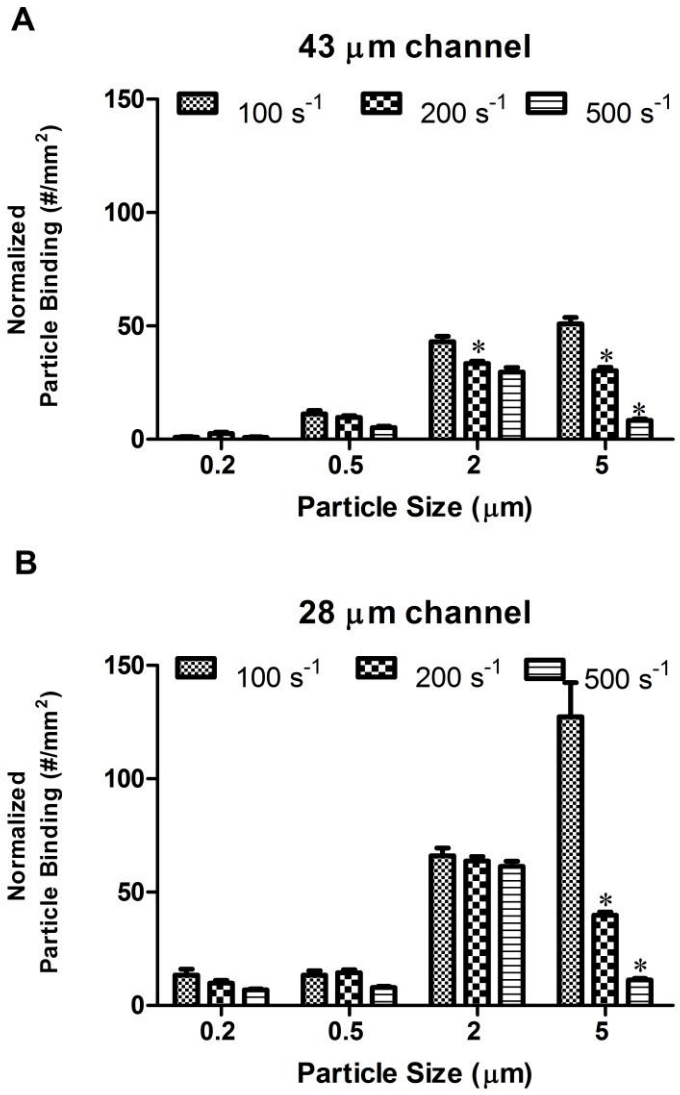

Figure 3-3 Normalized adhesion density of sLe^A-spheres to EC monolayer from laminar blood flow as a function of wall shear rate (WSR) in the (A) 43 μm and (B) 28 μm height channels. Reconstituted blood at 30% Hct is used. Data was normalized to the number of spheres passing over monolayer at 100 s^{-1} in the 28 μm height channel. * = $p < 0.05$ compare to binding of the same size at immediate lower WSR via one-way ANOVA. $n \geq 3$.

Overall, adhesion efficiency trended higher in the 28 μm channel relative to the 43 μm channel for all spheres though these increases were only significant for microspheres (Figure 3-3). The size of the RBC-FL in humans has been reported to be between 2 – 10 μm depending on the vessel size, WSR, and blood hematocrit, where RBC-FL typically decreases with decreasing vessel diameter at a fixed hematocrit [23-24]. Thus, a smaller RBC-FL, and hence a higher local concentration of spheres at a closer proximity to the wall, is anticipated in the 28 μm channel relative to the 43 μm channel. A higher concentration of spheres at the wall would in turn lead to higher adhesion efficiency. The lack of a significant difference in the adhesion of nanospheres in the 28 μm channel relative to the 43 μm channel is again likely explained by their aforementioned minimal localization to the RBC-FL.

3.3.2 Effect of blood hematocrit on sphere adhesion in microchannels

Blood Hct is an important factor that affects flow resistance in microvessels and the formation of the RBC-FL [25]. Thus, we investigated the impact of Hct on the binding of spheres in our microchannel system. Targeted spheres were introduced into channels at 10%, 30%, and 50 % Hct at a fixed WSR of 200 s^{-1}. As shown in Figure 3-4A, the adhesion density of 2 μm spheres significantly increased as the blood Hct increased from 10% to 50% in the 43 μm channel. This observation follows the expectation that a higher blood hematocrit in the flow channel would result in the shrinking of the RBC-FL, due to the enlargement of the RBC core, and hence a higher packing of small spheres closer to the targeted endothelial wall. The significantly steeper response to Hct observed for the adhesion of 2 μm spheres in the 43 μm channel relative to the nanospheres may be a result of the aforementioned minimal localization of nanospheres to the RBC-FL [6]. However,

the larger "RBC-FL-to-diameter" ratio exhibited by nanospheres that results in only modest packing of these spheres closer to the wall with changes in RBC-FL may also contribute to their shallower response relative to 2 μm spheres. The binding density of 5 μm spheres displayed a biphasic response to changes in Hct. The adhesion density of these spheres significantly increased when the Hct was increased from 10% to 30% but significantly decreased with a further increase to 50% Hct (Figure 3-4A). As aforementioned, the RBC-FL with human blood flow *in vivo* is reported to range from 2 -12 μm. Thus, at the 50% Hct evaluated in this study, it is likely that the RBC-FL is on the order of 5 μm or less, in which case 5 μm spheres in the microchannel likely experience "negative collisions" with RBCs in flow at this Hct to create an even higher disruptive force acting on their adhesion to the wall.

In light of the observed decrease in the adhesion of 5 μm spheres at 50% relative to 30% Hct, we sought to determine whether 2 μm spheres would still enjoy an almost linear increase in their adhesion with increase in Hct in the smaller height channel. As shown in Figure 3-4B, 2 μm spheres displayed the same biphasic adhesion pattern in the 28 μm channel as was observed for the 5 μm in the 43 μm channel with a peak adhesion occurring at 30% Hct. This is again consistent with the smaller RBC-FL layer anticipated in the 28 μm channel at higher Hct. The adhesion of 5 μm consistently decreased with increasing Hct from 10 to 50% in the 28 μm channel. Overall, in both channels, microspheres displayed the best adhesion (~3-7 fold higher than that of nanospheres) at the 30% Hct that likely best represents average Hct in human microvessels – lower Hct values than the average systemic Hct (~45% in human) have been reported in microvessels due to the Fahraeus and plasma skimming effects [26].

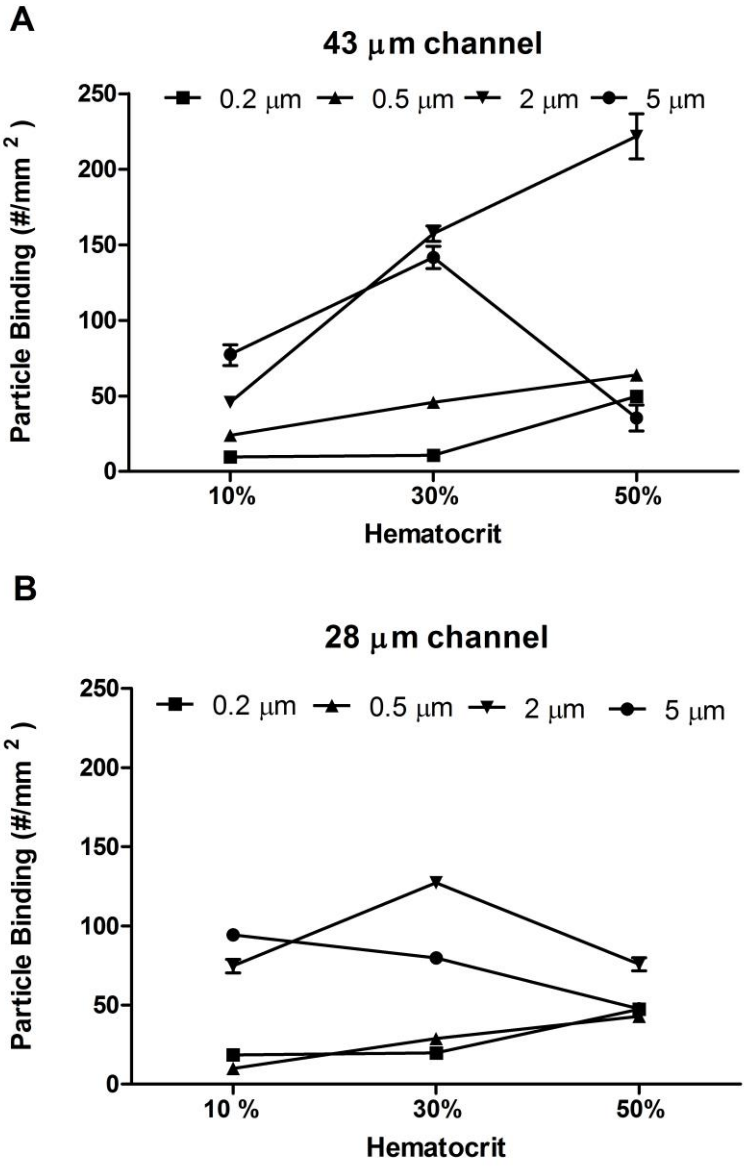

Figure 3-4 Adhesion density of particle as a function of blood hematocrit in the (A) 43 μm and (B) 28 μm height channels with laminar flow at a WSR of 200 s^{-1}. $n \geq 3$ and $p < 0.05$.

3.3.3 Effect of particle concentration on sphere adhesion in microchannels

Previous publications have argued that, owing to their much smaller size, nanoparticles can be injected into the bloodstream at a higher concentration than microspheres and that higher injection concentration would directly translate to their enhanced margination to the vascular wall. Thus, we evaluated the adhesion of all spheres in blood flowing at 200 s^{-1} in the 28 μm channel at 30% Hct (similar condition to Figure 3-2B) with a particle concentration of 2.5×10^6 spheres/ml – 5 times higher concentration than the one used in previous assays. The 28 μm channel is used for this analysis as it is expected to present the most dramatic effect of particle concentration, if present, due to its smaller RBC-FL relative to the 43 μm channel. As shown in Figure 3-5A, microsphere adhesion at the 5 times higher particle concentration was ~4.81 to 5.29 times higher than the adhesion reported in Figure 3-2B, i.e. microspheres maintained similar or slightly better margination at the higher particle concentration relative to the lower concentration. Conversely, the adhesion of nanospheres at the 5 times higher feed concentration was only ~1.96 – 2.62 times higher relative to their adhesion at the baseline particle concentration. This observed non-linear correlation between concentration and adhesion for nanospheres further supports our assertion that nanospheres do not effectively localize to the RBC-FL in bulk blood flow relative to small microspheres. More importantly, a disproportionately higher nanosphere concentration compared to small microspheres would likely be required to deliver similar particle numbers or volume density at the vascular wall, which would be problematic for delivery of highly potent drugs, as the majority of the nanospheres would remain in systemic circulation. While it is possible that the inherent equilibrium position of nanoparticles in the RBC-FL that places them sufficiently far from the wall such that

their adhesion is a weak function of concentration can explain the results shown in Figure 3-5A, a control adhesion experiment with buffer flow show 500 nm particles responding to a 5X increase in concentration in a nearly linear manner and with their response matching that of 2 μm spheres (Figure 3-5B). Furthermore, an observation of the RBC-FL for a 30% Hct blood flow in a PPFC at 200 s^{-1} via confocal microscopy visibly shows 2 μm spheres localizing to the wall at a significantly higher concentration than 500 nm spheres at the same high 5X particle concentration in blood (Figure 3-6). An analysis of the effect of particle concentration in flow on their localization wall via measurement of fluorescent intensity of confocal images also show result similar to Figure 3-5A, where the 500 nm spheres returned a ~2.x fold increase in localization for a 5 fold increase in particle blood concentration while the response was 1:1 for the 2 μm spheres.

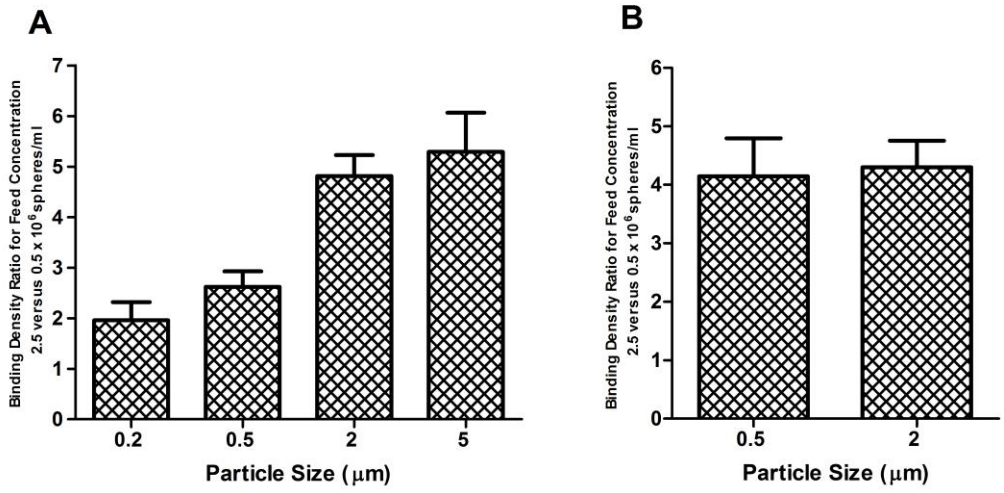

Figure 3-5 The ratio of particle adhesion density for the 2.5 x 10^6 relative to the 0.5 x 10^6 particles/ml feed concentrations in (A) reconstituted blood flow at 30%Hct, and in (B) Phosphate buffered saline at 200 s^{-1} in the 28 μm height channel. $n \geq 3$.

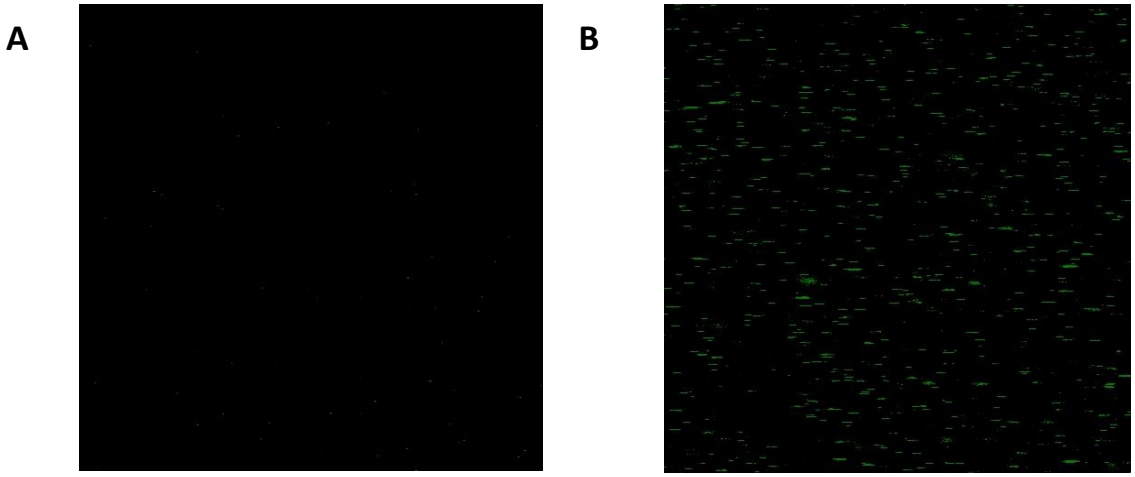

Figure 3-6 The confocal microscopy images of (A) 0.5 μm spheres and (B) 2 μm spheres in 30% Hct blood flow at 200 s^{-1} with the same high 5X particle concentration (2.5 x 10^6 particles/ml). The images were taken at the same plane on bottom surface of the chamber.

In conclusion, we evaluated the adhesion of sLe^A-coated nano- and microspheres to inflamed human endothelial cells from physiological human blood flow in microfluidic channels with dimensions on the order of human microvessels. Microspheres, particularly 2 μm spheres, were found to outperform nanospheres in all hemodynamic conditions evaluated due to the poor ability of the latter to localize to the blood vessel wall from blood flow. The presented work represented the first evidence that nanospheres may not exhibit significant "near wall excess" in microvessels. This finding may be of importance for the design of vascular-targeted carriers for imaging and treatment of cancer. While the majority of targeted delivery systems are designed to target capillaries in tumors, their potential ineffective localization in tumor arterioles and venules is likely consequential since (1) the bulk of blood flow that enters a capillary branching off an arteriole is skimmed from the wall region on the branch side (i.e. plasma skimming effect); therefore, low numbers of nanospheres would enter the capillaries, and (2) in some cases, tumor vasculature has been reported to exhibit a high percentage of arteriolar-to-venular shunt [27]. Thus, there remains a critical need for research to identify ways in which targeted nanosphere delivery to the vascular wall can be enhanced. Nanospheres will likely remain attractive for use as drug carriers due to the ease of their fabrication, their tendency to resist systemic clearance, and their capacity to undergo endocytosis and transcytosis upon contact with the endothelium. One promising avenue may be the use of micrometer-sized carriers to deliver encapsulated nanospheres to the vascular wall. However, this would require a design strategy that tightly balances the timing of microcarrier degradation and, hence, the release of nanospheres with the high rate of systemic clearance that tends to

exist for microspheres in the size range shown in this work. Our ongoing work is exploring this and other possibilities.

References

1. Bendas, G.; Krause, A.; Schmidt, R.; Vogel, J., Selectins as new targets for immunoliposome-mediated drug delivery:: A potential way of anti-inflammatory therapy. Pharm Acta Helv. 1998, 73 (1), 19-26.

2. Muro, S.; Dziubla, T.; Qiu, W.; Leferovich, J.; Cui, X.; Berk, E.; Muzykantov, V. R., Endothelial targeting of high-affinity multivalent polymer nanocarriers directed to intercellular adhesion molecule 1. J. Pharmol. Exp.Ther. 2006, 317 (3), 1161.

3. Sakhalkar, H. S.; Dalal, M. K.; Salem, A. K.; Ansari, R.; Fu, J.; Kiani, M. F.; Kurjiaka, D. T.; Hanes, J.; Shakesheff, K. M.; Goetz, D. J., Leukocyte-inspired biodegradable particles that selectively and avidly adhere to inflamed endothelium in vitro and in vivo. Proc. Natl. Acad. Sci. U.S.A. 2003, 100 (26), 15895.

4. Schnitzer, J. E., Vascular targeting as a strategy for cancer therapy. N. Engl. J. Med. 1998, 339 (7), 472-474.

5. Decuzzi, P.; Lee, S.; Bhushan, B.; Ferrari, M., A theoretical model for the margination of particles within blood vessels. Ann. Biomed. Eng. 2005, 33 (2), 179-190.

6. Charoenphol, P.; Huang, R. B.; Eniola-Adefeso, O., Potential role of size and hemodynamics in the efficacy of vascular-targeted spherical drug carriers. Biomaterials 2010, 31 (6), 1392-1402.

7. Charoenphol, P.; Mocherla, S.; Bouis, D.; Namdee, K.; Pinsky, D. J.; Eniola-Adefeso, O., Targeting Therapeutics to the Vascular Wall in Atherosclerosis-Carrier Size Matters. Atherosclerosis 2011, 217 (2), 364-370.

8. Huang, R. B.; Mocherla, S.; Heslinga, M. J.; Charoenphol, P.; Eniola-Adefeso, O., Dynamic and cellular interactions of nanoparticles in vascular-targeted drug delivery (review). Mol. Membr. Biol. 2010, 27 (7), 312-327.

9. Freitas, R. A., Nanomedicine, volume I: Basic capabilities. Landes Bioscience Georgetown, TX: 1999; Vol. 509.

10. Less, J. R.; Skalak, T. C.; Sevick, E. M.; Jain, R. K., Microvascular architecture in a mammary carcinoma: branching patterns and vessel dimensions. Cancer. Res. 1991, 51 (1), 265-273.

11. Tavana, H.; Zamankhan, P.; Christensen, P. J.; Grotberg, J. B.; Takayama, S., Epithelium damage and protection during reopening of occluded airways in a physiologic microfluidic pulmonary airway model. Biomed. microdevices 2011, 13 (4), 731-742.

12. Eniola, A. O.; Rodgers, S. D.; Hammer, D. A., Characterization of biodegradable drug delivery vehicles with the adhesive properties of leukocytes. Biomaterials 2002, 23 (10), 2167-2177.

13. Brunk, D. K.; Hammer, D. A., Quantifying rolling adhesion with a cell-free assay: E-selectin and its carbohydrate ligands. Biophys. J. 1997, 72 (6), 2820-2833.

14. Burns, A. R.; Walker, D. C.; Brown, E. S.; Thurmon, L. T.; Bowden, R. A.; Keese, C. R.; Simon, S. I.; Entman, M. L.; Smith, C. W., Neutrophil transendothelial migration is independent of tight junctions and occurs preferentially at tricellular corners. J. Immunol. 1997, 159 (6), 2893-2903.

15. Huang, R. B.; Eniola-Adefeso, O., Shear Stress Modulation of IL-1β-Induced E-Selectin Expression in Human Endothelial Cells. PloS One 2012, 7 (2), e31874.

16. Charoenphol, P.; Onyskiw, P. J.; Carrasco-Teja, M.; Eniola-Adefeso, O., Particle-cell dynamics in human blood flow: Implications for vascular-targeted drug delivery. J. Biomech. 2012, 45 (16), 2822-2828.

17 Nagaoka, T.; Yoshida, A., Noninvasive evaluation of wall shear stress on retinal microcirculation in humans. Invest. Ophthalmol. Vis. Sci 2006, 47 (3), 1113-1119.

18 Koutsiaris, A. G.; Tachmitzi, S. V.; Batis, N.; Kotoula, M. G.; Karabatsas, C. H.; Tsironi, E.; Chatzoulis, D. Z., Volume flow and wall shear stress quantification in the human conjunctival capillaries and post-capillary venules in vivo. Biorheology 2007, 44 (5), 375-386.

19. Nigro, P.; Abe, J.; Berk, B. C., Flow shear stress and atherosclerosis: a matter of site specificity. Antioxid. Redox Signaling 2011, 15 (5), 1405-1414.

20. Eckstein, E. C.; Tilles, A. W.; Millero, F. J., Conditions for the occurrence of large near-wall excesses of small particles during blood flow. Microvasc. Res. 1988, 36 (1), 31-39.

21 King, M.R.; Bansal, D.; Kim, M.B.; Sarelius, I.H., The effect of hematocrit and leukocyte adherence on flow directionin the microcirculation. Ann Biomed Eng 2004, 32 (6), 803-814.

22. Patil, V. R. S.; Campbell, C. J.; Yun, Y. H.; Slack, S. M.; Goetz, D. J., Particle diameter influences adhesion under flow. Biophys. J. 2001, 80 (4), 1733-1743.

23. Kim, S.; Ong, P. K.; Yalcin, O.; Intaglietta, M.; Johnson, P. C., The cell-free layer in microvascular blood flow. Biorheology 2009, 46 (3), 181-189.

24. Maeda, N.; Suzuki, Y.; Tanaka, J.; Tateishi, N., Erythrocyte flow and elasticity of microvessels evaluated by marginal cell-free layer and flow resistance. Am. J. Physiol.-Heart C. 1996, 271 (6), H2454-H2461.

25. Pries, A.; Secomb, T.; Gessner, T.; Sperandio, M.; Gross, J.; Gaehtgens, P., Resistance to blood flow in microvessels in vivo. Circ. Res. 1994, 75 (5), 904-915.

26. Pries, A.; Secomb, T.; Gaehtgens, P., Structure and hemodynamics of microvascular networks: heterogeneity and correlations. Am. J. Physiol.-Heart C. 1995, 269 (5), H1713-H1722.

27. Shubik, P., Vascularization of tumors: a review. J. Cancer Res. Clin. 1982, 103 (3), 211-226.

CHAPTER 4

VARIATION IN HEMORHEOLOGY BETWEEN HUMAN AND ANIMAL BLOOD AND THE EFFECT OF BINDING EFFICACY OF VASCULAR-TARGETED DRUG

Abstract

Several animal models are extensively used in experimental research as a mean to understand human diseases and evaluate new therapy. This includes the fields of vascular-targeted imaging and drug delivery. Despite the comparable *in vivo* physiological environment between most animal models and human, there are still many variations that can significantly alter the experimental results obtained with animal models relative to human system, especially, blood composition and physical properties of blood cells. In the vascular-targeted drug delivery field the effects of the variation in hemorheology, hemodynamics and the structure of vasculature between common animal models and human has typically been overlooked. This study aims to investigate the role of hemorheology of various animal models and human on dictating the binding efficiency of spherical vascular-targeted drug carriers (VTCs) at the wall in physiological blood flows. Specifically, the adhesion of sLe^A-coated particles, 0.2, 0.5, 2 and 5 μm, to inflamed endothelial cells monolayers were conducted via a parallel plate flow chamber assay

(PPFC). Particle binding was observed in RBCs-in-buffer (washed red blood cells (RBCs) suspended in saline) and whole blood, in laminar, pulsatile and recirculating flow. Our results suggest that RBCs size compared to the carrier size dictate the particle binding in blood flow. The cell free layer (CFL) width and formation of RBCs core may vary with RBC size and rheology, at fixed hematocrit (RBC volume fraction in blood), and this variation can affect the binding density/trend of particles since the proper ratio of particle size to CFL width is necessary for the optimal particle binding. Additionally, the presence of white blood cells also appears to affect the trend of particle adhesion in different animal species. Overall, this work sheds light on the potential deviation of results investigated *in vivo* by utilizing animal models from what might be the expected outcome in human.

---

* Content of this chapter is being prepared for publication.

4.1 Introduction

To date, vascular-targeted drug delivery remains of tremendous interest for use as an alternative for treating several diseases. To this end, several works have focused on characterizing the capacity for vascular-targeted drug carriers (VTCs) to markedly adhere to a targeted location either via various *in vitro* static and flow assays ranging in complexity from simple buffer to blood flows, e.g. [1-4], or in various animal models of human diseases, e.g. [5-8]. *In vivo* assays are preferentially used due to the many challenges associated with recreating the complexity of the human *in vivo* cellular and biochemical environment with *in vitro* assays. Animals prominently used in drug delivery research include rodents, rabbits, pigs, dogs and monkeys [9-12]. While the pathology of many human diseases can be faithfully represented in these animals at the cellular, and in some cases organ levels, many of them have differences in their physiology relative to human (e.g. vessel size and hemodynamics) that may limit the extrapolation of the generated data to human physiology [13]. This includes differences in shear rates, plasma protein compositions -that affect blood viscosity and red blood cell (RBC) aggregation, and blood cell properties (i.e. size, shape and deformability). The discrepancy in the physiology between laboratory animals and human is likely most critical in the evaluation of particulate delivery systems where the identified differences in hemorheology and hemodynamics impact the distribution and performance of these systems/therapy. Indeed, we recently reported that human RBCs have a significant influence on the binding efficiency of nano- and micro-particles targeted for binding to the inflamed endothelial cells (ECs) under physiological blood flow via in vitro flow assays [2, 8, 14-16]. We showed that small microspheres and micro-rods exhibit a high capacity to marginate

(localize and adhere) to inflamed human ECs at the wall from steady and disturbed human blood flow, while nanospheres and nanorods exhibit limited margination. The observed size effect on the margination of particles is due to the well-documented preferential migration of RBCs away from the wall and alignment at the center of the flow that creates a RBC-free layer (CFL) near the wall. This inward movement of RBCs causes microparticles (as well as micrometer sized leukocytes and platelets) in blood flow to concentrate in the CFL via exclusion, enhancing their collision and contact with the vascular wall. A significant fraction of nanoparticles in bulk blood flow, however, are entrapped within the RBC core resulting in their low margination - i.e. they exhibit a low capacity to localize to the CFL [8]. The CFL width has been reported to vary from 2.5 - 7μm in humans and some small animals depending on the hydrodynamic shear rate of flow, vessel size, the volume fraction of RBC or percent blood hematocrit (% Hct), and the aggregability and deformability of the RBCs [1, 17-20]. Therefore, any subtle differences in the physical properties of RBCs between various animal models that possibly result in their differential lateral migration, and hence the formation of CFL of various sizes, may eventually lead to variations in particle behavior and margination in different animal models.

Variations in RBCs and blood characteristics between human and other common laboratory animals prominent in drug delivery research have been reported, including for mice, pigs, rabbits, dogs and monkeys. For example, the volume, and aggregability of RBCs in mouse blood, a common animal species used for vascular-targeting research, are significantly smaller/lower than in humans [13, 21]. Yet, to date, very limited works have investigated the impact of these variations in hemorheology between animal models and

human on the hemodynamics of particulate carrier systems as it relates to their margination to the vascular wall. Thus, this study aims to elucidate the role of RBC dimension in dictating the binding efficiency of spherical particles of various sizes in blood flow of different patterns. Specifically, we evaluated the adhesion of inflammation-targeted polystyrene spheres in a parallel plate flow chamber (PPFC) to inflamed endothelial cells from physiological flow of RBC-in-buffer (washed RBCs suspended in saline at fixed 40 % Hct) from different animals species and human, rabbit , pig and mouse whole blood. Overall, our results show that the capacity of VTCs to marginate to the vascular wall is significantly influenced by blood flow types and most importantly, RBC size.

4.2 Methods

4.2.1 Preparation of vascular-targeted spheres

The preparation of VCTs in this chapter is described in detail in chapter 3.

4.2.2 Preparation of human endothelial cells (ECs) monolayer

The preparation of human umbilical vein endothelial cells (HUVECs) in this chapter is described in detail in chapter 3.

4.2.3 Preparation of RBC-in-buffer and whole blood (WB)

Human blood was collected from healthy adult donors via venipuncture into a syringe containing citrate anticoagulant (acetate-citrate-dextrose, ACD) same procedures as described in chapter 3.

To prepare human RBCs suspended in saline, a 6% wt dextran-250 solution (1.4 ml/10 mL of blood) was added into anti-coagulated whole blood. This mixture was kept at

room temperature for approximately 2 hr to allow RBCs to sediment separating from the leukocyte-platelet rich plasma layer at the top. RBCs collected from the bottom layer were washed with Dulbecco's phosphate buffered saline (DPBS) three times via centrifugation at 1000 g for 30 min, then the RBC pellet was collected and resuspended in DPBS+ with 1% BSA (flow buffer) to achieve a 40% Hct, i.e. volume fraction of RBCs to plasma [2]. To prepare animal RBCs-in-buffer, isolated pig, cow and rabbit RBCs were obtained commercially (Lampire Biological Lab, Pipersville, PA). For the murine RBC-in-buffer assays, mouse whole blood was collected from surplus mice generously provided by the breeding colony of Unit of Laboratory Animal Medicine (ULAM) according to a protocol approved by ULAM and University Committee on Use and Care of Animals (UCUCA) at the University of Michigan. Briefly, mouse blood was drawn from anaesthetized mice by a cardiac puncture into a syringe containing heparin as an anticoagulant. The obtained animal whole blood was then centrifuged at 1000 g for 30 min to collect RBCs. Isolated RBCs were then washed in DPBS to minimize the excess anticoagulant and/or plasma constituents and were spun down at 1000 g for 30 mins. The RBCs for all animals were then resuspended in DPBS+ with 1% BSA at 40% Hct to yield RBCs-in-buffer.

For whole blood experiments, mouse and rabbit whole blood containing heparin and human whole blood containing ACD were stored at 4°C overnight before use.

4.2.4 Flow adhesion experimental set up

A parallel plate flow chamber (PPFC) equipped with a straight (for laminar and pulsatile flow) or vertical step (for recirculating flow) gaskets forming the flow channel (GlycoTech, Gaithersburg, MD) were used for in vitro flow adhesion assays. Flow assays were constructed as described in a previous publication with minor modifications [2].

Briefly, a single straight gasket or a layered step channel was placed over an activated HUVEC monolayer cultured on a glass coverslip and vacuum-sealed to the flow deck to form the bottom adhesion substrate of the flow chamber assay. Vascular-targeted spheres of a given size suspended in buffer or blood at a fixed concentration of 5 $\times 10^5$ spheres/ml were introduced into the flow channel from an inlet reservoir via a programmable syringe pump (KD Scientific, Holliston, MA).

For laminar flow assays, the wall shear rate (WSR; $\boldsymbol{\gamma_w}$), was computed using the approximation (chapter 3)

$$\gamma_w(s^{-1}) = \frac{6Q}{wh^2} \qquad (1)$$

using the volumetric flow rate (***Q***) through the channel (mL/min), where ***h*** is the channel height (254 μm, unless otherwise noted) and ***w*** is the channel width (1 cm unless otherwise noted).

For pulsatile flow, a programmable syringe pump was used to induce two profiles of pulsatile flow in the horizontal PPFC as previously described [14]. For the first pulsatile profile (Profile I), blood was pulsed about 10 s^{-1} with a net flow in the forward direction. Specifically, the syringe pump was set to run continuous loops with 14 s of forward flow followed by 7 s of backward flow for at total experimental time of 5 minutes. Maximum Q was set at 3.225 mL/min (500 s^{-1}) or 6.45 mL/min (1000 s^{-1}) and WSR(t) computed from Q(t) according to equation (1).

For the second pulsatile profile (profile II), blood was pulsed only in the forward direction from a low WSR of 120 s^{-1} for 4 seconds to a high shear of 1200 s^{-1} for 2 seconds with the total flow time set at 5 min.

Recirculating flow was generated via a vertical-step gasket (VSFC) [24] that formed entrance and main channel heights of 127μm and 508 μm (0.5 cm width), respectively, as previously described [14]. The sudden expansion at the step generates recirculation in flow where a two-dimensional flow with a parallel (V_x) and a normal flow velocity (V_z) with respect to the channel bottom wall is established. The recirculation vortex extends from the step to a reattachment point where V_x=0 and only a negative V_z (pointing toward the bottom wall) is present. Beyond the reattachment, flow moves forward, and a laminar profile is reestablished at far downstream. The flow rate through the VSFC was set such that a laminar WSR of 200 s^{-1} was achieved in the main chamber for 5 min.

Flow adhesion assays were observed on a Nikon TE 2000-S inverted microscope fitted with a digital camera (Photometrics CoolSNAP EZ with a Sony CCD sensor). Digital recording of experiments was via Metamorph analysis software. All adhesion experiments were conducted at 37°C and each cell monolayer was used once.

4.2.5 RBC volume measurement

To determine the average RBC volume for all animal and human blood, 15 ml of whole blood was spun down at high-speed, 1000 rpm, for 30 mins, then the WBC layer and plasma were removed. 1 ml of RBCs, from the bottom part of RBC layer (assuming RBCs were completely packed), were collected and diluted in DPBS buffer (2000X, 5000X and 10,000X). RBCs concentrations were counted by hemocytometer. RBC volumes are calculated based on RBCs/volume. All processes were repeated 3 times.

4.2.6 Data analysis

Particle binding density (#/mm^2) in laminar and pulsatile flow is obtained by manual count of the number of particles bound on the cell monolayer after 5 min of flow and dividing this number by the area of the field of view (20x magnification, A = 0.152 mm^2, unless otherwise stated). For recirculating flow experiments, the number of particles bound downstream of the step channel was counted in 100 μm intervals (area of strip = 0.034 mm^2), as previously described [14]. For adhesion at far downstream where laminar flow is re-established [25], the adherent particles were counted at a distance of 5000 μm from the step. Each data point represents an average of at least three experiments and includes at least five fields of view per experiment. Standard error bars were plotted unless otherwise stated. Differences in adhesion levels were analyzed using a student t test and one-way ANOVA with Tukey post-test. A value of $p<0.01$ was considered statistically significant. To estimate a range of optimal particle size for each flow condition, we used a Monte Carlo method that incorporated the variability in particle size with the binding data [15].

4.3 Results

To study the effect of red blood cell (RBC) size (diameter and volume) on the localization and adhesion of VTCs to the vessel wall, sLe ^{A}-coated spherical particles, 0.2, 0.5, 2 and 5.7 μm diameter, were observed from their binding to inflamed endothelial cells in laminar flow of human, pig, mouse and rabbit RBCs-in-buffer (RBC in buffer at 40% Hct) or whole blood in a PPFC. The average diameter, volume, and the ratio of RBC

volume to diameter (VDR) of the different animal RBCs used are summarized in Table1 [26].

Table 4-1: Red blood cell average dimensions of human and different animal species

Species	Diameter (D)	Volume (V)	VDR
Human	7.3	95	13.88
Rabbit	6.1	76	13.35
Pig	5.81	61	11.17
Mouse	5.8	41	7.55

4.3.1 Effect of RBC size on particle adhesion in laminar flow

Figure 4-1 shows the average binding densities for sLe^A-particles observed in laminar RBCs-in-buffer flows at a wall shear rate (WSR) of 500 s^{-1}. Overall, the adhesion density of microspheres at this shear rate was significantly higher than the adhesion of nanospheres. We should note that for all but the 2 μm particles, adhesion in rabbit and pig's RBCs flow were not significantly different (Table 4-2). When focused on the binding of spheres of a giving size, the adhesion of the 2 μm spheres was found to significantly increase as the RBCs-in-buffer changed from mouse to pig to rabbit following the order of increase in RBC volume (from 41 to 61 to 76 μm^3 , respectively). Nevertheless, the adhesion of the 2 μm spheres in human RBCs-in-buffer flow was significantly lower than the density observed in both rabbit and pig RBCs flows despite the volume of the human RBC, 95 μm, being significantly larger than RBC volume in these animals. However, the binding density of 5 μm particles decreased significantly relative to 2 μm particles in mouse, pig and rabbit RBCs-in-buffer flow while binding increased in the human model. This observation suggest a trend in particle binding with RBC volume, albeit non-linear

one. To further probe how RBC geometry in the different animals affect the flow adhesion of particles of different sizes, we plotted the adhesion density data shown in Figure 4-1A as a function of RBC diameter, RBC volume, and reduced volume (defined as the ratio of the averaged RBC volume, to the volume of a sphere with the same diameter as the RBC), and we found no appreciable trend for particle binding. However, as shown in Figure 4-1B, particle adhesion seems to have a linear relation to the RBC volume to diameter ratio (VDR), except again for larger particles with human RBCs. This particle binding trend in RBCs-in-buffer flows relative to the RBC VDR is similar to the trend observed for particle binding as a function of RBC volume for the different particle sizes (in Figure 4-1A the bars are plotted in the order of increase volume left to right). This would suggest that RBC volume is more important than RBC diameter in the dynamic interactions of RBC and particles in blood flow. However, the lack of a general trend in the effect of RBC volume on binding for all particles sizes, and previous studies where we observed that binding density of particles larger than human RBCs drops drastically (e.g. 10 μm spheres [15]), prompted us to look at whether a correlation exist between particle and RBC size. Figure 4-1C shows the plot of particle binding density as a function of the ratio of particle diameter to RBC diameter, defined as ϕ, where we see a significant correlation. This ratio takes into account not only the size of the particle, but also how it compares to the size of the RBC. There was no clear fit of the data with RBC volume, diameter, reduced volume or VDR. However, when we normalized the particle sizes to the RBC size, we could see a quadratic relation similar to what was observed in [15] for particle binding in human RBC flow as a function of particle size. Thus, we estimated an optimal ϕ range using a Monte Carlo method that incorporates the variability in particles sizes with the binding data using

quadratic fit, as done in [15], which gave surprising results. For example, the optimal range for ϕ in figure 4-1 translates to the range $3.97 < d_{opt} < 4.55$ μm for human RBCs in 40% Hct, with an average R^2 of 0.94, where d_{opt} is the optimal particle diameter for the given flow. This agrees with the range of $3.8 < d_{opt} < 4.4$ μm in 45% Hct given in [15] for human RBC in plasma, as the optimal size decreases with increased hematocrit. For completeness, we looked at the relation between particle binding and the ratio of particle volume to RBC volume, which didn't yield a good fit.

To see if this size effect was the same when all components of blood were present, we ran the experiments with mouse, rabbit, pig and human whole blood flow at 500 s^{-1}. No binding was found for pig's whole blood, which may be linked to interference of proteins or complement in pig blood plasma with particle binding [4]. There was a general decrease in particle binding density in whole blood flow for the rest of the species for microparticles elative to adhesion in RBCs-in-buffer flows, being more pronounced for rabbit. Although a quadratic relation is still observed between ϕ and density binding, an R^2 of 0.75 suggests that non-geometric characteristics of blood, such as the proteins in plasma or number and size of white blood cells (WBCs), play a significant role in particle binding. For example, around 80% of WBCs in rabbits are lymphocytes, which are significantly smaller than a rabbit RBC, whereas the majority of human WBCs are neutrophils, which are almost twice the size of an RBC. This suggests that the large size of neutrophils in humans might aid the migration of particles to the wall.

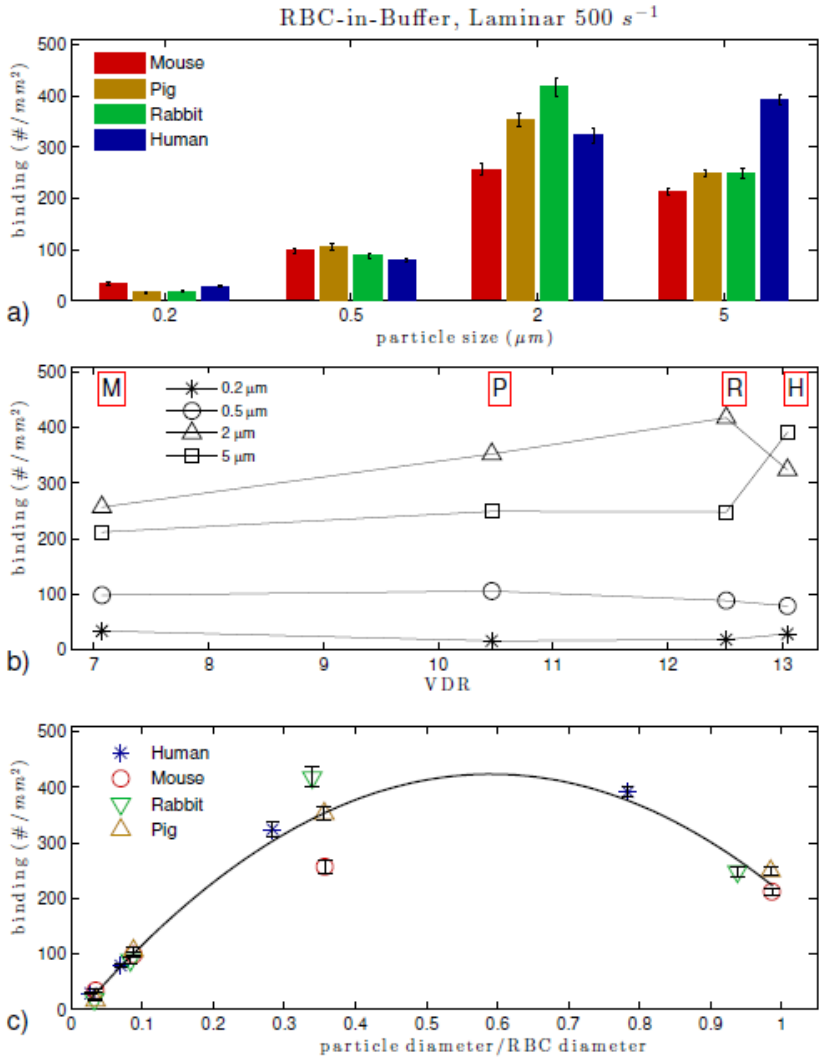

Figure 4-1 Adhesion of sLe^A-particles in human, pig, mouse and rabbit laminar RBCs-in-buffer flow, 40% Hct at 500 s^{-1} WSR (a) histogram, (b) vs VDR and (c) ratio of particle diameter to RBC diameter, $0.57 < \phi_{opt} < 0.65$, ($R^2 = 0.94$).

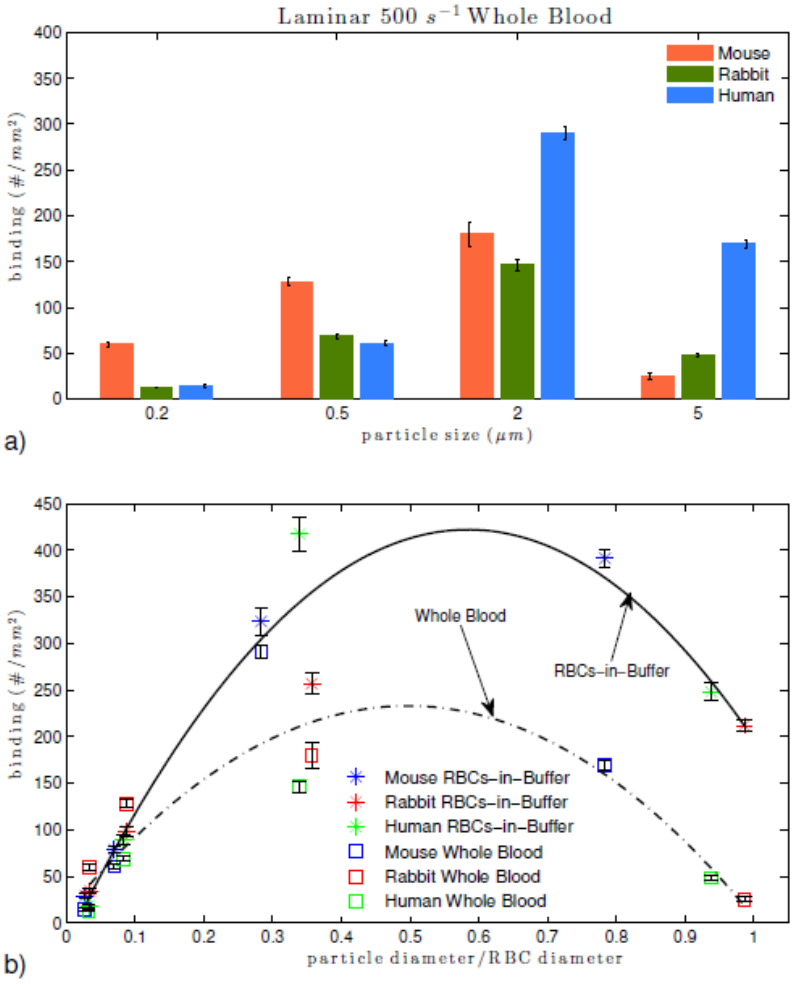

Figure 4-2 Adhesion of sLe^A-particles in human, mouse and rabbit laminar RBCs-in-buffer, 40% Hct, and whole blood flow at WSR 500 s^{-1}: (a) histogram, (b) particle to RBC diameter ratio (RBCs-in-buffer $0.54 < \phi_{opt} < 0.62$, $R^2=0.93$; Whole Blood $0.46 < \phi_{opt} < 0.53$, $R^2 = 0.75$).

4.3.2 Effect of RBC size on particle adhesion in pulsatile flow

To identify if particle binding trend in laminar RBC-in-buffer and blood flow can be generalized for the different flow patterns in circulation, we studied the adhesion of particles in pulsatile flow. First we used pulsatile profile I (described in method section), with mouse, pig, rabbit and human cells. In general, the adhesion levels were lower than in laminar flow due to the smaller volume of blood, thus number of particles that passed through the channel owing to the cycling between low and high shear rate for a fixed experimental time (figure 4-3A). For 0.5 and 2 μm particles, the difference between pig, rabbit and human RBCs-in-buffer flow adhesion levels was not significant (p>.01, see Table 4-2). All the animals followed a quadratic pattern with respect to the ratio ϕ, and no clear relation was found with volume, diameter, reduced volume or VDR as with laminar flow. The whole blood experiments were ran only for human, mouse and rabbit as the laminar flow experiments showed no adhesion in pig's whole blood. There was only a small decrease in adhesion in whole blood experiments compared to RBCs-in-buffer flow trials. This is likely due to the changes in shear force during flow that provides favorable conditions to overcome WBC competition. The quadratic fit of adhesion density vs ϕ yielded an R^2=0.78 for RBCs-in-buffer flow and R^2 = 0.81 for whole blood flow. The optimum particle size was found to be in the range $3.40 < d_{opt} < 4.92$ μm for humans, $2.84 < d_{opt} < 3.28$ μm for rabbits and $2.70 < d_{opt} < 3.12$ μm for mice in RBCs-in-buffer flow. In the case of whole blood the ranges are $3.28 < d_{opt} < 3.80$ μm for humans, $2.61 < d_{opt} < 3.02$ μm for rabbits and $2.75 < d_{opt} < 3.17$μm for mice.

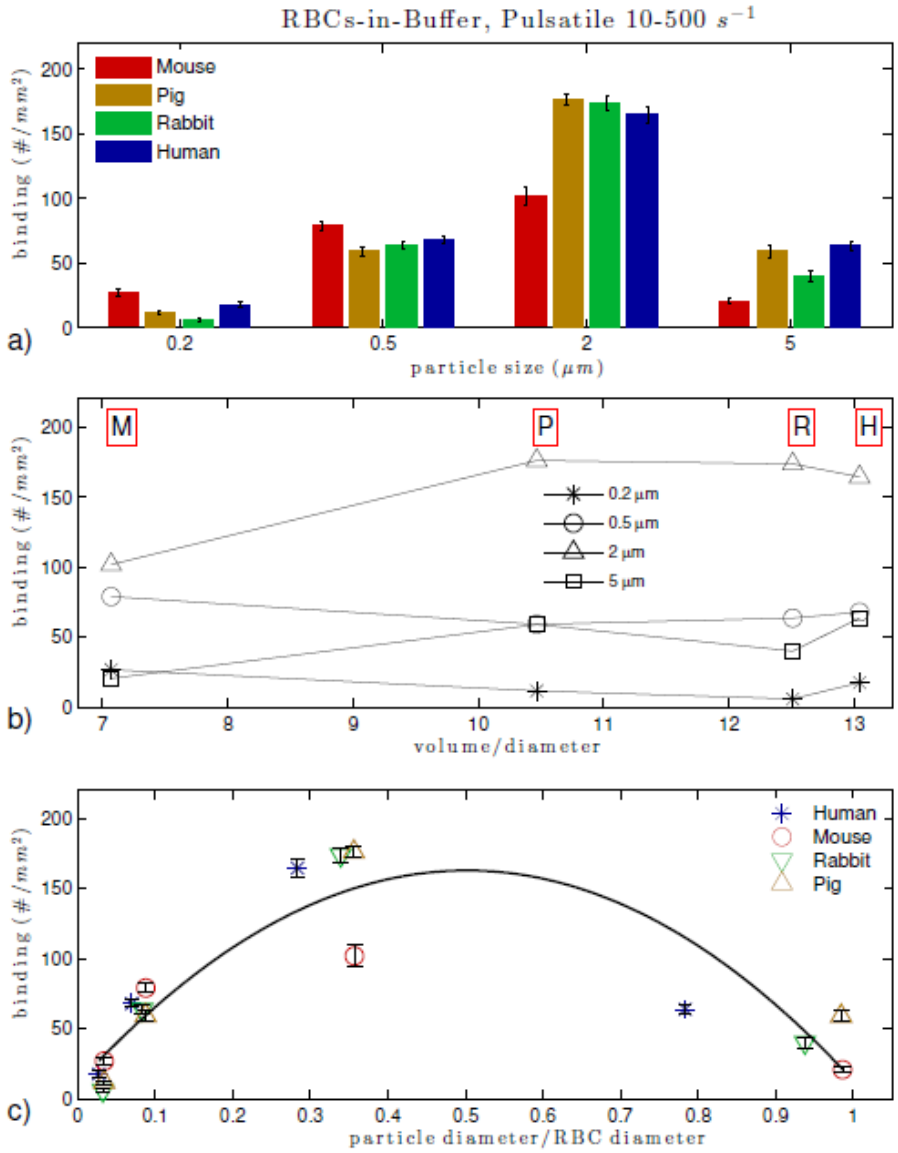

Figure 4-3 Adhesion of sLe^A-particles in human, mouse, pig and rabbit pulsatile RBCs-in-buffer flow at 40% Hct, 10-500 s^{-1} WSR: (a) histogram, (b) plot vs VDR, (c) particle to RBC ratio ($0.47 < \phi_{opt} < 0.54$, $R^2 = 0.78$).

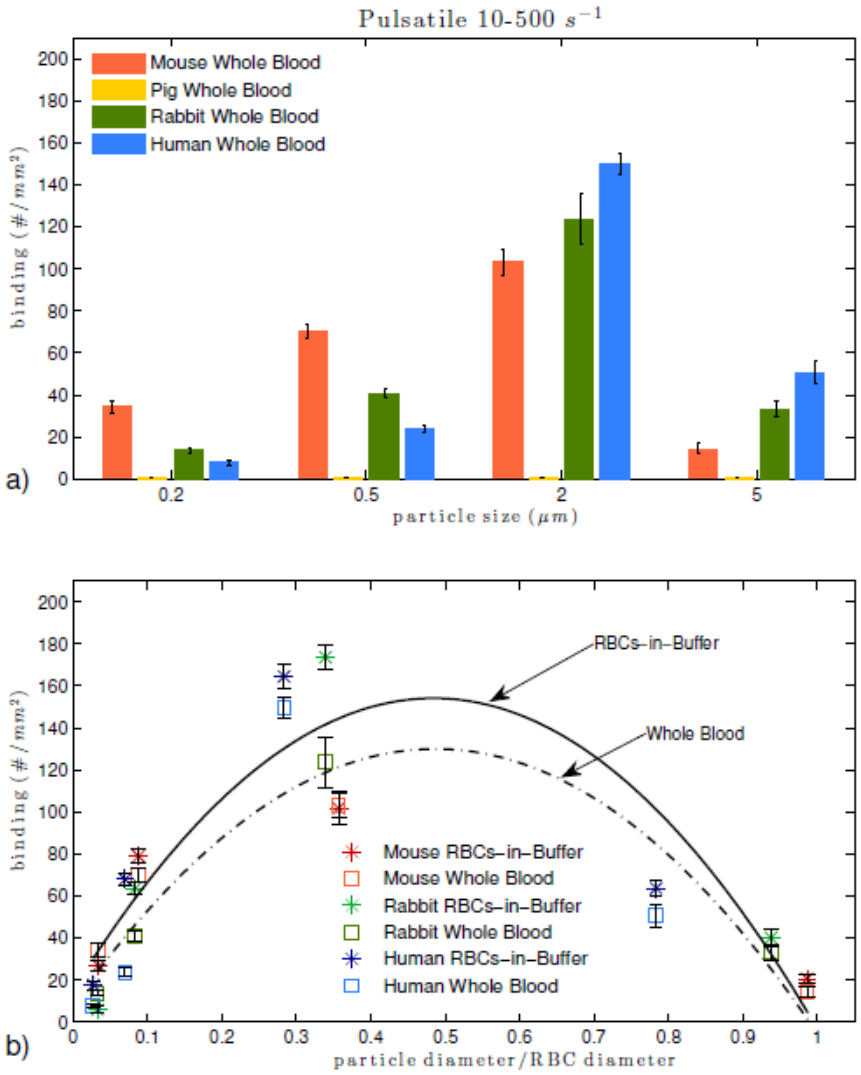

Figure 4-4 Adhesion of sLe^A-particles in human and mouse pulsatile RBCs-in-buffer and whole blood flow at 10-500 s^{-1} WSR: (top) histogram, (bottom) particle to RBC ratio (RBCs-in-buffer $0.45 < \phi_{opt} < 0.52$, R^2=0.78; Whole Blood $0.45 < \phi_{opt} < 0.52$, R^2 = 0.81).

To test further the effect of pulsatile flow, the WSR was fluctuated between 120 s^{-1} and 1200 s^{-1} using human and mouse RBCs-in-buffer flow and whole blood flow (figure 4-5). For both flows, the adhesion levels were higher than at the slower flow, which is somehow expected as the number of particles per experiment increases with WSR. The trend versus ϕ again yields a quadratic fit with an R^2=0.80 for RBCs-in-buffer flow, and R^2= 0.91 for whole blood. The optimal ranges for particle size decreased to $3.36 < d_{opt} < 3.87$ μm for humans and $2.67 < d_{opt} < 3.07$ μm for mice in both RBCs-in-buffer and whole blood flow.

Finally human and mouse whole blood flow was tested at a 50 - 500 s^{-1} fluctuating WSR (figure 6). The trend within each species was the same, with mouse peaking in the range of [2.38, 2.78] and human in [2.99, 3.50]. For 2 μm particles the adhesion density was higher for mouse than human, which didn't occur in any other case.

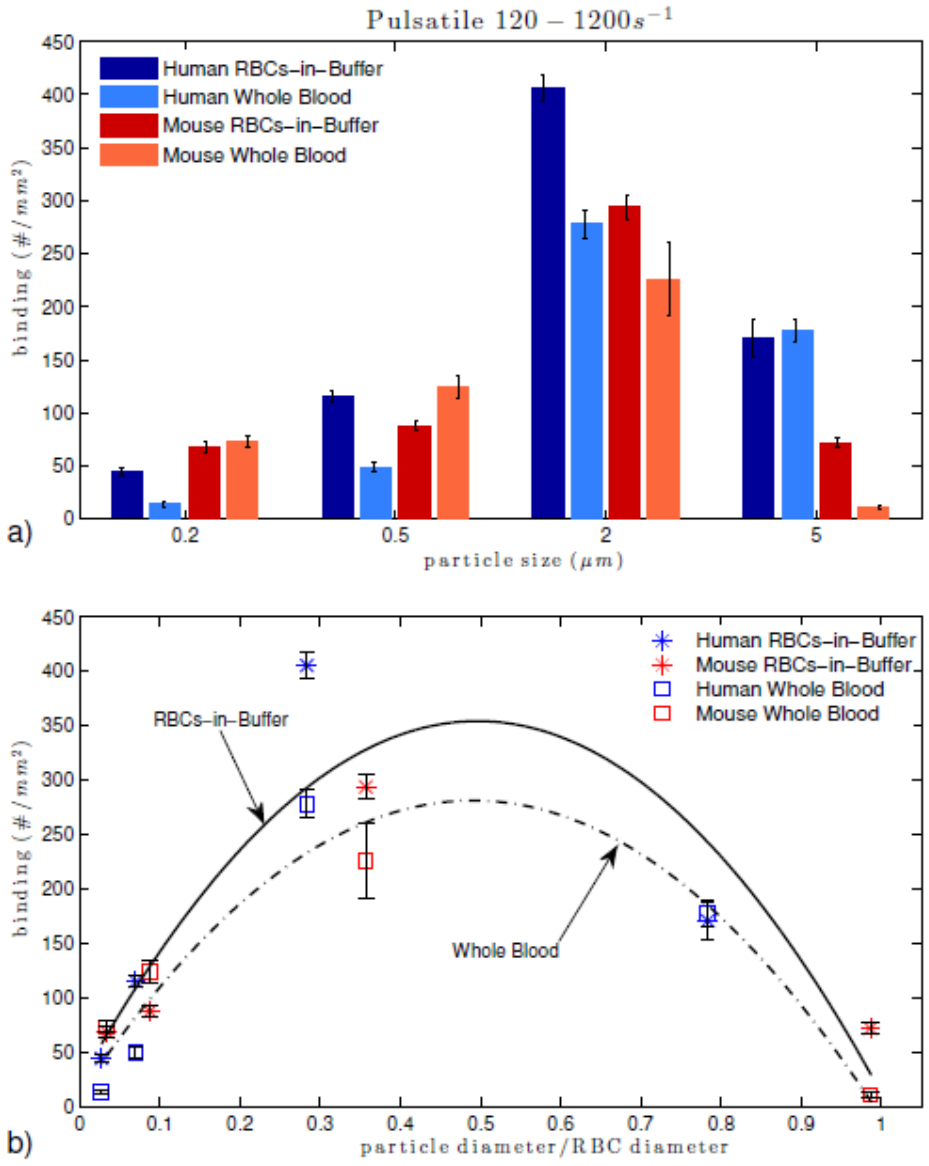

Figure 4-5 Adhesion of sLe^A-particles in human and mouse in pulsatile RBCs-in-buffer and whole blood flow at 40% Hct,120-1200 s^{-1} WSR: (top) histogram, (bottom) particle to RBC ratio (RBCs-in-buffer $0.46 < \phi_{opt} < 0.53$, $R^2 = 0.80$; Whole Blood $0.46 < \phi_{opt} < 0.53$, $R^2 = 0.91$).

4.3.3 Effect of RBC size on particle adhesion in recirculating flow

Recirculating flow was achieved by fitting a step at the entrance of the PPFC yielding a swirling effect. The flow was pumped at a flow rate Q=2.58 ml/min to achieve a WSR of 200 s^{-1} at the point of flow reattachment. We measured the density every 100 μm after the step, and downstream at 5000 μm where the flow stabilizes and behaves as laminar flow. Once again, human, mouse, rabbit and pig's RBCs-in-buffer were tested. In figure 4-6 adhesion densities are plot by size. The 0.2 and 0.5 μm particle adhesion levels are still very low, and no pattern can be discerned. For 2 μm particles, the adhesion levels increased, with rabbit doing better than the other species, while human did best for 5 μm particles, as in the other types of flow. The adhesion peaked around 500 μm from the step for the microparticles. At this location, human, mouse and pig adhesion levels increased with particle size, while rabbit showed a decrease from 2 μm to 5 μm particles (figure 4-7). Although there is still a quadratic pattern with respect to ϕ, the fit was poor with an R^2=0.81.

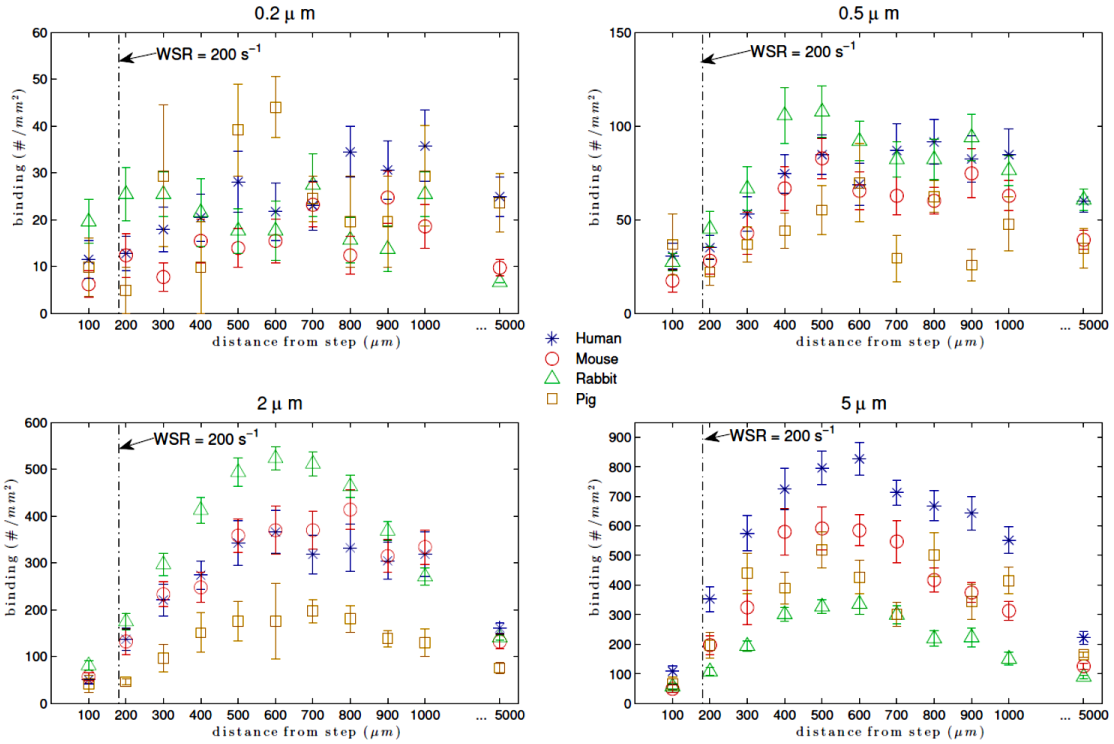

Figure 4-6 Adhesion of sLe^A-particles in human, mouse, rabbit and pig recirculating RBCs-in-buffer flow at 40% Hct, 200 s^{-1}.

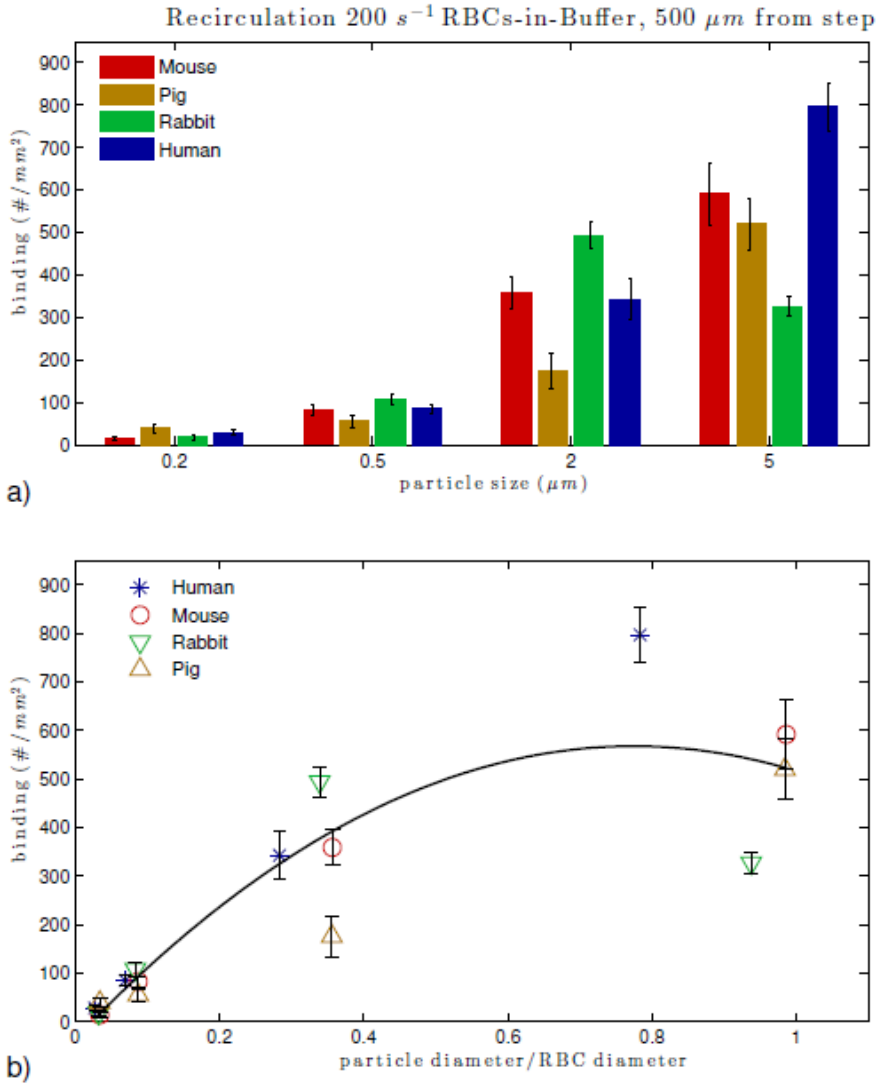

Figure 4-7 Adhesion of sLe^A-particles in human, mouse, rabbit and pig recirculating RBCs-in-buffer flow 40% Hct, 500 µm from step: (a) histogram, (b) particle to RBC diameter ratio ($0.74 < \phi_{opt} < 0.85$, $R^2 = 0.81$) .

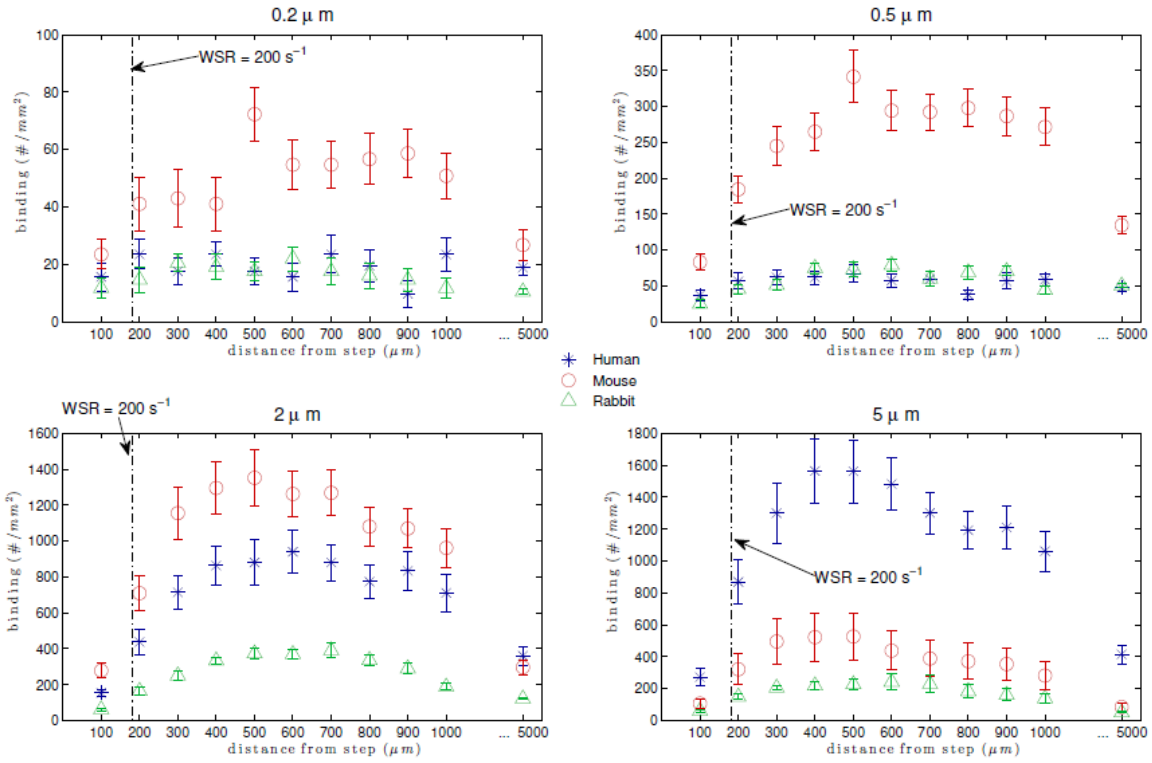

Figure 4-8 Adhesion of sLe^A-particles in human, mouse and rabbit recirculating whole blood flow at 40% Hct, 200 s^{-1}.

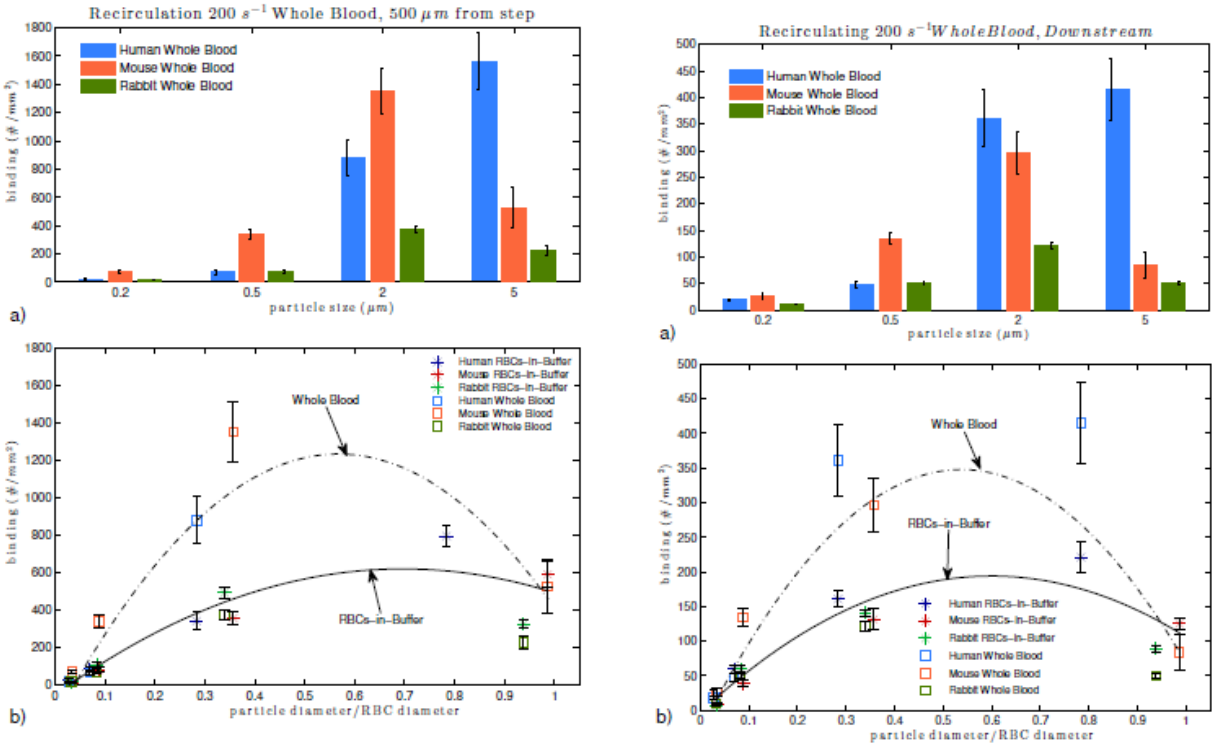

Figure 4-9 Adhesion of sLe^A-particles downstream in human and mouse recirculating flow at 40% Hct, 200 s^{-1}:(a) histogram, (b) adhesion vs particle to RBC diameter ratio (ϕ), (at 500 µm RBCs-in-buffer $0.65 < \phi_{opt} < 0.74$, $R^2 = 0.85$, Whole Blood $0.53 < \phi_{opt} < 0.61$, $R^2 = 0.67$; Downstream µm RBCs-in-buffer $0.49 < \phi_{opt} < 0.57$, $R^2 = 0.87$, Whole Blood $0.44 < \phi_{opt} < 0.51$, $R^2 = 0.67$).

The same analysis was made using whole blood in recirculating flow for mouse, rabbit and human (figure 4-8). Rabbit whole blood has low levels of binding across the board, indicating a WBC effect. Mouse whole blood did particularly well for medium to small particles; 200 nm 500 nm and 2 μm spheres. Particle binding in human whole blood increased along with particle size. Within each particle size, adhesion in human blood peaked around 500 μm from the step (figure 4-8) and declined along far downstream, where it almost tripled decrease of particle binding in downstream to the peak (500 μm from the step)(figure 4-9). It should be noticed that binding in whole blood flow was higher than in RBCs-in-buffer flow both at 500 μm from the step and downstream (figure 4-9), but the optimal range for particle size in human decreased from $5.40 < d_{opt} < 6.21$ μm in RBCs-in-buffer flow, to $4.74 < d_{opt} < 5.40$ μm in whole blood.

4.4 Discussion

Due to the many advantages gained from utilizing imaging modalities and vascular-targeted drug delivery in the early diagnosis and treatment of diseases, several research works have been focused on the design and engineering of the optimal vascular-targeted carriers used to localize contrast and/or therapeutic agents to a target site in several human diseases, including cancer and cardiovascular diseases. To ensure the *in vivo* functionality of designed delivery system, most researchers utilize animal models of human diseases, and this primarily represents the core of preclinical research prior to advancement to clinical testing. Mouse, rat, rabbit, pig, dog and monkey models are extensively used for testing in the preclinical research relating to vascular-targeting [9-12], despite the significant differences in blood rheology, hemodynamics and the vasculature structure of

these animals relative to human [13, 21, 27, 28]. Though the potential correlation and the suggested scaling factor of a particular animal to human, respective to their differences in macroscopic scale (e.g. shear stress) are available [27, 28], limited works have studied the potential implications of the variations in microscopic scale, including different size of blood cells and plasma constituents, on the efficiency of vascular-targeted drug delivery relative to human physiology. The few works that exist have primarily focused on platelet adhesion in high shear laminar flow. In [29], they found differences in platelet adhesion in whole blood flow of different mammalian species via controlled *in vitro* assays. Aarts et al. observed via flow assays with RBCs of various animals that the adhesion of human platelet increased with increasing RBC sizes [30]. Due to the significant influence of RBCs and other blood cells on particle margination in blood flow as thoroughly described in [14-16], it is likely that the distinct hemorheology that exists in animal models relative to humans, particularly the difference of red blood cell (RBC) size, can result in the differential pattern of targeted carrier localization and adhesion (margination) of particles of various sizes to the vascular wall. Herein, the adhesion of sLe^A coated particles, 0.2, 0.5, 2 and 5 μm in diameter, to the inflamed endothelial cells in flow of human, pig, mouse and rabbit RBCs-in-buffer (40% Hct RBCs suspended in saline) and whole blood was observed *in vitro* via parallel plate flow chamber (PPFC) assays with physiological shear conditions. Overall, the presented results showed that the binding efficiency of particles varies with the dimension of RBCs corresponding to different animal models, flow types and blood constituents.

In buffer flow, we know that the discrepancies in particle binding density are due to geometrical properties of their RBCs as there are no other variables present. We showed

that the particle diameter to RBC diameter ratio, ϕ, gives us a good statistical estimate of the effect. Nevertheless, to have a better fit, we would need to be able to vary all length variables in the experiments accordingly, for example, channel height, WSR and even RBCs rigidity, which is not feasible in our *in vitro* experimental setup. Thus, for example, since these adhesion experiments were observed in RBCs-in-buffer at fixed RBC volume fraction in the same channel size (at 40% Hct, which closely represents the *in vivo* conditions in the animals evaluated), a larger number of RBCs with smaller volume, e.g. mouse RBCs, relative to human, would be required to yield the same hematocrit in the same blood volume. Without adjusting the channel height and WSR for each species, formation of RBCs at center of the flow is different depended on the size and volume of RBCs, which would affect the size of the CFL and, therefore, of the particle margination. For this same reason, in whole blood experiments, the fit is not accurate due to the variety of the different blood components on each species, which in turn affects the margination in a non-linear way. Another factor to keep in mind is RBC deformability, as it is known to strongly affect the alignment of RBCs under shear flow, i.e. less rigid RBCs tend to migrate to the center of flow while more rigid RBCs, less susceptible to the shear flow, are likely to stay adjacent to the wall [31]. Even though mouse and pig's RBC average diameter is similar, and thus their corresponding ratios ϕ, there are two significant differences: firstly, mouse RBCs are more deformable than pig RBCs [32]; secondly, pig's average RBCs volume is larger than mouse's RBCs average volume (Table 4-1). These two factors would account for the difference in binding in both species, although there is no discernable pattern in adhesion density relating particle size and either deformability or volume. For instance, in laminar flow (figure 4-1), pig's adhesion is lower for 0.2 μm particles, but

higher for all other sizes, while in pulsatile flow (figure 4-3) pig's adhesion is lower than mouse's adhesion for nanoparticles, and higher for microparticles.

In whole blood flow, it is clear that the difference in adhesion levels depend strongly on the animal species, and therefore, on the specific blood constituents. For instance, in pig's model, there was no binding in any of the flow profiles, which is likely due to pig's protein composition that result in surface absorbed protein hindering the targeting ligands' ability to adhere to the wall [4]. For the other three species, human, mouse and rabbit, the RBCs diameter to particle diameter ration ϕ, still yields a good fit, although there is another effect on mouse and rabbit whole blood. As this effect is not as pronounced as in pig, we looked into the composition of mouse's and rabbit's blood, specifically white blood cells. The majority of mouse's and rabbit's white blood cells are lymphocytes, smaller than the RBCs, while humans have more neutrophils which is twice larger than human RBCs. Our previous study presents that human WBCs interfered with microparticle adhesion on EC [15], so the smaller size and concentration of WBCs may be other factors to dictate particle adhesion which still requires further study to confirm.

Overall, our findings address many important factors that help optimize the margination of micro- and nano-particles in different species. First of all, it showed the relevance of the relative size of the particle to the RBC, so that *in vivo* assays in animals have to be adjusted before applying them to humans. Although the effect of hematocrit was not investigated for the different animal species, this is not expected to affect the trend as we had previously showed that the trend does not change in human [15]. Second of all, although it didn't fully elucidate the role of plasma and other cells' components, it clearly showed that these have an effect in the binding efficiency of vascular-targeted carriers, thus

raising the awareness of potential deviation of results investigated in vivo and the expected outcome in human, which is an important message to many research fields.

Table 4-2: p-value from balance one-way ANOVA, only $p \geq 0.01$ are shown

Figure	Significance (ANOVA)
1	rabbit vs mouse 2 µm p = 0.05; human vs rabbit 0.2 µm p = 0.3, 0.5 µm p = 0.018
2	rabbit vs pig 0.2 µm p = 0.38, 0.5 µm p = 0.14, 5 µm p = 0.94; rabbit vs human 0.5 µm p = 0.21
3	rabbit, pig vs human 5 µm p = 0.015, 2 µm p = 0.30, 0.5 µm p = 0.11; human vs pig 0.2 µm p = 0.033; human vs rabbit 0.2 µm p = 0.012
4	rabbit vs human 2 µm p = 0.3134, 5 µm p = 0.16
5	human (RBCs vs whole blood) 0.2 µm p = 0.48, 2 µm p = 0.067; mouse (RBC vs whole blood) 5 µm p = 0.76
6	all p< 0.001
8	human vs rabbit vs mouse 0.2 µm p = 0.084, 0.5 µm p = 0.14

References

1. Zhang, N., et al., PLGA nanoparticle− peptide conjugate effectively targets intercellular cell-adhesion molecule-1. Bioconjugate chemistry, 2007. 19(1): p. 145-152.

2. Charoenphol, P., R.B. Huang, and O. Eniola-Adefeso, Potential role of size and hemodynamics in the efficacy of vascular-targeted spherical drug carriers. Biomaterials, 2010. 31(6): p. 1392-1402.

3. Klibanov, A., et al., Targeted ultrasound contrast agent for molecular imaging of inflammation in high-shear flow. Contrast media & molecular imaging, 2006. 1(6): p. 259-266.

4. Sobczynski, D.J., et al., Plasma Protein Corona Modulates the Vascular Wall Interaction of Drug Carriers in a Material and Donor Specific Manner. PloS one, 2014. 9(9): p. e107408.

5. McAteer, M.A., et al., Magnetic resonance imaging of endothelial adhesion molecules in mouse atherosclerosis using dual-targeted microparticles of iron oxide. Arteriosclerosis, Thrombosis, and Vascular Biology, 2008. 28(1): p. 77-83.

6. Deosarkar, S.P., et al., Polymeric particles conjugated with a ligand to VCAM-1 exhibit selective, avid, and focal adhesion to sites of atherosclerosis. Biotechnology and bioengineering, 2008. 101(2): p. 400-407.

7. Namdee, K., et al., < i> In vivo</i> evaluation of vascular-targeted spheroidal microparticles for imaging and drug delivery application in atherosclerosis. Atherosclerosis, 2014.

8. Namdee, K., et al., Margination propensity of vascular-targeted spheres from blood flow in a microfluidic model of human microvessels. Langmuir, 2013. 29(8): p. 2530-2535.

9. Hamberg, L.M., et al., Functional CT perfusion imaging in predicting the extent of cerebral infarction from a 3-hour middle cerebral arterial occlusion in a primate stroke model. American journal of neuroradiology, 2002. 23(6): p. 1013-1021.

10. Lazarous, D.F., et al., Comparative effects of basic fibroblast growth factor and vascular endothelial growth factor on coronary collateral development and the arterial response to injury. Circulation, 1996. 94(5): p. 1074-1082.

11. Tolentino, M.J., et al., Intravitreal injection of vascular endothelial growth factor small interfering RNA inhibits growth and leakage in a nonhuman primate, laser-induced model of choroidal neovascularization. Retina, 2004. 24(1): p. 132-138.

12. Moghadasian, M.H., Experimental atherosclerosis: a historical overview. Life sciences, 2002. 70(8): p. 855-865.

13. Windberger, U., et al., Whole blood viscosity, plasma viscosity and erythrocyte aggregation in nine mammalian species: reference values and comparison of data. Experimental Physiology, 2003. 88(3): p. 431-440.

14. Charoenphol, P., et al., Targeting Therapeutics to the Vascular Wall in Atherosclerosis-Carrier Size Matters. Atherosclerosis, 2011.

15. Charoenphol, P., et al., Particle-cell dynamics in human blood flow: Implications for vascular-targeted drug delivery. Journal of biomechanics, 2012.

16. Thompson, A.J., E.M. Mastria, and O. Eniola-Adefeso, The margination propensity of ellipsoidal micro/nanoparticles to the endothelium in human blood flow. Biomaterials, 2013. 34(23): p. 5863-5871.

17. Tateishi, N., et al., Flow dynamics of erythrocytes in microvessels of isolated rabbit mesentery: cell-free layer and flow resistance. Journal of biomechanics, 1994. 27(9): p. 1119-1125.

18. Yamaguchi, S., T. Yamakawa, and H. Niimi, Cell-free plasma layer in cerebral microvessels. Biorheology, 1992. 29(2-3): p. 251.

19. Sharan, M. and A.S. Popel, A two-phase model for flow of blood in narrow tubes with increased effective viscosity near the wall. Biorheology, 2001. 38(6): p. 415-428.

20. Bagchi, P., Mesoscale simulation of blood flow in small vessels. Biophysical journal, 2007. 92(6): p. 1858-1877.

21. Gregory, T.R., Animal genome size database, 2001, TR Gregory.

22. Huang, A.J., et al., Effects of human neutrophil chemotaxis across human endothelial cell monolayers on the permeability of these monolayers to ions and macromolecules. Journal of cellular physiology, 1988. 135(3): p. 355-366.

23. Huang, R.B. and O. Eniola-Adefeso, Shear Stress Modulation of IL-1β-Induced E-Selectin Expression in Human Endothelial Cells. PloS one, 2012. 7(2): p. e31874.

24. Chiu, J.-J., et al., Effects of disturbed flow on endothelial cells. Journal of biomechanical engineering, 1998. 120(1): p. 2-8.

25. Skilbeck, C., et al., Dependence of adhesive behavior of neutrophils on local fluid dynamics in a region with recirculating flow. Biorheology, 2001. 38(2): p. 213-227.

26. Lewis, J.H., Comparative Hemostasis, in Comparative Hemostasis in Vertebrates1996, Springer. p. 325-359.

27. Weinberg, P.D. and C. Ross Ethier, Twenty-fold difference in hemodynamic wall shear stress between murine and human aortas. Journal of biomechanics, 2007. 40(7): p. 1594-1598.

28. Greve, J.M., et al., Allometric scaling of wall shear stress from mice to humans: quantification using cine phase-contrast MRI and computational fluid dynamics. American Journal of Physiology-Heart and Circulatory Physiology, 2006. 291(4): p. H1700-H1708.

29. Grabowski, E., et al., Platelet adhesion to foreign surfaces under controlled conditions of whole blood flow: human vs rabbit, dog, calf, sheep, pig, macaque, and baboon. ASAIO Journal, 1977. 23(1): p. 141-149.

30. Aarts, P., et al., Red blood cell size is important for adherence of blood platelets to artery subendothelium. Blood, 1983. 62(1): p. 214-217.

31. Fedosov, D.A., et al., Blood Flow and Cell-Free Layer in Microvessels. Microcirculation, 2010. 17(8): p. 615-628.

32. Smith, J.E., N. Mohandas, and S.B. Shohet, Variability in erythrocyte deformability among various mammals. Am. J. Physiol, 1979. 236(5): p. 725-730.

CHAPTER 5

PLASMA PROTEINS IN DIFFERENT ANIMALS DIFFERENTIALLY AFFECT THE FUNCTIONALITY OF VASCULAR-TARGETED CARRIER

Abstract

Animal *in vivo* assays in drug delivery research are preferentially compared with human *in vitro* study. However, these animals still have many differentiations relative to humans, which may obstruct the extrapolation to human physiological data such as shear rate, blood cell properties, and plasma protein composition. In this study, we investigate the potential role of different animal plasma proteins in dictating the adhesion efficiency of vascular targeted carriers (VTCs) of different material types to the vascular wall from blood flow *in vitro*. Specifically, PS, PLGA, silica and titanium particles were used as model VTCs in this study, and a monolayer of endothelial cells (ECs) at the bottom wall in a parallel flow channel served as a model vascular wall. The result showed that differences in plasma proteins composition in different species affect the capacity for VTCs to effectively bind to vascular wall in blood flow. The negative adhesion of VTCs was most pronounced with PLGA in all animal blood and for all particle types in porcine blood. This study also show blood composition and blood properties play an importance role for

the binding efficiency of vascular-targeted carrier. Overall, we address the crucial factors of plasma protein-VTC interaction in different animal species with various VTC material types, which impact the validity of animal models for predicting VTCs outcome in human.

* Content of this chapter is being prepared for publication.

5.1 Introduction

Vascular-targeted carriers (VTCs) offers tremendous promise for use as an alternative for diagnosing and treating several human diseases due to the provided benefit of non-invasive and highly localized delivery to the disease area [1, 2]. To date¸ much research on the functionality of VTCs has mainly focused on novel strategies for targeting and drug release formulation [2] that allow for precise delivery and optimal drug release. However, these previous works assume successful VTC margination (localization and adhesion) to vascular wall in the blood flow. Recent publications have highlighted the importance of various physical and surface properties of VTCs, including size, shape and material characteristics, on the capacity to efficiently bind to the vascular wall in flow models ranging in complexity from simple *in vitro* buffer to *in vitro* blood flow assays [3-8] to various animal models of human diseases [9-11]. *In vivo* assays are preferentially used in drug delivery research due to the (1) in ability of *in vitro* systems to fully recreate the complexity of the *in vivo* environment despite access to human tissues and cells *ex vivo*; and (2) the capacity to generate models of many human diseases in these animals at the cellular and molecular. Several animal species are used in drug delivery research, including rodents, rabbits, pigs, dogs and monkeys [12-15]; however, differences in the physiology of these animals relative to humans, such as blood vessel size, blood flow magnitude, blood cell properties (aggregation, deformation, size and shape) and plasma protein composition, may prevent extrapolation of *in vivo* pre-clinical experimental results to clinic application in human [16] . In our recent research studies, we found that the human plasma protein has a negative effect on the vascular wall interaction of vascular-targeted carriers (VTCs) constructed from poly(lactic-co-glycolic-acid) (PLGA) polymer in a donor

(human) dependent manner [17]. However, little is known about the potential differential interaction of other animal plasma protein with VTCs in their bind to vascular wall endothelial cell, which is an essential component in understanding the translation of *in vivo* data to clinical relevance in human.

To date, several publications have highlighted the importance of the plasma corona protein on targeted drug carriers, that differs for carriers of different material types[18], to their *in vivo* functionality; however, these studies have mainly concentrated on opsonization of particles and the impact recognition and clearance from bloodstream by phagocytic cells [19-21]. Only recently have a few works present evidence that particle corona protein characteristics can affect particle ligand-receptor interaction necessary for target recognition/specificity [22-24] . In addition, some studies claimed that persons express different biomolecules and form different corona in their blood [17, 25, 26], and the protein corona also can be applied for cancer diagnostic markers [27]. However, it is not yet known to what extent targeted particle interaction with plasma protein differ in different animal species and how such differences affect the carrier targeting outcome, especially in a complex environment such as blood flow.

In this study, we investigate the differential vascular wall interaction of model VTCs in the flow blood from different animal in order to elucidate the impact of differential plasma protein corona for different material types via *in vitro* assays. Specifically, PS, PLGA, silica and titanium particles were used as VTCs model in this study. We characterize the adhesion of Sle^A conjugated particles to inflamed endothelial cells (overexpressing E-selectin) in laminar blood flow via a parallel plate chamber (PPFC) from different animal species (mouse, rabbit, porcine and human). This study offers the first

evaluation of plasma protein in different animal species to determine how they affect VTCs under blood flow assays.

5.2 Methods

5.2.1. Particle fabrication

Fabrication of 5 μm PLGA sphere, the oil-in-water solvent evaporation technique were applied as previously described [17, 28, 29]. Briefly, 50:50 PLGA polymer with acid (carboxyl) end group (Evoniks; Parsippany, NJ) was dissolved at 2 mg/mL in 20 ml of dichloromethane (DCM) (oil phase), and then the solution was filled in glass syringe and injected into 90 mL of polyvinyl alcohol (PVA)/poly(ethylene-alt-maleic anhydride) (PEMA) solutions (aqueous phase) under mixing batch. The emulsion was stirred for 2 hr in order to evaporate DCM. Subsequently, the emulsion was washed with ID water via differential centrifugation to diminish residual PVA on the particle surface. Finally, the particle solution was frozen and dried on a lyophilizer, and then stored dry at −20°C until use. The 500 nm PLGA spheres were obtained from Phosphorex, Inc. (Hopkinton, MA). These particles were also fabricated from acid (carboxyl)-terminated PLGA polymer with 50:50 glycolic: lactic co-monomer ratio. The caboxylate-modified 500 nm silica spheres were purchased from Nanocomposix, Inc. (San Diego,CA). The 500 nm titanium spheres were procured from EPRUI Nanoparticles and Microspheres Co. Ltd. (Nanjing, China).

5.2.2 Preparation of vascular-targeted particle

Carboxylate-modified polystyrene spheres of 500 nm and 5.0 μm in size (Bangs Laboratories Inc., Fishers, IN) were covalently coupled with NeutrAvidin protein (Pierce

Biotech Inc., Rockford, IL) via carbodiimide (EDAC) chemistry as previously described [3-5]. Briefly, 5 mg/mL NeutrAvidin in 50 mM MES buffer (800 µL) was incubated with avidin-coated spheres ($5.6x10^8$ beads) on rotor for 15 min at room temperature. Then, 75 mg/mL EDAC in 50 mM MES buffer (800 µL) was put in the avidin-particle mixture and adjusted pH to 9.0 via 1M NaOH. After 20 hrs incubation, the reaction was quenched by adding 100 mM glycine (concentration in mixture) and incubating for 30 mins. Avidin conjugated spheres were washed twice and resuspended in 50 mM PBS 1000 µL (50mM sodium dihydrogen phosphate and 50 mM sodium phosphate dibasic, pH 7.4). Particles were kept at 4°C until use.

Avidin-coated spheres were conjugated with biotinylated multivalent sialyl Lewis A (sLe ^{A}; GlycoTech, Gaithersburg, MD) as previously described [3, 4]. Briefly, avidin-coated sphere were incubated with sLe ^{A} in 50 mM PBS with 1% BSA on rotor for 45 mins at room temperature. The concentration of sLe ^{A} for each sphere types was varied to fix the same surface density for all sphere types. After conjugation, spheres were washed twice and resuspended with 1000 µL 50 mM PBS. Sphere surface ligand densities were quantified via BD FACsCalibur. A site density of approximate 1000 to 3000 sites/μm^2 was used for in vitro experiments with sLe ^{A}. All procedures of avidin and sLe^A conjugation were applied to PLGA, Silica and Titanium sphere as well.

5.2.3 Preparation of human endothelial cells (ECs)

The preparation of human umbilical vein endothelial cells (HUVECs) in this chapter is described in detail in chapter 3 via the well-known collagenase perfusion method [30, 31]. Confluent HUVEC monolayers were cultured on coverslips treated with gelatin

cross-linked with glutaraldehyde [32], and then activated with IL-1β at 1 ng/mL for a 4 hr period prior to use for experiments.

5.2.4 Preparation of RBC-in-buffer and whole blood (WB)

Human blood was collected from healthy adult donors via venipuncture as described in detail in chapter 3.

To prepare human RBCs suspended in buffer, whole blood was spun down at 1000g for 30 min via centrifugation. RBCs was collected from the bottom layer, and plasma on the top layer was spun down again at 2250g for 30 min to diminish palettes and WBCs. RBCs layer was washed with PBS 3 three times via centrifugation at 1000 g for 30 min to minimize the excess anticoagulant and/or plasma constituents, then the RBC pellet was collected and resuspended in buffer (DPBS+ with 1% BSA (flow buffer)), viscous buffer (1.4% dextran in flow buffer), or plasma (spun plasma) to achieve a 40% hematocrit (% Hct), i.e. volume fraction of RBCs to plasma [4]. To prepare animal RBCs-in-buffer, isolated pig and rabbit RBCs were obtained commercially (Lampire Biological Lab, Pipersville, PA). For the murine RBC-in-buffer assays, mouse whole blood was collected from surplus mice, generously provided by the breeding colony of Unit of Laboratory Animal Medicine (ULAM) according to a protocol. Mouse procedures were approved by ULAM and University Committee on Use and Care of Animals (UCUCA) at the University of Michigan. Briefly, mouse blood was drawn from anaesthetized mice by a cardiac puncture into a syringe containing heparin as an anticoagulant. All the obtained animal whole bloods were prepared in the same way as human whole blood. For whole blood

experiments, mouse, pig and rabbit whole blood containing heparin and human whole blood containing ACD were stored at 4°C before use.

5.2.5 Flow adhesion experimental set up

A parallel plate flow chamber (PPFC) equipped with a silicon rubber gaskets forming the flow channel (GlycoTech, Gaithersburg, MD) were used for *in vitro* flow adhesion assays. Flow assays were constructed as described in a previous publications [4-6]. Briefly, a single straight gasket was placed over an activated HUVEC monolayer cultured on a glass coverslip and vacuum-sealed to the flow deck to form the bottom adhesion substrate of the flow chamber assay. Vascular-targeted spheres were suspended in buffer or reconstituted blood at a fixed concentration of 5×10^5 beads/mL were introduced into the flow channel from an inlet reservoir via a programmable syringe pump (KD Scientific, Holliston, MA). Flow adhesion were observed on a Nikon TE 2000-S inverted microscope fitted with a digital camera (Photometrics CoolSNAP EZ with a Sony CCD sensor). Digital recording of experiments was via Metamorph analysis software.

For laminar flow assays, the wall shear rate (WSR; γ_w), was computed using the approximation (chapter 3 and 4)

$$\gamma_w(s^{-1}) = \frac{6Q}{wh^2}$$

using the volumetric flow rate (Q) through the channel (mL/min), where h is the channel height (254 µm) and w is the channel width (1 cm). The wall shear stress (τ w - dynes/cm^2) can be calculated by multiplying the WSR by blood viscosity (μ), which is a function of temperature, Q, and blood hematocrit.

5.2.6 Data analysis

Particle binding density (#/mm^2) is obtained by manual count of the number of particles bound on the cell monolayer after 5 min of flow and dividing this number by the area of the field of view (20x magnification, A = 0.152 mm^2) as previously described [5]. The data was collected at a constant position along the length of the chamber for all experiments. Each data point represents an average at least three experiments and includes at least 10 fields of view per experiment. Standard error bars were plotted unless otherwise stated. Differences in adhesion levels were analyzed using a student t test and one-way ANOVA with Tukey post-test. A value of $p<0.01$ was considered statistically significant [6].

5.3 Result

5.3.1 Effect of plasma protein on microsphere adhesion in buffer flows

The purpose of this study is to evaluate the potential role of the plasma protein surface coating on the adhesion of targeted carriers to the vascular wall under flow condition. Polystyrene (PS) and PLGA spheres in 5 μm in diameter were conjugated with Sle^A at the same site density (~1,000 sites/μm^2). Both sphere types were incubated with flow buffer, human plasma, animal plasmas (rabbit, porcine and mouse) for 1 hr before running through the system. After 1 hr, spheres were washed before being introduced into the flow system with PBS buffer. We evaluate the binding efficiency of the sphere to an activated EC monolayer in low shear rate (200 s^{-1}) laminar flow. On average (Figure 5-1), the adhesion of PS microspheres is significantly lower than PLGA

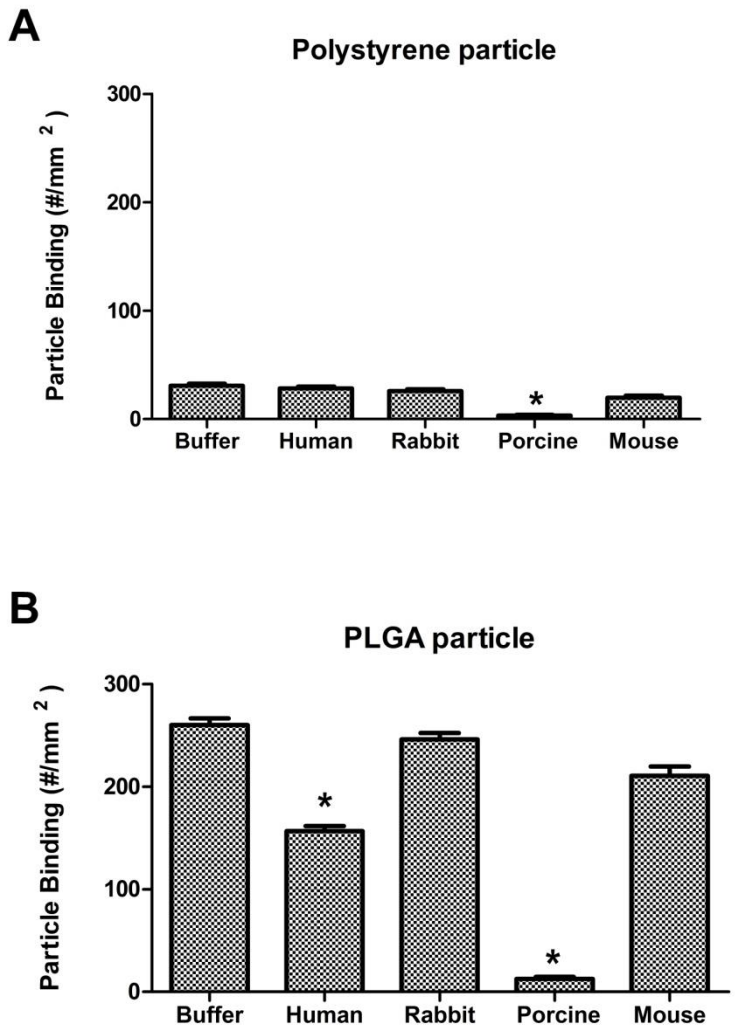

Figure 5-1. The adhesion efficiency of 5 µm spheres from buffer flow to an activated endothelial monolayer. (A) Adhesion of 5 µm polystyrene sphere to HUVEC monolayer under 200 s^{-1} laminar buffer flow for 5 mins, and (B) for 5 µm PLGA sphere. Particles were incubated in buffer (control) and pure plasmas (human, rabbit, porcine and mouse) for 1 hr before operating flow system. Particle concentration = 5e5 spheres/mL. * = $p<0.05$ relative to buffer control trial via one-way ANOVA. $n \geq 3$.

microspheres in a simple flow buffer system, but not for porcine plasma soaked spheres (no significant difference between two sphere types). For the adhesion of PS sphere (Figure5-1A), all conditions have the same level of adhesion as buffer control. However, porcine plasma soaked spheres have 89% lower adhesion relative to the adhesion in buffer soaked spheres. Similarly, the EC adhesion of PLGA sphere opsonized in porcine plasma show radically 99% lower adhesion than their binding level in a simple buffer control as well (Figure5-1B). Moreover, for human plasma opsonized PLGA spheres, adhesion level also displays 41% reduction from the simple buffer (similar result to previous study [17]), while rabbit and mouse plasma immersed spheres show a similar level as the buffer control.

5.3.2 Evaluation of plasma protein and blood component effect to microsphere in blood flow

In this study, adhesions of 5 μm spheres both PS and PLGA were analyzed for several species to validate any variations in particle adhesion that may link to differences in the plasma protein and blood composition of each species. To determine the effect of plasma protein and blood component to particle adhesion under mimic physical conditions, RBCs were introduced into the flow system with viscous buffer (VB) (matching plasma viscosity) in order to increase particle-blood interactions compared to whole blood. Animal and human whole bloods were spun down to separate plasma layer (top part) and WBC (interface layer) out of the RBC layer (bottom part). The RBC layer was washed 3 times with PBS-/- to diminish the excess anticoagulant and plasma constituents. For all species, RBCs were adjusted to 40%hct in VB. Similar to the previous study, particles were opsonized in pure plasma for 1 hr before running the flow experiment with RBCs in VB in order to observe the effect of plasma protein on the particles.

Overall adhesion of polystyrene spheres shows an increase with RBC in VB compared to simple flow buffer (previous study), while an across the broad adhesion of PLGA sphere shows decrease from the previous buffer trial. These results are similar to our previous report [4, 17].

As shown in Figure 5-2A, for the adhesion level of PS spheres in human, the opsonized PS sphere had significant decrease binding compared to RBC in VB and whole blood (35% and 41% reduction, respectively). This result presents the negative plasma protein interference with the PS sphere binding correlated with plasma exposure time (particles were added into whole blood right before running flow assays). On the other hand, for the adhesion efficiency of PS spheres in the rabbit and mouse plasma the negative plasma protein effect on the spheres was absent, yet the binding of particles decreased in whole blood relative to RBC in VB in both rabbit and mouse (28% and 64% reduction, respectively). These results suggest that other blood components (WBCs and platelets) in rabbit and mouse bloods also have the potential role in particle adhesion. Interestingly, the adhesion level of PS particles in porcine declined in both plasma opsonized particle and whole blood relative to RBC in VB, 42% and 95% reduction, respectively. This observation suggests that both plasma protein and blood component have negative effect on particle binding in porcine blood.

Overall, adhesion of PLGA sphere (Figure 5-2B) had a strong negative effect on plasma protein and WBCs rather than the PS sphere. Specially, PLGA adhesion in human whole blood significantly dropped off from human RBC in VB, unlike the PS sphere.

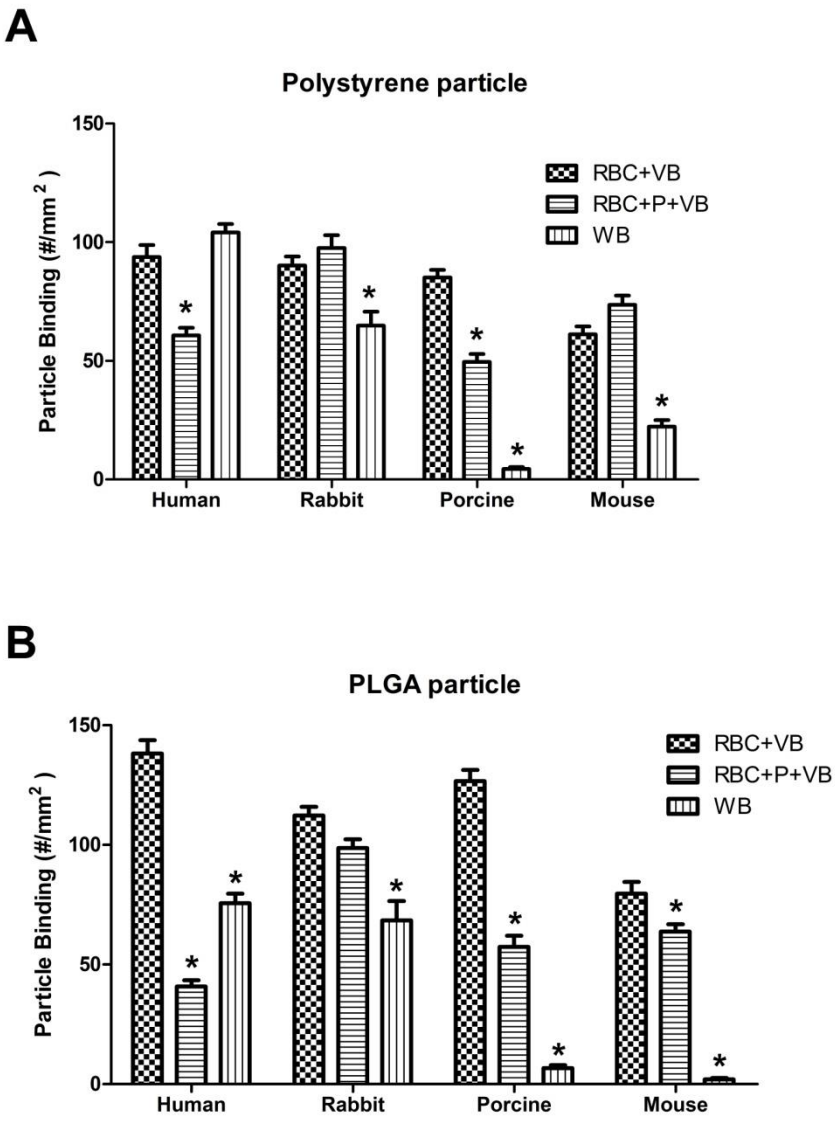

Figure 5-2. Particle adhesion to activated HUVEC in laminar flow of blood at 200 s^{-1} for 5 min. (A) Adhesion of 5 µm polystyrene sphere, and (B) Adhesion of 5 µm PLGA sphere. Both particle types were evaluated in human, rabbit, porcine and mouse blood. RBC+VB = washed RBCs in matched plasma viscous buffer, RBC+P+VB = 1 hr plasma opsonized particle in washed RBCs with matched plasma viscous buffer, and WB = whole blood. Particle concentration = 5e5 spheres/mL. * = $p<0.05$ relative to RBC+VB trial via one-way ANOVA. $n \geq 3$.

Moreover, the plasma protein interference with binding was slightly present in plasma opsonized PLGA microparticles in rabbit and mouse. These results suggest that extent of the negative adhesion effect of plasma protein occurred on PLGA sphere.

To further determine whether the protein absorption on PLGA particle or blood constituent cause more differential adhesion to activated ECs, especially in porcine and mouse blood flow, washed RBCs in pure plasma (cell removed plasma) assay was included in the extended experiment. Figure 5-3A shows a noticeable decrease particle binding in porcine RBCs in plasma and porcine whole blood relative to RBCs in VB and plasma incubated particles (RBC+P+VB). This result shows that the plasma protein corona effect on adhesion of PLGA particle overcomes the effect of other blood components (WBCs and platelet) in porcine blood flow. In contrast to mouse blood (Figure 5-3B), there is no significant difference between adhesions in both mouse plasma opsonized PLGA particle in VB and mouse RBC in plasma, which moderately decrease from mouse RBC in VB (20% and 31% reduction, respectively). However, the adhesion of PLGA sphere is absent in mouse whole blood flow. It exhibits that mouse blood constituent has a potential role in PLGA particle binding rather than mouse plasma protein corona effect.

5.3.3 Evaluation on plasma protein effect to nanoparticles in various material types under blood flow.

According to the previous experiment, the effect of plasma protein absorption on PLGA microparticle adhesion was pronounced in porcine, human and mouse, respectively. To further study whether this observed plasma protein effect distinctly appears in PLGA microparticles or expands to nanoparticles or other material types too,

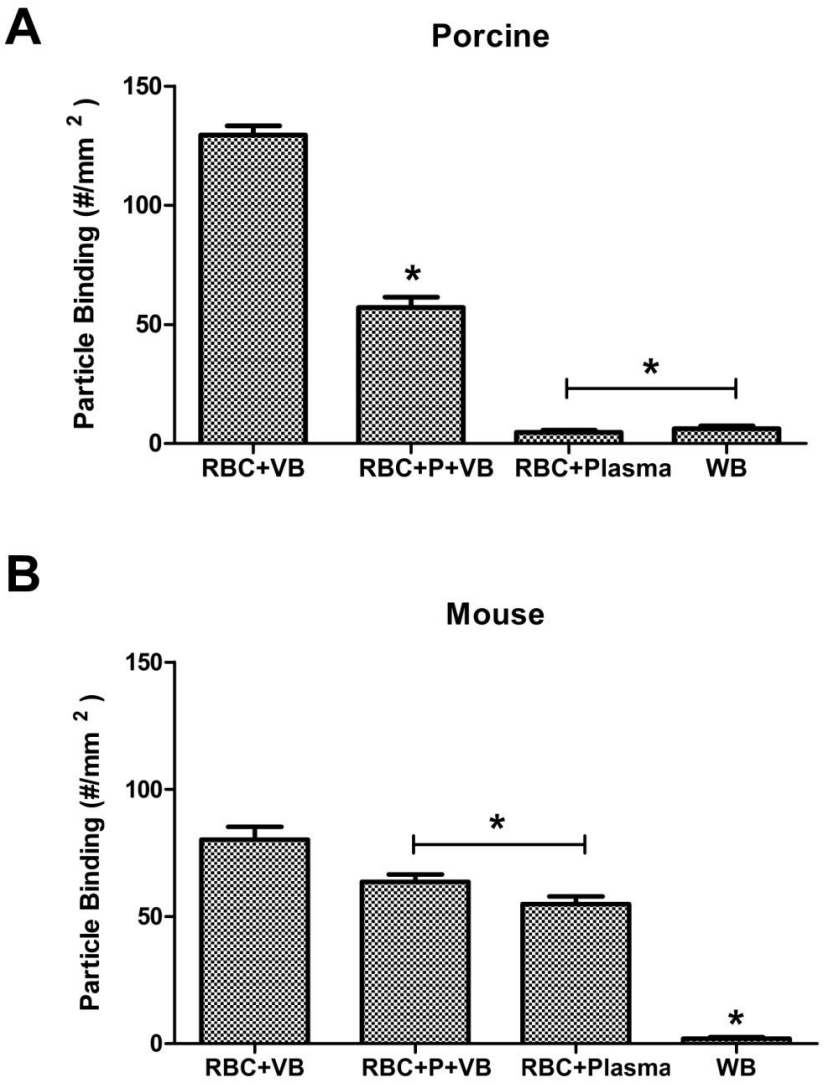

Figure 5-3. Adhesion of PLGA microparticle to activated HUVEC in laminar flow of blood at 200 s^{-1} for 5 min. (A) Porcine blood flow, and (B) Mouse blood flow. RBC+VB = washed RBCs in matched plasma viscous buffer, RBC+P+VB = 1 hr plasma opsonized particle in washed RBCs with matched plasma viscous buffer, RBC+plasma = washed RBCs in pure plasma (cells removed plasma), and WB = whole blood. Particle concentration = 5e5 spheres/mL. * = $p<0.05$ relative to RBC+VB trial via one-way ANOVA. $n \geq 3$.

we evaluated the adhesion of PS, PLGA, silica and titanium nanoparticles (500 nm) to activated ECs from porcine and mouse laminar blood flow similar to the previous experiment.

Similar to previous results, the extent of the negative adhesion effect of porcine plasma protein is more prominent in all material types of nanoparticles compared to mouse plasma (Figure 5-4A). Even though some level adhesion of nanoparticles were observed in silica and titanium nanosphere with porcine RBC in plasma and whole blood trial, these adhesion levels still do not fully recover the adhesion level under buffer conditions. Additionally, the adhesions of 500 nm silica and titanium particle are significant higher than PS and PLGA nanosphere in RBC in VB. This result shows the positive adhesion effect of high density material similar to our previous report.

The adhesion levels of nanospheres in mouse RBC with plasma flow are highest in all material types, and lowest in mouse whole blood flow(Figure 5-4B), which is in contrast to porcine blood flow. This result interestingly reveals that the protein plasma corona effect was absent in adhesion of nanospheres with mouse blood flow; however, mouse blood component still negatively affect the nanoparticle binding which is shown in whole blood results. Moreover, overall adhesions of nanospheres with mouse whole blood flow are higher than adhesion of microparticles (5 μm PS and PLGA spheres), which suggests that nanoparticles are less detached by mouse WBCs and platelets than micro sized particles. In addition, the responsive adhesion of particle to viscosity of buffer is more pronounced in nanoparticles than in microparticles, particularly in mouse blood (small RBC) (Figure 5-5). Therefore, adhesions of nanoparticles in mouse RBC in plasma are significant higher than in VB for all material types (Figure 5-4B).

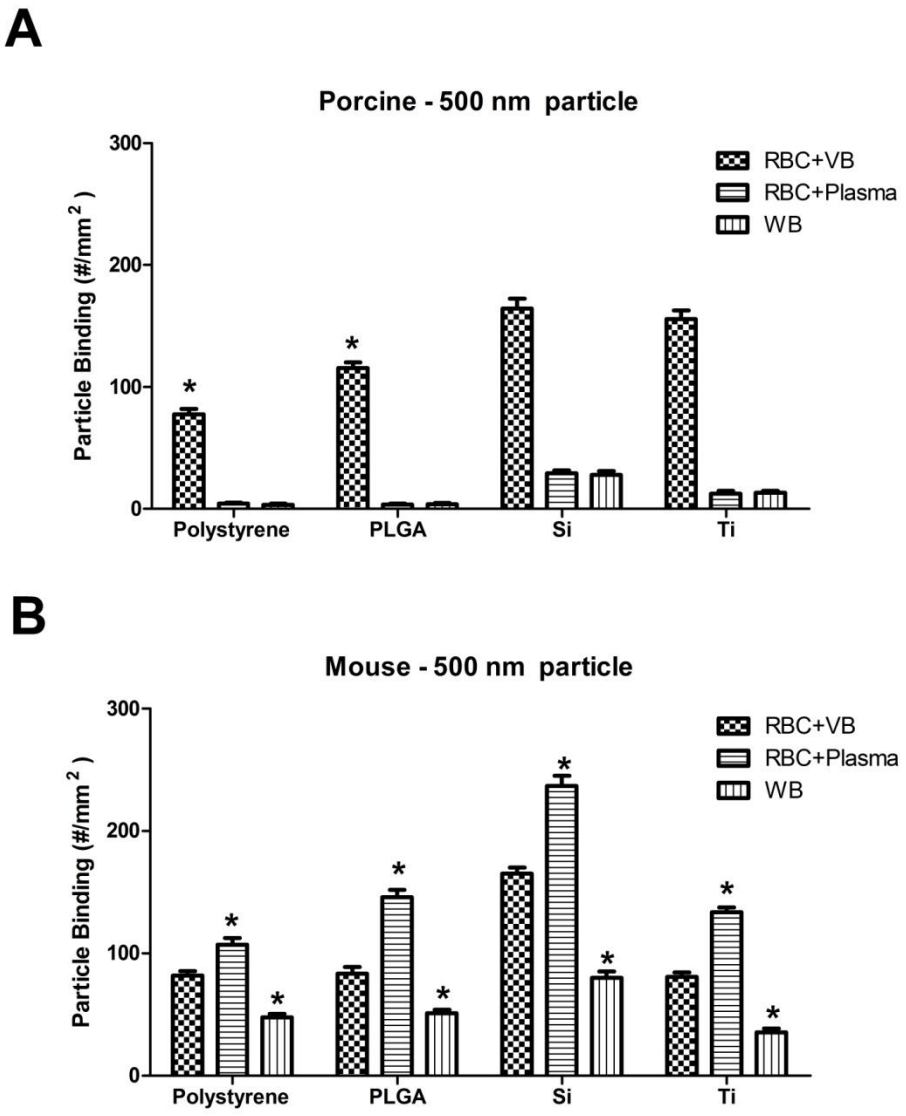

Figure 5-4. Adhesion of nanoparticles (500 nm) to activated HUVEC in laminar flow of blood at 200 s^{-1} for 5 min. There are 4 material types in this set of experiment; polystyrene, PLGA, silica and titanium**.** (A) Porcine blood flow, and (B) Mouse blood flow. RBC+VB = washed RBCs in matched plasma viscous buffer, RBC+plasma = washed RBCs in pure plasma (cells removed plasma), and WB = whole blood. Particle concentration = 5e5 spheres/ml. * = $p<0.05$ relative to RBC+VB trial via one-way ANOAVA. $n \geq 3$.

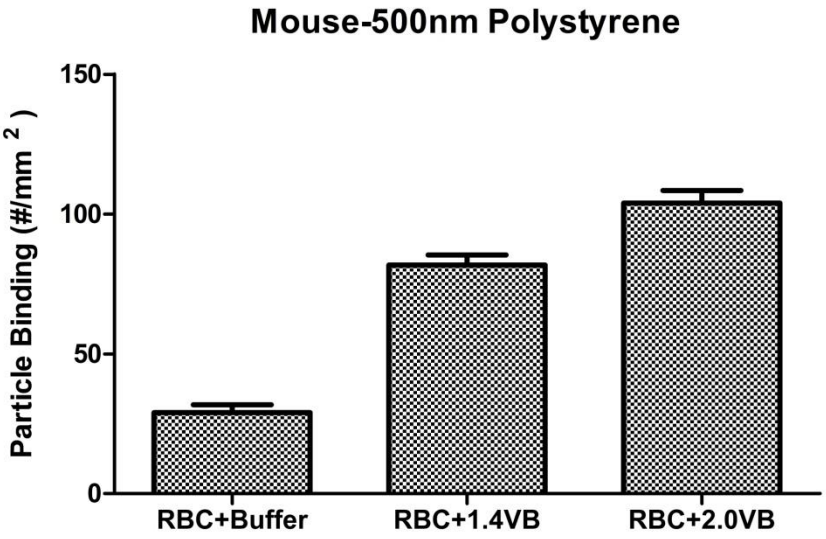

Figure 5-5. Adhesion of polystyrene nanoparticles (500 nm) to activated HUVEC in laminar flow of washed mouse RBCs at 200 s^{-1} for 5 min with different viscosity of buffer (PBS buffer, 1.4%(w/v) Drextran in PBS buffer and 2.0% (w/v)Drextran in PBS buffer).

5.4 Discussion

In biological fluids (plasma or otherwise), a range of proteins associate with VTCs to form a "protein corona" that defines the biological character of the particle. The protein corona formation depends on the geometric and physicochemical properties of the targeted drug carrier, such as size, charge, material type, curvature and targeting moieties on their surfaces [21, 33, 34]. Many recent publications have focused on identification of corona protein composition on plasma opsonized particles and the downstream effect of *in vivo* circulation time and blood clearance; however, few studies have shown that corona protein interferes with the ligand-receptor interaction on particles [22-24]. In particular, there is limited understand on explored how the plasma protein type and composition in different animal species affects particle adhesion in blood flow. In this study, we investigated the role of plasma protein in different animal species on micro and nano particles in various material types under laminar blood flow. The data in Figure 5-1 illustrates that overall adhesions of PS microsphere are significantly lower than adhesion of PLGA microsphere in buffer flow. This result is linked to material density, which is linked when higher density material has more force to break through stream line in flow and marginate to ECs. Therefore, PLGA (1.34 g/cm^3) has higher density than PS (1.05 g/cm^3), resulting in higher binding in PLGA particles. Also, the adhesion of porcine plasma opsonized particles in both PLGA and PS microparticle is radically low compared to other species. We conclude that porcine plasma has a strongly negative protein effect on the adhesion of microparticles, and it may form different corona protein compositions from other species on the surface of the particles as well. Additionally, human plasma soaked PLGA microparticle exhibit reduced vascular wall binding relative to buffer control, which exhibits the critical negative

plasma proteins specific to material type (PLGA particle). This effect is not observed for PS microspheres, which is supported by our previous study as well [17]. Our results are similar to other reports, which claim that different material types affect the different adsorbed corona proteins on particles with the same size and surface charge [17, 18].

In a further study, we introduced blood cell and matched plasma viscous buffer with particles into flow assays. The particle-blood cell interactions have previously been reported between microspheres and RBCs and WBCs [6]. The adhesion of 5 μm PS particles drastically increase in laminar flow when adding RBCs into the flow which is also shown in Figure 5-2A for all PS microparticles binding. The data (Figure 5-2) agrees with the buffer flow study that showed porcine plasma has a strongly negative effect on the adhesion of particles. Moreover, the significant decrease of both PS and PLGA microspheres in human plasma soak particles comparative to whole blood and viscous buffer implies that the negative protein depends on plasma exposure time, which also was revealed in the previous study [17]. The negative plasma protein effect to particle binding is still more pronounced for the PLGA microparticle (both human and porcine) compared to PS in general. Interestingly, the negative protein effect is completely absent in rabbit and mouse plasma in PS microparticle binding and has a slight effect on PLGA microparticle binding; however, all these adhesions are significantly lower in whole blood flow relative to RBC in VB both rabbit and mouse. This result suggests that there are other components in blood beyond RBCs and plasma proteins affecting microparticle binding. WBCs and platelets might play a potential role in particle margination under blood flow. Chareonphol *et al.* reported that leukocytes can cause the collision-induce removal of bound microsphere or the enhancement of microsphere binding depending on share rate,

blood flow pattern and %hct [6]. In an extended study, washed RBCs in pure plasma was included in the experiment. Our results show that the effect of plasma protein is dominant for the negative adhesion of PLGA microparticles in porcine blood, but the reduced adhesion of particle in mouse whole blood is mostly due to the impact of other blood cell components (WBCs and platelets).

Some studies have found that for copolymer, gold, or other metal nanoparticles with various diameters, the amount of absorbed protein on surface varied with size and surface curvature, and the qualitative changes of protein also depend on the size of the particles in the obtained corona protein[17, 18, 21]. The potential explanation is a larger ratio of surface to volume which allows more protein to bind to smaller particles than to particles of larger sizes, and total surface area differences [17, 21]. Moreover, some investigators also pointed out that nanoparticles with different material and different sizes are associated with different corona proteins [35]. Therefore, we included nanoparticles (500 μm sphere) of various materials (PS, PLGA, silica and titanium) in our expanded study. The strong negative adhesion effect of porcine plasma protein to particle is still observed in all material types of nanoparticles, but silica and titanium nanospheres slightly recover from this effect. The results suggest that porcine plasma may consist of a variety and a larger amount of protein than other species, which can be associated with biomaterial forming broad corona protein layers and also interfere with targeting moieties on the material surface. On the other hand, the negative plasma protein effect to nanoparticle adhesion absent in mouse blood relative to porcine blood. The distinction of negative plasma protein effect on particle adhesion is less pronounced for nanospheres evaluated in mouse blood likely because adhesion can be overcome by an induced effect of a blood cell-particle interaction for

nanoparticles. We previously reported that the adhesions of 500 nm particles show a significant increase in mouse blood which has small RBCs relative to other species blood [chapter 4]. Therefore, herein the adhesion of nanoparticles in mouse whole blood also shows an increase compared to adhesion of microparticles similar to the previous study [chapter 4]. However, the significant difference in the adhesion of nanoparticles in mouse whole blood and mouse RBCs in plasma assays suggests that the mouse blood component still has a negative effect compared to nanoparticle adhesion which is not shown in human whole blood [6]. In mouse blood composition, the main component of the mouse's WBCs is lymphocytes which is smaller than mouse RBCs, while humans have more neutrophils which are twice as large as human RBCs. As mentioned above, human WBCs interfere with microparticle binding [6], so the smaller size of WBCs may interfere with particle adhesion as well. Additionally, the adhesion of nanoparticles in mouse RBCs in VB (matched with human plasma) is lower than in mouse RBCs in plasma and data from Figure 5-5 would suggest that the viscosity of plasma is another factor which dictates nanoparticle adhesion; however this requires further study in order to be verified.

In conclusion, our study addresses many potential factors that concern the adhesion of micro and nanoparticles in different species which can be translated to human data. First, the study shows that the plasma proteins in different species affect the different level of particle binding, especially in porcine which shows strong negative effect to particle adhesion. This crucial factor is a matter of concern for further *in vivo* studies in animal model or pre-clinical trials for drug delivery. Second, this study shows blood composition (RBCs and WBCs) and blood properties (size) play an importance role in the binding efficiency of vascular-targeted carriers. Third, using different material types of particles

causes in differences in corona protein formation which interfere with particle adhesion. Lastly, although it's not clear what role the viscosity of plasma on nanoparticle binding, our study shows that it has an effect on the adhesion of nanoparticles with small RBCs as mouse blood. Overall, by addressing the crucial factors of plasma protein- particle interaction in different animal species with various material types of particles, we reveal potential deviation of results in animal models and the predictable outcome in humans. This is an important for many research fields, particularly, drug delivery and diagnostics in cardiovascular.

References

1. Psarros, C., et al., Nanomedicine for the prevention, treatment and imaging of atherosclerosis. Maturitas, 2012. 73(1): p. 52-60.

2. Hajitou, A., R. Pasqualini, and W. Arap, Vascular targeting: recent advances and therapeutic perspectives. Trends in cardiovascular medicine, 2006. 16(3): p. 80-88.

3. Thompson, A.J., E.M. Mastria, and O. Eniola-Adefeso, The margination propensity of ellipsoidal micro/nanoparticles to the endothelium in human blood flow. Biomaterials, 2013. 34(23): p. 5863-5871.

4. Charoenphol, P., R.B. Huang, and O. Eniola-Adefeso, Potential role of size and hemodynamics in the efficacy of vascular-targeted spherical drug carriers. Biomaterials, 2010. 31(6): p. 1392-1402.

5. Charoenphol, P., et al., Targeting Therapeutics to the Vascular Wall in Atherosclerosis-Carrier Size Matters. Atherosclerosis, 2011.

6. Charoenphol, P., et al., Particle-cell dynamics in human blood flow: Implications for vascular-targeted drug delivery. Journal of biomechanics, 2012.

7. Klibanov, A., et al., Targeted ultrasound contrast agent for molecular imaging of inflammation in high-shear flow. Contrast media & molecular imaging, 2006. 1(6): p. 259-266.

8. Zhang, N., et al., PLGA nanoparticle− peptide conjugate effectively targets intercellular cell-adhesion molecule-1. Bioconjugate chemistry, 2007. 19(1): p. 145-152.

9. McAteer, M.A., et al., Magnetic resonance imaging of endothelial adhesion molecules in mouse atherosclerosis using dual-targeted microparticles of iron oxide. Arteriosclerosis, Thrombosis, and Vascular Biology, 2008. 28(1): p. 77-83.

10. Namdee, K., et al., < i> In vivo</i> evaluation of vascular-targeted spheroidal microparticles for imaging and drug delivery application in atherosclerosis. Atherosclerosis, 2014.

11. Deosarkar, S.P., et al., Polymeric particles conjugated with a ligand to VCAM-1 exhibit selective, avid, and focal adhesion to sites of atherosclerosis. Biotechnology and bioengineering, 2008. 101(2): p. 400-407.

12. Hamberg, L.M., et al., Functional CT perfusion imaging in predicting the extent of cerebral infarction from a 3-hour middle cerebral arterial occlusion in a primate stroke model. American journal of neuroradiology, 2002. 23(6): p. 1013-1021.

13. Lazarous, D.F., et al., Comparative effects of basic fibroblast growth factor and vascular endothelial growth factor on coronary collateral development and the arterial response to injury. Circulation, 1996. 94(5): p. 1074-1082.

14. Katz, L.N., Experimental atherosclerosis. Circulation, 1952. 5(1): p. 101-114.

15. Tolentino, M.J., et al., Intravitreal injection of vascular endothelial growth factor small interfering RNA inhibits growth and leakage in a nonhuman primate, laser-induced model of choroidal neovascularization. Retina, 2004. 24(1): p. 132-138.

16. Weinberg, P.D. and C. Ross Ethier, Twenty-fold difference in hemodynamic wall shear stress between murine and human aortas. Journal of biomechanics, 2007. 40(7): p. 1594-1598.

17. Sobczynski, D.J., et al., Plasma Protein Corona Modulates the Vascular Wall Interaction of Drug Carriers in a Material and Donor Specific Manner. PloS one, 2014. 9(9): p. e107408.

18. Deng, Z.J., et al., Differential plasma protein binding to metal oxide nanoparticles. Nanotechnology, 2009. 20(45): p. 455101.

19. Monopoli, M.P., et al., Physical− chemical aspects of protein corona: relevance to in vitro and in vivo biological impacts of nanoparticles. Journal of the American Chemical Society, 2011. 133(8): p. 2525-2534.

20. Yan, Y., et al., Differential roles of the protein corona in the cellular uptake of nanoporous polymer particles by monocyte and macrophage cell lines. ACS nano, 2013. 7(12): p. 10960-10970.

21. Lundqvist, M., et al., Nanoparticle size and surface properties determine the protein corona with possible implications for biological impacts. Proceedings of the National Academy of Sciences, 2008. 105(38): p. 14265-14270.

22. Mirshafiee, V., et al., Protein corona significantly reduces active targeting yield. Chemical Communications, 2013. 49(25): p. 2557-2559.

23. Salvati, A., et al., Transferrin-functionalized nanoparticles lose their targeting capabilities when a biomolecule corona adsorbs on the surface. Nature nanotechnology, 2013. 8(2): p. 137-143.

24. Fleischer, C.C., U. Kumar, and C.K. Payne, Cellular binding of anionic nanoparticles is inhibited by serum proteins independent of nanoparticle composition. Biomaterials science, 2013. 1(9): p. 975-982.

25. Anderson, N.L., et al., The human plasma proteome. Mol Cell Proteomics, 2004. 3(4): p. 311-326.

26. Boraschi, D., L. Costantino, and P. Italiani, Interaction of nanoparticles with immunocompetent cells: nanosafety considerations. Nanomedicine, 2012. 7(1): p. 121-131.

27. Huo, Q., et al., A facile nanoparticle immunoassay for cancer biomarker discovery. J Nanobiotechnology, 2011. 9: p. 20.

28. Heslinga, M.J., E.M. Mastria, and O. Eniola-Adefeso, Fabrication of biodegradable spheroidal microparticles for drug delivery applications. Journal of Controlled Release, 2009. 138(3): p. 235-242.

29. Watts, P., M. Davies, and C. Melia, Microencapsulation using emulsification/solvent evaporation: an overview of techniques and applications. Critical reviews in therapeutic drug carrier systems, 1989. 7(3): p. 235-259.

30. Huang, R.B. and O. Eniola-Adefeso, Shear Stress Modulation of IL-1β-Induced E-Selectin Expression in Human Endothelial Cells. PloS one, 2012. 7(2): p. e31874.

31. Huang, A.J., et al., Effects of human neutrophil chemotaxis across human endothelial cell monolayers on the permeability of these monolayers to ions and macromolecules. Journal of cellular physiology, 1988. 135(3): p. 355-366.

32. Burns, A.R., et al., Analysis of tight junctions during neutrophil transendothelial migration. Journal of cell science, 2000. 113(1): p. 45-57.

33. Tenzer, S., et al., Nanoparticle size is a critical physicochemical determinant of the human blood plasma corona: a comprehensive quantitative proteomic analysis. ACS nano, 2011. 5(9): p. 7155-7167.

34. Nel, A.E., et al., Understanding biophysicochemical interactions at the nano–bio interface. Nature materials, 2009. 8(7): p. 543-557.

35. Cedervall, T., et al., Understanding the nanoparticle–protein corona using methods to quantify exchange rates and affinities of proteins for nanoparticles. Proceedings of the National Academy of Sciences, 2007. 104(7): p. 2050.

CHAPTER 6

CONCLUSIONS AND FUTURE WORKS

6.1 Conclusions and Significant Contributions

Drug delivery systems (DDS) remain one of the most distinguished aspect in the field of biomedical and pharmaceutical engineering, particularly DDS developed for the targeting of therapeutics or imaging moieties to the vascular wall in human diseases. Vascular-targeted DDS are advantageous due to the benefits of decreased in side effect associated with the localized delivery, the ability to sustain drug release and the increase in patient compliance. Because these advantages improve the traditional therapies, many variants of vascular targeting carriers have been proposed for use as alternative treatment for cancer as well as for pulmonary and cardiovascular diseases. In order to design an efficient drug carrier for targeted drug delivery, there are three crucial criteria that must be considered: targeting properties, physical properties, chemical properties and hemodynamics properties.

6.1.1 Targeting Properties

To achieve the targeting specificity, the surface of drug carriers is typically altered by decorating with ligand molecules with affinity to proteins and other molecules specifically expressed at the target. In this study, we focus on sialyl-lewis A (Sle^{A})

(Chapter 3, 4 and 5), a carbohydrate ligand specific affinity to selectin, as the targeting ligand on vascular-targeted drug carrier with specificity for the E-selectin protein expressed on inflamed endothelial cells. Sle^A was use as the model ligand because Sle^A –coated particles are effectively captured under high-shear flow similar to leukocyte binding to the vessel wall. However, these particles have weak adhesion force which can detach under high shear rate or by WBCs rolling motion. Therefore, the particles in chapter 2 were decorated with dual-targeted ligands (Sle^A and anti-VCAM) at the optimal ratio because antibody molecules (anti-VCAM) help particles to resist the high shear force and still adhere under *in vivo* condition.

6.1.2 Physical Properties

Beyond specifically binding to the targeted sites, the VTCs must also be able to marginate (localize and adhere) to vessel wall through the bulk blood flow. The physical properties of drug carrier are important factors to localize VTCs to the vascular wall in blood flow. In chapter 2, we concluded that particle shape, particle size, and targeting moiety all play a role in prescribing the adhesion and biodistribution profile in a mouse model of atherosclerosis. Specifically, we found that the ellipsoidal microparticles of aspect ratio (AR4) with volume equivalent to 2 μm diameter spheres are more efficient on the targeting inflamed endothelium in the aorta of atherosclerotic mice than microspheres of equal volume and nanoparticles, especially in plaque areas. Further, these micro-rods, when untargeted, displayed a similar level of minimal mechanical entrapment in the lung capillaries compared to their spherical particles. Thus, the ellipsoidal geometry at the appropriate aspect ratio may be an advantageous shape to use when designing drug carriers for targeting the aorta, in order to deliver the highest possible payload of therapeutics or

diagnostics in atherosclerosis. However, more targeted micro-rods than microspheres and nanoparticles are retained in the lungs at higher levels compared to their untargeted particles due to molecular interaction with inflammatory molecules in the pulmonary vasculature of atherosclerotic mice.

1.6.3 Chemical Properties

In addition to the geometry of particles, the material type is also a crucial factor in particle binding efficiency due to differences in density and physicochemistry of particle. The discussion in chapter 5 confirms that the plasma protein-particle interaction in different material types of particles causes the differences in corona protein formation on the particle surface which interferes with particle adhesion as well. As the results show in chapter 5, human plasma soaked PLGA microparticle reduced binding relative to buffer control, which exhibits the critical negative plasma proteins specific to material type (PLGA particle), and this effect is not observed for PS microspheres. These discoveries are beneficial to VTCs design and imaging techniques because the provided optimal physical properties (size, shape and material) can be utilized to effectively deliver medication.

6.1.4 Hemodynamic Properties

Hemodynamics, the movement of blood cells in the circulatory system, is enforced by flow dynamics that can be changed by the characteristic of blood vessel and blood properties. Chapter 3 reveals that the adhesion efficiency of particles is dependent on the vessel size, WSR and blood hematocrit because these parameters effect “cell free layer” formation and particle-RBC interaction. The cell free layer typically decreases with decreasing vessel diameter at a fixed hematocrit. Therefore, a smaller cell free layer is

anticipated in the 28 μm channel height relative to the 43 μm channel height, which likely results in a higher local concentration of spheres at a closer proximity to the wall. A higher concentration of spheres at the wall would in turn lead to higher adhesion efficiency. The results of chapter 3 also show that the shear rates (WSR) also affect particle binding, especially given that the adhesion efficiency of 5 μm particles significantly decreased for all WSR increases in both channels. Because 5 μm particles exist in a reaction-limited regime (RLR), in which a high slip velocity is exhibited by these spheres and the higher disruptive force acting on them inhibit their adhesion at high WSRs, hence the decrease in adhesion density is observed for the 5 μm particle as the channel WSR increases. Lastly, the results in chapter 4 also show that flow pattern also plays an importance role in the adhesion of particles. Specifically, pulsatile flow tends to decrease microparticle binding, but recirculating flow enhances the adhesion of microparticles, particularly the reattachment point which presents low shear rate (favored for microparticles). Understanding the role of hemodynamics on prescribing the VTCs binding efficiency is valuable since these discoveries allow for flexibility in VTCs design for various conditions of diseases and blood vessels.

Furthermore, rheology is one of the crucial factors for efficacy of particle adhesion, including %Hct, RBC dimension, and plasma protein. In chapter 3, the studies shows that %Hct is an important factor that affects flow resistance in microvessels and the formation of the cell free layer. As shown in chapter 3, the adhesion density of 2 μm particle significantly increased as the blood Hct increased from 10% to 50% in the 43 μm channel, but the adhesion of 5 μm particle dropped when increased to 50%hct. These result is due to the shrinking of the cell free layer in response to the enlargement of the RBC core and

hence a higher packing of small particles closer to the endothelial wall. However, for larger particles there is increased in collision with RBCs with the larger RBC core and this disruptive force lead to detachment of large particles. Additionally, this study also sheds light on the relevance of the relative size of the particle to the RBC dimension in different species on particle binding, as discussed in chapter 4. According to the results, the optimal diameter of particles can be predicted with a mathematic model for each species along with blood flow patterns. Last but not least, the studies in chapter 5 conclude that the plasma proteins in different species affect the different levels of particle binding, especially in porcine which shows strong negative effects on particle adhesion. Overall, these studies reveal potential deviations of results observed in animal models and the predictability of the outcome in humans. This is important for drug delivery and diagnostics in cardiovascular research fields.

6.1.5 Implication of hemorheology in clinical aspect

Our studies and results particularly concentrate on application for atherosclerosis, however; this studies also can be applied into several physiological and pathophysiological conditions in human.

As discussed earlier, particle adhesion efficiency is strongly dependent on hemodynamic and hemorheology. In physiological condition, whole blood viscosity is reflected by hematocrit level. Hematocrit in a given individual may not remain constant but may change significantly as a part of physiological and pathophysiological conditions. An acute rise in hematocrit might be the result of a relative increase of RBCs mass in circulatory system caused by fluid loss by various means such as gastrointestinal and urinary tract, and by constriction of the volume of the circulatory system. These conditions

also affect the protein concentration of plasma and increasing plasma viscosity too. In addition, high hematocrit can also be caused by erythrocytosis, which is the production of more red blood cells by bone marrow, polycythemia vera and Cor pulmonale (COPD, chornic sleep apnea, pulmomary embolism). According to the correlation of these physical conditions and symptoms with our previous studies in chapter 3, the margination of nanoparticle may be optimized in these conditions.

Additionally, our study also show the relevance of the relative size of the particle to the RBC dimension, as discussed in chapter 4. The physical properties of RBC such as dimension and deformability have significant effect on flow resistance in vascular system and hence also impact the adhesion of VTCs. Several diseases that show unusual property of RBCs such as macrocytic anemia which RBCs have insufficient concentration of hemoglobin resulting larger than their normal volume which have more interaction with larger particle during blood flow. On the other hand, microcytic anaemia caused by iron deficiency anemia and thalassemia show smaller RBCs than normal dimension which may enhance nanoparticle adhesion as deliberated in chapter 4.

In addition to the hematocrit and dimension of RBCs, their rheological properties are also important determinants of blood fluidity. The unique shape and structure of RBCs provide special mechanical properties, which they can changes their shape responding to dynamic force known as RBC deformability resulting the formation of RBC core layer in vessel during blood circulation. This study demonstrated that most of nanoparticle tend to be entrapped into RBC core layer, which limits the particle margination to vessel wall as discussed in chapter 3. However, several diseases such as sickle cell anemia could have abnormal, rigid, inelastic and sickle-like shape RBCs effecting deformability in blood flow

and also RBCs core layer which may decrease the entrapment of nanoparticle between RBC and then enhance margination of nanoparticle to the vessel wall.

Lastly, according to chapter 5, we found that plasma viscosity also play important role in particle adhesion due to shear force on vessel wall during blood flow. In general, the level of plasma viscosity is good indicator of disease process and pathophysiological condition associated with acute phase reaction related to the protein content of plasma. Plasma viscosity can increase up to 5-6 cP (normal plasma viscosity is 1.10-1.35 cP) in patients with abnormal protein levels known as paraproteinemais which presence of excessive amounts of papraprotein or single monoclonal gammaglobulin in the blood. As discussed in chapter 5, immunoglobulins are one class of protein prominently present in the protein corona on the surface of particle interfere with particle adhesion.

Overall, these studies reveal potential correlation between hemodynamics describing particle adhesion extended into clinical side by providing the cases of physiological and pathophysiological conditions in human. This is essential for designing drug delivery in other hematological conditions beside atherosclerosis.

6.2 Future Works

Even though this dissertation evaluates the role of particle geometry (size and shape), hemodynamics, and hemorheology, which are significant strategies necessary in designing the optimal vascular-targeted carriers (VTCs) used in imaging and therapeutic delivery in cardiovascular diseases, the investigation in this field could be further developed and extended in the following directions.

(1) Extend development of the *in vitro* flow adhesion assay to acheive the physiological conditions as encountered in human.

(1.1) Use the cylinder flow system. Since most of this study uses rectangular channel as *in vitro* flow assay, which does not represent the real vessel geometry, thus, the cylinder flow system would be more suitable to be use as the assay. The particle binding trend in the cylinder tube could be different due to various factors including the velocity profile that occurred in different coordinating systems. However, this system still has limitations in channel fabrication and culture cells at the system wall.

(1.2) Observe the adhesion of VTC at smaller channel height (10-15 μm) with bifurcation or capillary network mimicking flow channel, which are the characteristics of disease sites such as atherosclerotic plaque area in arterioles and vascular network in cancer tissue. These studies would determine the trend of particle binding and possibly suggest the optimal VTC geometry used for targeting specifically to lesion areas.

(2.) Investigate the potential role of other materials on particle behavior in blood flow. Though the serveral material types (PS, PLGA, silica and titanium), VTCs used in chapter 5, are commonly employed for in vitro assays only PLGA is biodegradable

material. Therefore, other material such as polycaprolactone (PCL), hydrogel or biological materials would be preferable for in vivo research due to their biodegradability and biocompatibility. Due to the different properties of these materials such as density, surface characteristics and physicochemistry, the behavior in blood flow and the interaction with blood cells of these particles could be different and thus may effect their binding efficiency as well.

(3) Further investigate the potential role of WBCs in the different particle binding density in difference animal species, previously observed in Chapter 5. Specifically, the effect of WBC size, WBC concentration and specific WBC type in various animals on particle binding may need to be revisited and carefully examined.

(4) Identify the specific plasma protein interfering with particle binding in blood flow. As shown in chapter 5, some species such as porcine and bovine have a strongly negative protein plasma effect on the adhesion of particles; otherwise some species such as rabbit and mouse show a slight effect on plasma protein. However, we have not known which specific proteins in each animal plasma have strong interactions with targeting molecule and material surface, and then reduce binding efficiency of the particles. Thus, characterization of plasma protein on particles is crucial for enhancing affinity and sustain the particle in the circulation system.

(5) Include blood that is similar to the human physiology in the study such as orangutan or chimpanzee, due to the similarity in blood geometry and plasma protein to humans. This would result in a more accurate prediction as the ape blood data would be complied in the results in chapter 4 and 5 and could be add to mathematical model.

(6) Determine the role of particle physical properties (e.g. size, shape and surface charge) in dictating the internalization of VTCs in the endothelial cells and macrophage under blood flow condition.

Even though there is much room for further study, the studies presented here as a preliminary provide several crucial factors for designing drug delivery system and enhancing drug efficiency. They are essential for drug delivery and diagnostics in further cardiovascular research fields.